The combination of amperometry and mass spectrometry as a novel dual detection concept for capillary electrophoresis

Dissertation

zur Erlangung des Doktorgrades der Naturwissenschaften (Dr. rer. nat.)
der Fakultät für Chemie und Pharmazie
der Universität Regensburg

vorgelegt von

Daniel Böhm

aus Holzheim am Forst

im Januar 2023

Die vorliegende Dissertation entstand in der Zeit von Februar 2020 bis Januar 2023 am Institut für Analytische Chemie, Chemo- und Biosensorik der naturwissenschaftlichen Fakultät IV -Chemie und Pharmazie- der Universität Regensburg.

Die Arbeit wurde angeleitet von Prof. Dr. Frank-Michael Matysik.

Promotionsgesuch eingereicht am:	26. Januar 2023
Termin des Kolloquiums:	21. April 2023

Prüfungsausschuss:

Vorsitzender:	Prof. Dr. Oliver Tepner
Erstgutachter:	Prof. Dr. Frank-Michael Matysik
Zweitgutachterin:	PD Dr. Katja Dettmer-Wilde
Drittprüfer:	Apl. Prof. Dr. Rainer Müller

Danksagung

Ich möchte mich an dieser Stelle bei allen bedanken, die mich auf dem Wege zur Promotion unterstützt und begleitet haben.

Mein besonderer Dank gilt dabei in gleicher Weise:

- *Herrn Prof. Dr. Frank-Michael Matysik für die Betreuung der Arbeit und die wertvollen Diskussionen.*
- *Dem weiteren Prüfungsausschuss bestehend aus Prof. Dr. Oliver Tepner, PD Dr. Katja Dettmer-Wilde und Apl. Prof. Dr. Rainer Müller für die Begutachtung der Dissertation und für die Durchführung des Promotionskolloquiums.*
- *Der Feinmechanischen und Elektronischen Werkstatt, ohne deren Unterstützung einige Projekte kaum möglich gewesen wären.*
- *Nicole Herl, Dr. Thomas Herl, Dr. Timo Raith, Dr. Bernhard Durner und Dr. Stefan Wert für die wertvollen Ratschläge und Anregungen.*
- *Johannes Eidenschink, Martin Koall und Joachim Rewitzer für den großartigen Zusammenhalt, das einzigartige Arbeitsklima und die unterhaltsamen Mittagspausen.*
- *Meiner Familie Christian, Irmingard und Hans Böhm und meiner Freundin Angelina Hirmer für den stetigen Rückhalt, deren Verständnis und die Unterstützung in allen Lebenslagen.*

Die Promotion wurde finanziell von der Deutschen Forschungsgemeinschaft (DFG) unterstützt (Projektnummer: MA1491/12-1*)*.

Berge werden bezwungen, indem man sich auf den Weg macht.

(Autor unbekannt)

Table of contents

List of publications

Peer-reviewed articles

Characterization of linearly coupled capillaries with various inner diameters in the context of capillary electrophoresis

Böhm D, Matysik F-M. Characterization of linearly coupled capillaries with various inner diameters in the context of capillary electrophoresis. Monatsh Chem. 2021;152:1053–60.

Abstract

As a result of continuous instrumental progress, capillary electrophoresis (CE) has become an established separation technique. However, the choice of the suitable capillary inner diameter (ID) is sometimes difficult due to different instrumental requirements concerning injection, separation, or detection. To overcome this problem, we assembled two capillaries with different IDs, meaning that the ID of the capillary at the injection side was different from that at the detection side. Since this was a rather uncommon approach, we focused on the associated effects in this proof-of-concept study. For the experiments, a non-aqueous model system was used, consisting of an acetonitrile-based background electrolyte and the two ferrocene derivates, ferrocenemethanol and decamethylferrocene. Utilizing capillary flow injection analysis hyphenated to capacitively coupled contactless conductivity detection, it could be shown that fragmented capillaries of the same ID had slightly lower volume flow rates than non-fragmented capillaries. With non-aqueous CE hyphenated to UV detection, it was found that the coupling of capillaries with different IDs had a much stronger effect on the CE flow than combinations with the same ID. Additionally, if the ID of the second capillary was larger than the ID of the first capillary, a higher theoretical plate number and an increased sensitivity were found. Furthermore, it was found that there was no significant peak tailing introduced by the coupling.

Dead volume–free flow splitting in capillary electrophoresis

Böhm D, Koall M, Matysik F-M. Dead volume-free flow splitting in capillary electrophoresis. Electrophoresis. 2022;43:1438–45.

Abstract

In recent years, several dual detection concepts (DDCs) for capillary electrophoresis (CE) were developed, which consisted of at least one non-destructive detector. For these DDCs, a linear detector arrangement could be used, which is not possible when both detectors are destructive. To overcome this problem, we developed a concept for the splitting of the CE stream utilizing commercially available flow splitters (FSs) that allow the parallel positioning of two destructive detectors. In this proof-of-concept study, T- and Y-shaped FSs were characterized regarding their suitability for DDCs. To keep it simple, an UV/Vis photometric detector (UV) and a capacitively coupled contactless conductivity detector (C^4D) were used for the characterization. The model system consisted of an acetonitrile-based background electrolyte and two model substances (ferrocenylmethyl)trimethylammonium iodide and caffeine. CE hyphenated to UV measurements revealed that the split ratio was about 50% for both FSs. CE hyphenated to C^4D was used to evaluate the peak shape in front of and behind the FSs. These measurements showed that there was no significant peak broadening introduced by the FSs. Additionally, there were no changes in the limits of detection in front of and behind the FSs. Furthermore, the flexibility of the new FS approach allowed the usage of capillaries with different inner diameters (25–75 µm) for injection and detection.

Combining amperometry and mass spectrometry as a dual detection approach for capillary electrophoresis

Böhm D, Koall M, Matysik F-M. Combining amperometry and mass spectrometry as a dual detection approach for capillary electrophoresis. Electrophoresis. 2023;44:492-500.

Abstract

Dual detection concepts (DDCs) are becoming more and more popular in analytical chemistry. In this work, we describe a novel DDC for capillary electrophoresis (CE) consisting of an amperometric detector (AD) and a mass spectrometer (MS). This detector combination has a good complementarity as the AD exhibits high sensitivity, whereas the MS provides excellent selectivity. Both detectors are based on a destructive detection principle, making a serial detector arrangement impossible. Thus, for the realization of the DDC, the CE flow was divided into two parts with a flow splitter. The DDC was characterized in a proof-of-concept study with ferrocene derivates and a non-aqueous background electrolyte. We could show that splitting the CE flow was a suitable method for the instrumental realization of the DDC consisting of two destructive detectors. By lowering the height of the AD compared to the MS, it was possible to synchronize the detector responses. Additionally, for the chosen model system, we confirmed that the AD was much more reproducible and had lower limits of detection (LODs) than the MS. The LODs were identical for the DDC and the single-detection arrangements, indicating no sensitivity decrease due to the CE flow splitting. The DDC was successfully applied to determine the drug and doping agent trimetazidine.

Conference contributions

Oral presentations

2020 **16th International Students Conference Modern Analytical Chemistry**, online, Title: The effects of linearly assembled capillaries with various inner diameters on capillary electrophoresis, September 17-18, 2020.

2021 **3rd Cross-Border Seminar on Electroanalytical Chemistry (CBSEC)**, online, Title: Development of a novel dual detection concept (amperometric detection/ mass spectrometry) for capillary electrophoresis, April 8-9, 2021.

2022 **4th Cross-Border Seminar on Electroanalytical Chemistry (CBSEC)**, Prague (CZ), Title: Novel dual detection concept (amperometric detection/mass spectrometry) for capillary electrophoresis, April 11-13, 2022.

2022 **Electrochemistry 2022**, Berlin (DE), Title: A novel dual detection concept for capillary electrophoresis featuring amperometric detection and mass spectrometry, September 27-30, 2022.

2023 **33. Doktorandenseminar des AK Separation Science der GDCh**, Hohenroda (DE), Title: The marriage of amperometry and mass spectrometry as a novel dual detection approach for capillary electrophoresis, January 8-10, 2023.

Awards and honors

2020 **Metrohm award** for the best presentation in the field of electroanalytical chemistry at the 16th Modern Analytical Chemistry in Prague (CZ)

2022 **Front cover**: “Dead volume-free flow splitting in capillary electrophoresis” in ELECTROPHORESIS (July 2022)

2022 **Honorable mention**: “Dead volume-free flow splitting in capillary electrophoresis” in ELECTROPHORESIS (July 2022)

2022 **Award for one of the best presentations** at the 4th Cross-Border Seminar on Electroanalytical Chemistry in Prague (CZ)

2023 **Award for the third best presentation** at the 33. Doktorandenseminar des AK Separation Science der GDCh in Hohenroda (DE)

2023 **Honorable mention**: “Combining amperometry and mass spectrometry as a dual detection approach for capillary electrophoresis” in ELECTROPHORESIS (March 2023)

Declaration of collaboration

Most of the practical and theoretical work of this thesis was done by the author. A small part of the obtained results was achieved in cooperation with other researchers. In accordance with § 8 Abs. 1 Satz 2 Punkt 7 of the Ordnung zum Erwerb des akademischen Grades eines Doktors der Naturwissenschaften (Dr. rer. nat.) an der Universität Regensburg vom 18. Juni 2009 (Änderungssatzung vom 2. Juni 2022), this section describes the nature of these collaborations. The collaborations are described within this section.

4.1 Characterization of linearly coupled capillaries with various inner diameters in the context of capillary electrophoresis

The measurements were planned and done by the author. The manuscript was written by the author. The project was done under the supervision of Prof. Dr. Frank-Michael Matysik.

4.2 Dead volume–free flow splitting in capillary electrophoresis

The measurements were planned by the author. Most of the measurements were done by the author. Martin Koall did some of the measurements under the supervision of the author in the frame of a research internship. The manuscript was written by the author. The front cover was designed by the author. The project was done under the supervision of Prof. Dr. Frank-Michael Matysik.

4.3 Combining amperometry and mass spectrometry as a dual detection approach for capillary electrophoresis

The measurements were planned by the author. Most of the measurements were done by the author. Martin Koall did some of the measurements under the supervision of the author as part of the equipment instruction for his master thesis. The manuscript was written by the author. The project was done under the supervision of Prof. Dr. Frank-Michael Matysik.

7 Appendix

The user-friendly, miniaturized CE device with a novel capillary positioning concept for research purposes was developed by the author based on previous versions of miniaturized CE devices. The project was technically implemented by the mechanical and electronic workshops of the Faculty of Chemistry and Pharmacy of the University of Regensburg. The project was done under the supervision of Prof. Dr. Frank-Michael Matysik.

List of abbreviations

In this section, the most important abbreviations used in this thesis are summarized in alphabetical order. Special abbreviations are introduced in the corresponding chapters.

Table 1. List of the main abbreviations

Abbreviation	Full name
ACN	Acetonitrile
AD	Amperometric detection
BGE	Background electrolyte
Caf	Caffeine
C^4D	Capacitively coupled contactless conductivity detection
CE	Capillary electrophoresis
CE-AD	CE hyphenated to AD
CE-AD/MS	CE hyphenated to AD and MS
CE-C^4D	CE hyphenated to C^4D
CE-MS	CE hyphenated to MS
CE-UV	CE hyphenated to UV
CFIA	Capillary flow injection analysis
CFIA-C^4D	CFIA hyphenated to C^4D
DDC	Dual detection concept
dMFc	Decamethylferrocene
EOF	Electroosmotic flow
ESI	Electrospray ionization
FcMeOH	Ferrocenemethanol
$[FcMTMA]^+$	(Ferrocenylmethyl)trimethylammonium ion
FS	Flow splitter
FST	T-shaped FS
FSY	Y-shaped FS
ID	Inner diameter
LOD	Limit of detection
MS	Mass spectrometry
m/z	Mass-to-charge ratio
OD	Outer diameter
PEI	Polyetherimide
RSD	Relative standard deviation
SD	Standard deviation
S/N	Signal-to-noise ratio
TMZ	Trimetazidine
TOF	Time-of-flight
TPN	Theoretical plate number
UV	UV/Vis photometric detection
VFR	Volume flow rate

1 Introduction

The pioneering work of Jorgenson and Lukacs [1] in 1981 is considered as the birth of capillary electrophoresis (CE). Since then, CE has been improved by many research groups worldwide. Its separation principle is based on the different migration behavior of charged species in a high-voltage electrical field. For many analytes, primarily biologically relevant compounds, CE has a much higher separation efficiency than liquid or gas chromatography [2]. Furthermore, CE is appreciated for the fast separation times, simple instrumental setup, and low sample and solvent consumption [3–6]. CE is nowadays used in fields like medicine [7], environmental research [8], biochemistry [9], and pharmacy [10].

However, an efficient separation method like CE requires a powerful detection method. In the case of CE, finding a suitable detection method is challenging, due to the small sample volumes and the small dimensions. A detection method that can be easily miniaturized and adapted to the small dimensions of CE is amperometric detection (AD) [11–13]. AD is considered as one of the most sensitive detection methods for electroactive species [6, 14, 15]. Additionally, it has excellent long-term stability in combination with non-aqueous background electrolytes (BGEs). The good reproducibility allows the quantification by external calibration or standard addition method [16–18]. One drawback of AD is the lack of selectivity since analytes can hardly be identified. Moreover, it is not possible to distinguish comigrating substances. Furthermore, the AD is a very specific detector that is only suitable for electroactive analytes [12, 19].

In contrast to AD, mass spectrometry (MS) is an universal detection method for a wide range of analytes. The most significant advantage of MS is its unmatched selectivity. With MS, it is possible to identify analytes by their molecular weight, characteristic fragmentation, and isotopic patterns. Furthermore, comigrating substances can be distinguished by MS [20–22]. The coupling of CE and MS is achieved via electrospray ionization (ESI), which has a low inter- and intraday reproducibility. Thus, for quantification mainly isotope-labeled internal standards are added. However, these standards are expensive and not available for all substances. The limits of detection (LODs) of MS depend on the ionization efficiency of the analyte. In most cases, the AD has much lower LODs than the MS [23–26].

For these reasons, one could conclude that every detector is particularly suited for a specific application. The AD is ideal for quantification, whereas the MS is perfect for identification. A powerful way to combine the benefits of two different detectors are dual

detection concepts (DDCs). With DDCs, the disadvantages of one detector could be compensated by the advantages of the other detector and vice versa [27]. The combination of AD and MS has excellent complementarity and provides a promising DDC.

Several DDCs for CE are already described in literature [7, 28–33]. However, a DDC consisting of an AD and a MS for CE is to the best of our knowledge not described so far. Most of the established DDCs use a serial detector arrangement because this is easiest to implement [13]. For the serial detector arrangement, a non-destructive detector is placed in front of a second detector which could be non-destructive or destructive [7, 29–31]. In some other DDCs, the detectors use the same detection spot [28, 32, 33]. Both detectors (AD and MS) have a destructive detection principle and must be decoupled from the high-voltage electrical field of the CE. Hence, the established implementation strategies (serial detector arrangement and detection at one spot) are not suitable for the novel DDC (CE-AD/MS). For the realization of the DDC, the CE flow must be divided into two parts. This was achieved by a flow splitter (FS), which allowed the parallel positioning of the detectors. A scheme of the novel DDC (CE-AD/MS) is shown in Fig. A.1

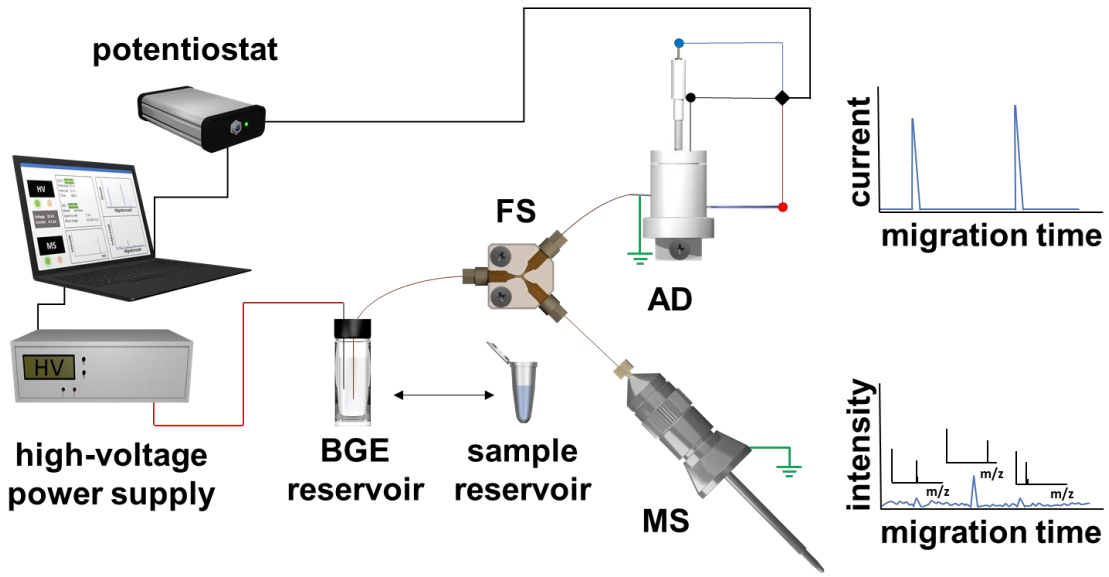

Figure A.1. Scheme of the novel CE-AD/MS setup. The FS in the center splits the CE flow into two parts and allows the parallel positioning of the AD and the MS. The scheme was designed by Dr. Thomas Herl

According to our knowledge, no DDC for CE utilizes an FS. In CE, a kind of flow splitting is only done for the realization of 2D separations or the concurrent analysis of cations and anions. These approaches are technically realized via micro-structured chips or valves [34–36]. However, this is unsuitable for implementing the DDC (CE-AD/MS) because a continuous CE separation without decoupling from the high-voltage field is required for the technical implementation of the novel DDC.

This thesis describes the development of the novel DDC (CE-AD/MS). The development was started with the linear coupling of capillaries and the evaluation of the corresponding effects. In the next step, different types of FS were tested regarding their suitability for DDCs. The project was concluded by realizing the final DDC and its characterization. Additionally, a user-friendly, miniaturized CE device with a novel capillary positioning concept for research purposes was developed.

References

1. Jorgenson JW, Lukacs KD. Zone electrophoresis in open-tubular glass capillaries. Anal Chem. 1981;53:1298–302.
2. Grundmann M, Matysik F-M. CE ergänzt HPLC: Kapillarelektrophorese-Massenspektrometrie. Nachrichten aus der Chemie. 2011;59:1081–3.
3. Voeten RLC, Ventouri IK, Haselberg R, Somsen GW. Capillary electrophoresis: trends and recent advances. Anal Chem. 2018;90:1464–81.
4. Ramos-Payán M, Ocaña-Gonzalez JA, Fernández-Torres RM, Llobera A, Bello-López MÁ. Recent trends in capillary electrophoresis for complex samples analysis: A review. Electrophoresis. 2018;39:111–25.
5. Furter JS, Boillat M-A, Hauser PC. Low-cost automated capillary electrophoresis instrument assembled from commercially available parts. Electrophoresis. 2020;41:2075–82.
6. Holland LA, Chetwyn NP, Perkins MD, Lunte SM. Capillary electrophoresis in pharmaceutical analysis. Pharm Res. 1997;14:372–87.
7. Cieslarova Z, Magaldi M, Barros LA, do Lago CL, Oliveira D, Fonseca FAH, et al. Capillary electrophoresis with dual diode array detection and tandem mass spectrometry to access cardiovascular biomarkers candidates in human urine: Trimethylamine-N-Oxide and l-carnitine. J Chromatogr A. 2019;1583:136–42.
8. Rojano-Delgado AM, Luque de Castro MD. Capillary electrophoresis and herbicide analysis: present and future perspectives. Electrophoresis. 2014;35:2509–19.
9. Kristoff CJ, Bwanali L, Veltri LM, Gautam GP, Rutto PK, Newton EO, et al. Challenging bioanalyses with capillary electrophoresis. Anal Chem. 2020;92:49–66.
10. Suntornsuk L. Recent advances of capillary electrophoresis in pharmaceutical analysis. Anal Bioanal Chem. 2010;398:29–52.
11. Matysik F-M. Elektrochemische Detektion für miniaturisierte Fließsysteme und Trennverfahren. Nachrichten aus der Chemie. 2000;48:632–5.
12. Cammann K. Instrumentelle Analytische Chemie: Verfahren, Anwendungen, Qualitätssicherung. Heidelberg: Spektrum Akademischer Verlag; 2001.
13. Opekar F, Stulík K. Some important combinations of detection techniques for electrophoresis in capillaries and on chips with emphasis on electrochemical principles. Electrophoresis. 2011;32:795–810.
14. Holland LA, Lunte SM. Capillary electrophoresis coupled to electrochemical detection: a review of recent advances. Anal Commun. 1998;35:1–4.
15. Matysik F-M. End-column electrochemical detection for capillary electrophoresis. Electroanalysis. 2000;12:1349–55.

16. Matysik F-M. Special aspects of detection methodology in nonaqueous capillary electrophoresis. Electrophoresis. 2002;23:400–7.
17. Riekkola M-L. Recent advances in nonaqueous capillary electrophoresis. Electrophoresis. 2002;23:3865–83.
18. Matysik F-M. Application of non-aqueous capillary electrophoresis with electrochemical detection to the determination of nicotine in tobacco. J Chromatogr A. 1999;853:27–34.
19. Kubán P, Hauser PC. Fundamentals of electrochemical detection techniques for CE and MCE. Electrophoresis. 2009;30:3305–14.
20. Beutner A, Scherer B, Matysik F-M. Dual detection for non-aqueous capillary electrophoresis combining contactless conductivity detection and mass spectrometry. Talanta. 2018;183:33–8.
21. Skoog DA, Holler FJ, Crouch SR. Instrumentelle Analytik. 6th ed. Berlin, Heidelberg: Springer Spektrum; 2013.
22. Hesse M, Bienz S, Meier H, Bigler L, Fox T. Spektroskopische Methoden in der organischen Chemie. 9th ed. Stuttgart, New York: Georg Thieme Verlag; 2016.
23. Samskog J, Wetterhall M, Jacobsson S, Markides K. Optimization of capillary electrophoresis conditions for coupling to a mass spectrometer via a sheathless interface. J. Mass Spectrom. 2000;35:919–24.
24. Wang L, Li Y, Chen D, Chen DDY. Electrospray ionization stability and concentration sensitivity in capillary electrophoresis-mass spectrometry using a flow-through microvial interface. Electrophoresis. 2021;42:360–8.
25. Issaq HJ, Janini GM, Chan KC, Veenstra TD. Sheathless electrospray ionization interfaces for capillary electrophoresis–mass spectrometric detection. J Chromatogr A. 2004;1053:37–42.
26. Maxwell EJ, Chen DDY. Twenty years of interface development for capillary electrophoresis-electrospray ionization-mass spectrometry. Anal Chim Acta. 2008;627:25–33.
27. Beutner A, Herl T, Matysik F-M. Selectivity enhancement in capillary electrophoresis by means of two-dimensional separation or dual detection concepts. Anal Chim Acta. 2019;1057:18–35.
28. Szarka M, Szigeti M, Guttman A. Imaging laser-induced fluorescence detection at the Taylor cone of electrospray ionization mass spectrometry. Anal Chem. 2019;91:7738–43.
29. Beutner A, Cunha RR, Richter EM, Matysik F-M. Combining C4D and MS as a dual detection approach for capillary electrophoresis. Electrophoresis. 2016;37:931–5.

30. Huhn C, Ruhaak LR, Mannhardt J, Wuhrer M, Neusüß C, Deelder AM, et al. Alignment of laser-induced fluorescence and mass spectrometric detection traces using electrophoretic mobility scaling in CE-LIF-MS of labeled N-glycans. Electrophoresis. 2012;33:563–6.
31. Chicharro M, Bermejo E, Ongay S, Zapardiel A. Determination of maleic hydrazide in potato samples using capillary electrophoresis with dual detection (UV-electrochemical). Electroanalysis. 2008;20:534–41.
32. Qiu H, Yin X-B, Yan J, Zhao X, Yang X, Wang E. Simultaneous electrochemical and electrochemiluminescence detection for microchip and conventional capillary electrophoresis. Electrophoresis. 2005;26:687–93.
33. Zhong M, Zhou J, Lunte SM, Zhao G, Giolando DM, Kirchhoff JR. Dual-electrode detection for capillary electrophoresis/electrochemistry. Anal Chem. 1996;68:203-7.
34. Sydes D, Kler PA, Hermans M, Huhn C. Zero-dead-volume interfaces for two-dimensional electrophoretic separations. Electrophoresis. 2016;37:3020–4.
35. Pham TTT, Mai TD, Nguyen TD, Sáiz J, Pham HV, Hauser PC. Automated dual capillary electrophoresis system with hydrodynamic injection for the concurrent determination of cations and anions. Anal Chim Acta. 2014;841:77–83.
36. Jooß K, Scholz N, Meixner J, Neusüß C. Heart-cut nano-LC-CZE-MS for the characterization of proteins on the intact level. Electrophoresis. 2019;40:1061–5.

2 Fundamentals and background

2.1 Capillary electrophoresis

2.1.1 Fundamentals

In 1897, Kohlrausch [1] discovered the principle of electrophoresis. After several years (1930), it was used as an analytical method for proteins by the Swedish scientist Tiselius. He already recognized that capillaries with a small inner diameter (ID) are necessary for efficient heat removal (Joule heating) to get high separation efficiencies. However, only the technical development of capillaries with small IDs in the early 1980s made CE possible [2, 3]. Jorgenson and Lukacs [4] performed CE measurements for the first time in 1981. Since then, CE has become an established separation technique whose separation principle is based on the different migration behavior of charged species in an electrical field. It can be used for various analytes, from small ions to large macromolecules like proteins and DNA. Additionally, with CE enantiomers can be separated [2, 5]. Due to this wide range of applications, CE is used in many fields like medicine [6], environmental research [7], chemical [8] and food industries [9], pharmacy [10], and biochemistry [11]. Further advantages of CE are the high separation efficiency, the small sample and solvent consumption, the simplicity of the instrumental setup, and the short analysis times [12–15]. In contrast to classical flatbed electrophoresis, CE can easily be automated [2].

There are different types of CE described, such as capillary zone electrophoresis, micellar electrokinetic chromatography, capillary electrochromatography, capillary isotachophoresis, capillary gel electrophoresis, and capillary isoelectric focusing. This thesis focuses on capillary zone electrophoresis, which is the most frequently used CE type [2]. The following text refers to capillary zone electrophoresis.

Various forces act on charged species in an electrical field. On the one hand, the species are accelerated by the electrical force. On the other hand, the friction force decelerates the species. Both forces are in equilibrium resulting in a constant, substance-specific electrophoretic velocity (v_{EPH}) of the species in the electrical field (equation 1) [2, 5].

$$v_{EPH} = \frac{q}{f_c} \cdot E = \mu \cdot E \qquad (1)$$

with v_{EPH} = electrophoretic velocity

q = charge of the ion

f_c = friction coefficient

E = electrical field strength

μ = electrophoretic mobility

If two species differ in their charge (q) or in their friction coefficient (f_c) they can be separated [3]. In equation 1 also the electrophoretic mobility (μ) is introduced, which is a substance-specific proportionality factor between v_{EPH} and the electrical field strength (E) [2, 5].

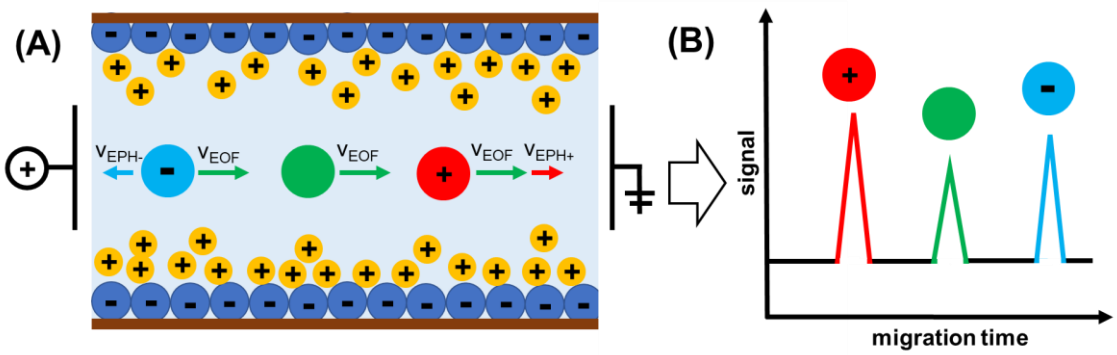

Figure B.1. Migration behavior of cationic (red), neutral (green), and anionic species (blue) in CE (A). The electropherogram (B) shows the migration order. Cationic species are detected first, then neutral species, and finally anionic species are detected. Adapted from [2]

An important phenomenon in CE is the electroosmotic flow (EOF). For pH values greater than four, the terminal silanol groups at the inner wall of the fused silica capillary are deprotonated [5]. Cations from the background electrolyte (BGE) interact with the negatively charged capillary wall and form a double layer (Stern-model). The double layer consists of a static part which is located close to the capillary wall and a dynamic part which is connected to the static part. The cations of the dynamic part move to the cathode whenever a separation voltage is applied. This generates a suction effect which is termed EOF. The EOF can be influenced by the electrical field strength (E), pH-value,

ionic strength, different additives, and capillary coatings [2, 5]. The formation of the EOF is depicted in Fig. B.1A. The electroosmotic velocity (v_{EOF}) can be calculated with equation 2 [2].

$$v_{EOF} = \frac{\varepsilon \cdot \zeta \cdot E}{4 \cdot \pi \cdot \eta} \quad (2)$$

with v_{EOF} = electroosmotic velocity
ε = dielectric constant
ζ = zeta-potential
E = electrical field strength
η = viscosity

The migration velocity of the analytes is the sum of the electrophoretic velocity (v_{EPH}) and the electroosmotic velocity (v_{EOF}) [2, 3]. Cationic species have the highest migration velocity and shortest migration times since v_{EPH+} and v_{EOF} have the same direction. Next, neutral substances migrate, which move with v_{EOF}. However, all neutral substances migrate simultaneously with the EOF and are not separated from each other. Anionic species show the slowest migration behavior because v_{EPH-} and v_{EOF} have different directions. Usually, v_{EOF} is higher than v_{EPH-}, thus the anions move to the cathode as well. Therefore, it is possible to detect all species at the side of the cathode [2, 5]. The migration behavior of the different species is illustrated in Fig. B.1.
Another advantage of the EOF is the flat flow profile in contrast to the parabolic flow profile of liquid chromatography (pump-driven flow), which is depicted in Fig. B.2. The flat flow profile of CE results in low band-broadening and narrow peaks [2, 5].

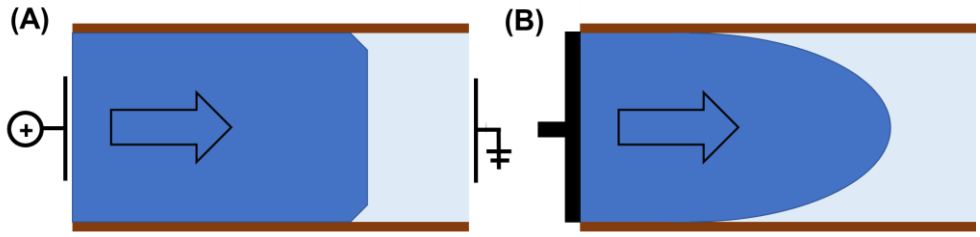

Figure B.2. Flat flow profile of the EOF (A) in comparison to a parabolic flow profile of liquid chromatography (B). Adapted from [3]

2.1.2 Instrumental aspects

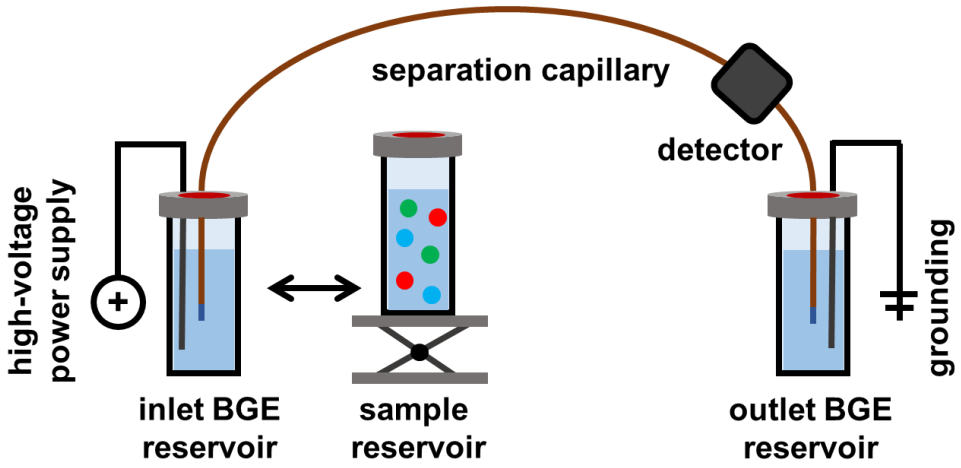

Figure B.3. Scheme of a basic CE setup consisting of an inlet and outlet BGE reservoir, separation capillary, detector, positive high-voltage power supply and grounding. In this scheme, the injection is done hydrodynamically via a gravity-driven flow introduced by a height different between the sample and outlet reservoir. Adapted from [3]

In contrast to other separation methods, the experimental setup for CE is quite simple [2]. A scheme with the basic components for CE is depicted in Fig. B.3. A CE system consists of an inlet and outlet reservoir filled with BGE, connected to each other by a separation capillary. For CE, usually fused silica capillaries with IDs ranging from 5 to 100 µm are utilized, but also capillaries made of borosilicate glass, polytetrafluoroethylene and polyether ether ketone are suitable. Due to the small dimensions in CE only minimal sample volumes of 0.5 - 50 nL are required. There are commonly two injection concepts used for CE, the hydrodynamic injection (excess pressure at the injection site, vacuum at the detection side, or gravity-driven flow) and the electrokinetic injection (high-voltage at the injection site) [2, 5, 16]. Another innovative injection concept was developed by Backofen et al. [17]. In the so-called capillary batch injection, the sample is directly injected into the separation capillary utilizing a second capillary. This is especially useful for the handling of minimal sample volumes. However, in this thesis only the gravity-driven hydrodynamic injection was used, which was achieved by a height difference between the sample and outlet reservoir. The CE setup further consists of two electrodes which are immersed in the BGE reservoirs and connected to a high-voltage power supply. A positive high-voltage is usually applied at the electrode in the inlet reservoir (anode) and the electrode in the outlet reservoir is grounded (cathode). In CE, high-voltages up to 30 kV are used. The applied voltage creates an electrical field that is responsible for the separation of the analytes. The migration behavior depends on the

charge and size of the analytes. For most applications, the detector is placed at the side of the cathode. CE can be hyphenated to various detector types. The most common ones are so-called on-column detectors as UV/Vis photometric detection (UV), laser-induced fluorescence detection, and capacitively coupled contactless conductivity detection (C^4D). Examples of detectors positioned at the capillary end are MS and AD [2, 3, 5]. Some of these detectors (UV, C^4D, MS, and AD) were used in this thesis and are described in the following chapters.

2.1.3 Non-aqueous capillary electrophoresis

Non-aqueous BGEs consisting of organic solvents are an interesting alternative to the predominately used aqueous BGEs in CE. The first application of non-aqueous CE was done by Walbroehl and Jorgenson in 1984 [18]. Suitable organic solvents are among others methanol, dimethyl sulfoxide, and acetonitrile (ACN). With non-aqueous BGEs analytes are accessible to CE, which are not dissolvable in water. Furthermore, the selectivity of CE can be tuned by mixing different solvents. Primarily, ACN is used for non-aqueous CE. It has a large dielectric constant-to-viscosity ratio which enables fast separations. ACN also has favorable characteristics for the combination with various detectors. Combined with AD, it shows enhanced long-term stability of the electrochemical detector response. In aqueous BGEs, the potential window is limited to about 2 V, whereas for ACN-based BGEs have a wider potential window. Therefore, the range of possible analytes for AD is increased. According to the volatility and low surface tension, ACN-based BGEs are also favorable for electrospray ionization (ESI)-MS. It facilitates the formation of a stable electrospray. In addition, grounding problems between CE and the ESI interface are reduced due to the low electrophoretic currents of non-aqueous BGEs [19–21]. Due to these advantages, an ACN-based BGE was used for the development of the novel DDC (CE-AD/MS).

2.2 UV/Vis photometric detection

UV is a spectrophotometric detection method. The detection principle is based on the absorbance of light. Thus, the analytes must show absorbance in the UV/Vis region (190 – 800 nm) [3, 22]. The profile of the fused-silica capillary is used as detection window. Therefore, the hyphenation of CE with UV is simple since the detector can be placed on-column. However, the polyimide coating of the capillary is impermeable to light and must be removed at the detection area. The coating can be removed using a flame, razor blade, or concentrated sulfuric acid [2, 3, 22]. Often modified detectors for liquid chromatography are used for CE [5]. UV is inexpensive and can be applied to various analytes. Therefore, it is installed in almost every commercial CE device [22]. One drawback of CE-UV is the lack of sensitivity. According to the Lambert-Beer law, the absorbance is directly proportional to the optical path length. However, this is limited by the ID of the capillary, which is usually smaller than 100 µm. Different approaches can be used to increase the optical path length, like z-cells, bubble cells, and multi-reflection cells. With these innovations, the sensitivity of UV can be improved, but there is a loss in selectivity due to the broader optical path length [3, 22]. There are basically two types of UVs. UVs with variable wavelengths have a monochromator in front of the detection window and light of a specific wavelength passes the detection window. In contrast, diode-array detectors have a grating monochromator after the detection window and polychromatic light passes the detection window. After the detection window, the light is split into the spectral range and analyzed with an array of diodes. In contrast to UVs with variable wavelengths, diode-array detectors allow the identification of substances due to the measured UV/Vis spectra [2, 22].

2.3 Capacitively coupled contactless conductivity detection

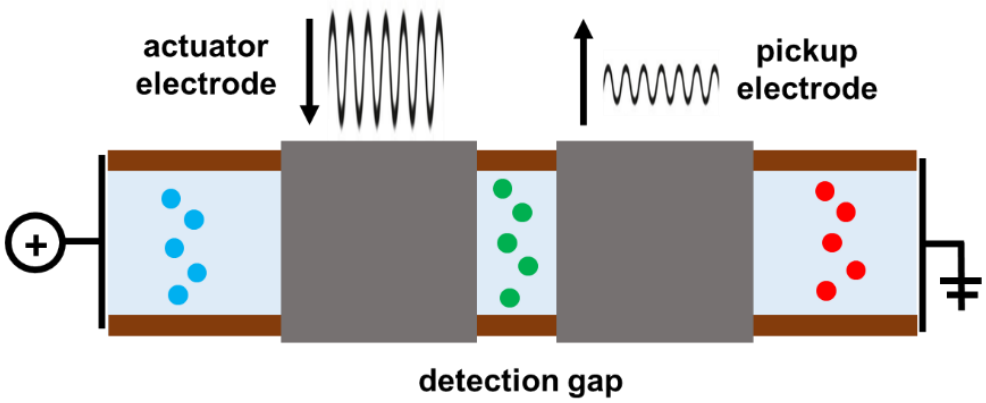

Figure B.4. C^4D with axial electrode alignment. The actuator electrode applies the oscillating frequency. The pickup electrode recognizes a change in the conductivity in the detection gap. Adapted from [22, 23]

CE is an excellent method for the separation of charged species. Thus, conductivity detection is a very suitable detection method for CE. According to its universal nature, it can be used for a wide variety of analytes that were otherwise difficult to detect, like small inorganic ions or non-UV/Vis absorbing species [22, 24]. There are different instrumental approaches for the hyphenation of CE with conductivity detection. In these approaches, the sensing electrodes were placed inside the capillary [25] or at the capillary end [26]. However, the success of conductivity detection as a detection method for CE began with the introduction of C^4D with an axial cell design [27, 28]. In C^4D, the electrodes are not in direct contact with the analyte or BGE. A sketch illustrating the detection principle of a C^4D is depicted in Fig. B.4. An oscillating frequency with a certain amplitude is applied at the actuator electrode and collected by the pickup electrode. Between both electrodes, there is a certain distance which is called detection gap. The conductivity changes when ions pass the detection gap. The pickup electrode registers this conductivity change within the capillary. The BGE also has a specific conductivity which results in a constant signal. For optimal sensitivity, the conductance difference between the analyte zones and the BGE must be as high as possible. Thus, for most BGEs, a compromise must be found between separation and detection [22, 24, 29].

There are several advantages since the sensing electrodes do not come into contact with the sample solution in C^4D:

- There are no problems with electrode fouling or analyte carryover.

- There is no problem with interfering effects between the high-voltage electrophoretic circuit of the CE and the C^4D.
- According to the on-column detection, it can be hyphenated with other detection systems like UV or MS
- Not limited to fused silica as capillary material [22]

Further advantages of C^4D are that cations and anions can be detected without modifications in the experimental setting and that the EOF can be monitored without adding an EOF marker [30].

2.4 Mass spectrometry

2.4.1 Fundamentals

The first application of MS was already described in 1910 for the separation of isotopes [31]. Since that time, the method has been continuously improved. Especially the development of the two soft ionization techniques, electrospray ionization (ESI) and matrix-assisted laser desorption ionization enabled the application of MS for large biomolecules. Nowadays, MS is considered as the most versatile detection technique because it can identify and quantify a broad range of analytes [2, 3]. It is mainly known for its excellent selectivity. With MS, it is possible to determine the mass-to-charge ratio (m/z) of ions in a vacuum. Substances can be identified with MS by their molecular weight, characteristic fragmentation, and isotopic patterns. [3, 31].

The essential components of a MS are a sample inlet, an ion source, a mass analyzer, a detector, and a data processing system. A mandatory requirement for MS is the ionizability of the analytes. Thus, in a first step the analytes are transformed into gaseous ions. The sample inlet and the ion source are often combined [31]. There are different ionization techniques like electron ionization, chemical ionization, fast atom bombardment, ESI, and matrix-assisted laser desorption ionization. A distinction is made between hard and soft ionization methods. Electron ionization is a typical example of a hard ionization technique. Due to the high energy transfer, the molecules are decomposed into many fragments, which is helpful for structure elucidation and the determination of functional groups. In contrast, ESI is a soft ionization technique where almost no fragments are produced. With ESI predominately molecule ions are formed giving information about the molecular weight of the analyte. After the ionization process, the ions enter the mass analyzer where they are separated under high vacuum according to their m/z. The vacuum is necessary to prevent the ions from collisions with

components present in the atmosphere. The most common mass analyzers are quadrupole and time-of-flight (TOF) mass analyzers [3, 5, 31]. Combinations of several mass analyzers are also possible. In the final step, the fractionated ions are detected with a faraday cup or a secondary electron multiplier [2].

The obtained mass spectrum is the two-dimensional representation of the relative ion frequency versus m/z [2]. In a mass spectrum the m/z with the highest signal intensity is called base peak and is defined to the value 100. The intensities of the remaining peaks are scaled to this base peak. The m/z which corresponds to the ion of an intact molecule structure is called molecular ion peak [3, 31].

2.4.2 Electrospray ionization

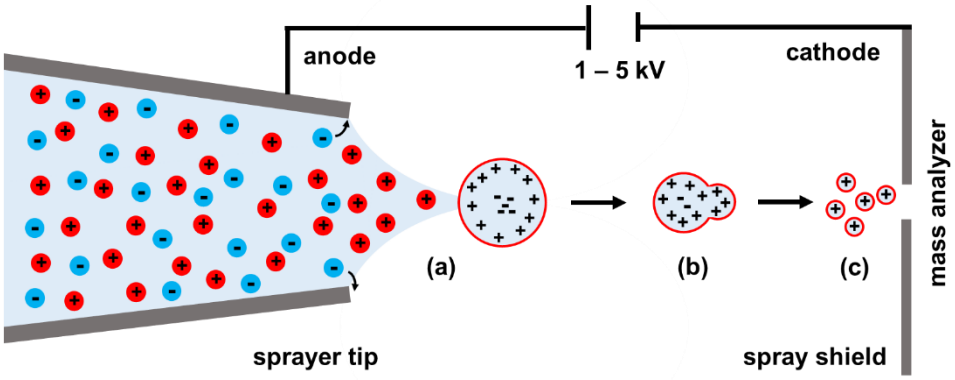

Figure B.5. Scheme showing a positive ESI process. At the tip of the ESI sprayer, a Taylor cone is formed (a) and multiple charged droplets are generated. After solvent evaporation Coulomb explosions occur (b) and gaseous ions are formed (c). Adapted from [31]

It is challenging to generate ions from solutions and to transfer them into the MS. The biggest challenge is the selective ionization of an analyte in the presence of huge amounts of solvents. An ionization technique that masters this task and could be directly coupled to a liquid-based separation system like CE is ESI. ESI was developed in the mid-80s and is especially useful for determining the molecular weight of large biomolecules since ions with an intact molecular structure are formed by protonation, deprotonation, or the addition of an alkali metal ion. In the positive ESI process (depicted in Fig. B.5) cations are generated. The sprayer acts as an anode and the spray shield of the MS as a cathode. For negative ESI the potential would be reversed and anions would be generated. A high-voltage of 1 - 5 kV is applied between the ESI sprayer and the spray shield. At the tip of the ESI sprayer positively charged ions accumulate and form

a fine filament called Taylor cone (Fig. B.5, a). At this point droplets with multiple positive charges are created. On their way to the spray shield the size of the droplets is shrinking due to the solvent evaporation. The charge at the surface of the droplets increases until the Rayleigh limit is reached (Fig. B.5, b). When this limit is reached Coulomb explosions occur and the droplets break up into smaller droplets. The droplets undergo this process several times until gaseous ions are formed (Fig. B.5, c). Finally, the ions are transferred into the mass analyzer. The ESI process takes place under atmospheric pressure, but the determination of the ions in the mass analyzer is done under high vacuum and is described in the next chapter [2, 31].

2.4.3 Time-of-flight mass spectrometry

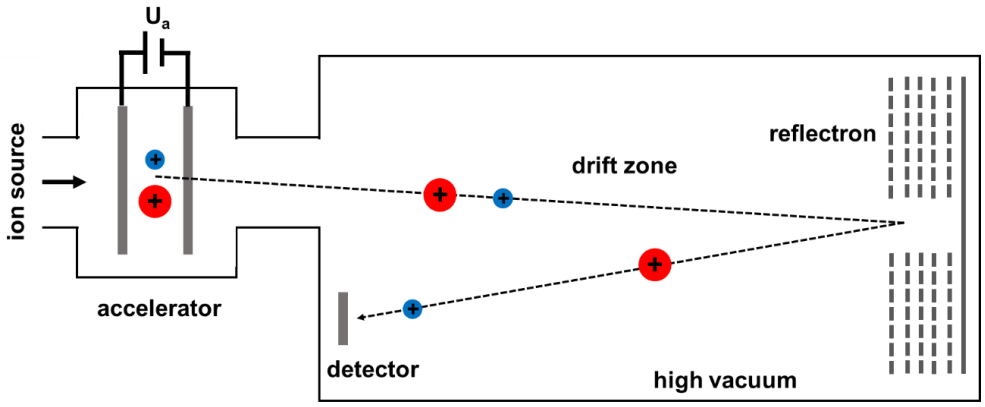

Figure B.6. Scheme showing the principle of a TOF-MS. First, the ions are expedited by an acceleration voltage (U_a). Next, they are separated in the field-free drift zone according to their m/z. Finally, the ions are detected at different times due to their different velocities. Adapted from [2]

TOF mass analyzers are known for their robustness, wide mass range, and high scan rates [3, 5]. The working principle of a TOF-MS is depicted in Fig. B.6. In the first step, the ions are expedited by an acceleration voltage (U_a) in the accelerator. At this point, all ions with equal charge number (z) get the same energy which is transferred into kinetic energy (E_{kin}, equation 3) [2].

$$E_{kin}=\frac{1}{2}\cdot m\cdot v^2=z\cdot e\cdot U_a \text{ with } v=\frac{L_{TOF}}{t_{TOF}} \quad (3)$$

with m = mass
v = velocity
z = charge number
e = elemental charge
U_a = acceleration voltage
t_{TOF} = flight time
L_{TOF} = length of the drift zone

Next, the ions are separated in the field-free and evacuated drift zone. This is possible since all ions have the same kinetic energy (E_{kin}) and due to their different masses, they move with different velocities through the drift zone. For example, lighter ions have higher velocities and reach the detector earlier than heavier ones. From equation 3 one could derive that the m/z is proportional to the square of the flight time (equation 4) [2, 31].

$$\frac{m}{z}\propto(t_{TOF})^2 \quad (4)$$

The m/z can be calculated from the measured flight times (t_{TOF}). The calibration is done with a reference substance of known m/z [2]. The reflectron which is also shown in Fig. B.6 increases the length of the field-free drift zone and compensates energy differences between ions with identical m/z. Therefore, it improves the mass accuracy and the resolution of the TOF-MS [31].

2.4.4 Hyphenation of capillary electrophoresis and mass spectrometry

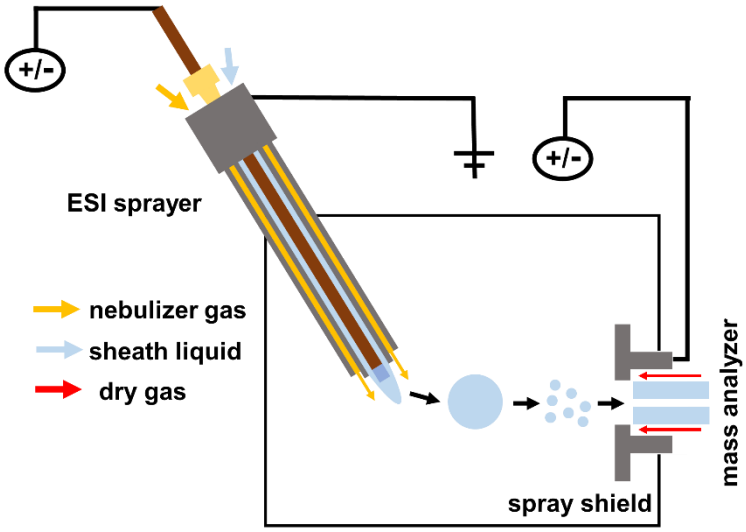

Figure B.7. Scheme showing the hyphenation of CE and MS via a grounded, sheath liquid ESI sprayer. Adapted from [22, 32]

In recent years MS has become a very popular detection method for CE [33, 34]. Both methods (CE and MS) have a good complementarity. With CE it is for example possible to separate isobaric substances (identical molecular weight), which cannot be distinguished with MS. However, comigrating substances from CE with different molecular weights can be identified with MS [22]. The coupling of CE and MS was the first time described by Smith and coworkers [35]. The hyphenation of both techniques is usually achieved via ESI. CE and ESI are both electric field-driven and their electrical circuits must be separated. The most elegant way to accomplish this is by grounding the ESI sprayer. With a grounded ESI sprayer, it is for example possible to apply a negative potential at the inlet of the MS. This allows positive ions to enter the MS (positive ESI). However, if a positive potential is applied at the inlet of the MS, negative ions will enter the MS (negative ESI). Also, a positive or negative potential could be applied at the injection side of the CE due to the grounded ESI sprayer. Hence, different modes of CE and MS (positive or negative) can be realized. Fig. B.7 shows the different combinations for CE and MS possible with a grounded ESI sprayer. Furthermore, the used BGE must be MS compatible and should only consist of volatile components like ammonium salts, formic acid, or acidic acid [2, 22, 32].

Another point that must be considered is a robust closure of the electrical circuit of the CE. There are two concepts described, the sheathless and the sheath flow interfaces. In the sheathless interfaces, electrical contact is achieved via wires inserted into the

capillary tips, metal-coated capillary tips, or liquid junctions [2, 22]. Maxwell and Chen [36] give a detailed overview of different sheathless approaches. A drawback of sheathless methods is the lack of reproducibility due to the formation of gas bubbles and the usual laboratory-constructed interfaces. Sheath flow interfaces are more robust and commercially available. In this approach, a conductive sheath liquid generates an electrical contact between the capillary and the grounded ESI sprayer. Since the volume flow in CE is relatively low, the sheath liquid also supports the generation of a stable ESI spray. A nebulizer gas (nitrogen) is added to get a uniform spray. A detailed view of a grounded, sheath flow ESI sprayer is given in Fig. B.7. A drawback of the sheath liquid approach is the loss of sensitivity due to the dilution of the analyte [22, 36, 37]. In this thesis, it was tried to compensate this disadvantage through the additional use of an AD, which is described in the next chapter.

2.5 Amperometric detection

2.5.1 Fundamentals

Various electrochemical detection techniques, like amperometry, voltammetry, or conductometry, are used in analytical chemistry [3]. In literature, the term “electrochemical detection” is often used as an equivalent for AD because it is the most common electrochemical detection mode [38]. Within this section, the focus will be only on amperometry which is used as a detection method in sensors or for the endpoint control of titrations [39]. Amperometry is also used as a detection method for different flow stream systems like capillary flow injection analysis [40], liquid chromatography [41], and CE [42]. In amperometry, a certain potential is applied at the working electrode which oxidizes or reduces the analyte. The current resulting from electrochemical processes at the electrode surface is directly proportional to the analyte concentration. The most common mode of amperometry is chronoamperometry, where a constant detection potential is applied at the working electrode. There are also different pulsed amperometric methods that are not discussed in this work. The AD usually consists of a three-electrode setup (working, counter, and reference electrode) [5, 43]. For example, the working electrode could be made of gold, platinum, copper, or carbon [44]. Whereas for the counter electrode, mainly platinum or stainless steel is used [3]

AD is described as one of the most sensitive detection methods for electroactive substances with LODs down to 10^{-10} M [43, 45]. However, the LODs in AD strongly depend on the nature of the electrode reaction. Additionally, the AD has a wide linear concentration range that starts near the LOD and goes up to the mM range. Furthermore, the AD has usually a simple design and can be constructed using low-cost components [43, 46]. One drawback of AD is the lack of selectivity, which can be

improved by selecting the detection potential, modifying the electrode surfaces, or using different electrode materials [38, 43, 47]. One problem of AD is the direct contact of the electrodes with the sample solution. This can lead to a passivation of the electrode surface by corrosion or electrode fouling. As electrode fouling the deposition of electrochemically generated products at the electrode surface is known. Electrode fouling can result in a decrease in sensitivity and poorer reproducibility. The electrode can be cleaned by mechanical polishing or by applying an electrode pretreatment protocol (application of different potentials) [5, 23].

2.5.2 Hyphenation of capillary electrophoresis and amperometric detection

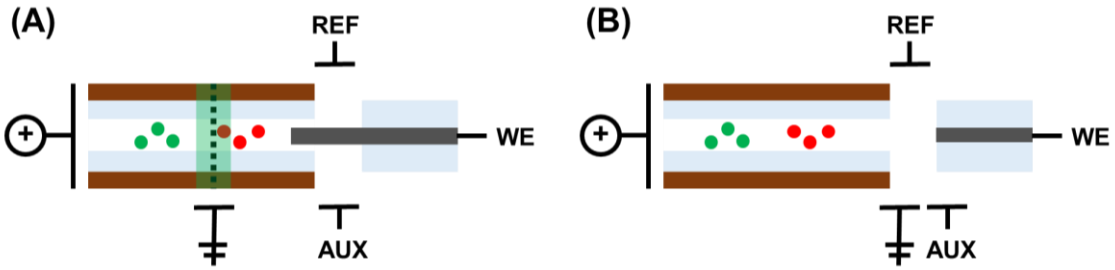

Figure B.8. Schematic representation of two decoupling strategies for CE-AD, off-column AD (A) and end-column AD (B). The off-column AD has its grounding in front of the detection zone, whereas the end-column AD is grounded at the capillary end. Each AD consists of a working (WE), auxiliary (AUX), and reference electrode (REF). Adapted from [44]

The small injection volumes, the limited size of the separation channels, and the high separation efficiency of CE require powerful and down-scalable detection techniques. AD is a suitable detection method for CE. AD has a high sensitivity for electroactive analytes, a high tolerance to various BGEs, permits a low dead volume, and can be miniaturized without loss in sensitivity [43, 46–48]. However, care must be taken to the interference of the high-voltage separation field of the CE and AD circuit [43]. In CE a high separation voltage of several kV is used, and the current is in the µA region. However, for AD a moderate detection potential of a few V is applied to the working electrode and a current is measured down to the pA region [19]. To avoid interference effects between CE and AD, the two electrical circuits must be decoupled from each other. For CE-AD there are two ways to reduce interference effects, which are shown in Fig. B.8. The first approach is called off-column AD (Fig. B.8A) and was introduced by Wallingford and Ewing [42] in 1987. An off-column AD is characterized by an electrical

field decoupler which is implemented in front of the detection zone and serves as grounding for the CE. Usually, an electrical field decoupler is generated by a fracture in the capillary. Due to the fracture, a small gap for the grounding is produced, which is covered by a semipermeable membrane, but also porous joints can be used as electrical field decouplers [19, 23, 48]. There are a lot of other approaches for electrical field decouplers which are partly summarized by Voegel and Baldwin [49]. After the decoupler, the EOF pushes the analytes to the AD [38]. In off-column AD there is almost no effect of the high-voltage electrical field of the CE behind the decoupler, and the working electrode can even be placed in the capillary. The drawbacks of off-column AD are peak broadening caused by the movement of the analytes in the field-free capillary part behind the decoupler, the potential loss of cations due to the fracture in the capillary and the inconvenient implementation of the electrical field decoupler due to the small dimensions [19, 23, 48].

End-column AD is a more straightforward approach without an electrical field decoupler (Fig. B.8B). The first CE-AD without a decoupler was developed by Sloss and Ewing [50]. In end-column AD, a wall-jet configuration is usually used, and the working electrode is placed at a certain distance from the capillary outlet. There is no need for an electrical field decoupler because the capillary acts as an ohmic resistance, causing a voltage drop across the capillary. Additionally, there is an exponential potential drop at the end of the capillary according to the lager cross-section of the BGE outside the capillary [19, 23]. With a proper positioning of the working electrode in the proximity of the capillary outlet, interference effects can be reduced [20]. However, without decoupler the AD is not completely decoupled from the high-voltage field of the CE and effects of the high-voltage electrical field must be considered [43]. The potential shift at the working electrode is determined in situ under electrophoretic conditions and depends on the applied high-voltage, the electrode geometry, the capillary dimensions and the capillary-to-electrode alignment. The potential shift can be determined by the performance of cyclic voltammograms with and without separation voltage [19, 51]. For end-column AD, capillaries with very small IDs (<25 µm) are usually used. These capillaries have a higher ohmic resistance than capillaries with a wider ID resulting in smaller electrophoretic currents. Therefore, the detector signal is less affected by the high-voltage electrical field of the CE. The ohmic resistance of the capillary could also be increased by the usage of a non-aqueous BGE instead of an aqueous BGE. Due to the higher ohmic resistance of non-aqueous BGEs capillaries with bigger IDs could be used in combination with end-column AD [44, 48]. It is possible to couple end-column AD with capillaries up to 75 µm, which is more practicable than capillaries with IDs smaller than 25 µm. Wide-bore

capillaries have the advantage that they have reduced problems with clogging and bubble entrapment at the detection zone [19].

Since the technical implementation of an end-column AD is simpler, it is utilized more frequently than off-column AD. Nevertheless, CE-AD is according to our knowledge exclusively used in research laboratories. One reason for this is that the sensitivity depends on the capillary-to-electrode alignment. Furthermore, for the reproducibility a reliable capillary-to-electrode alignment is necessary. This is often achieved with an x,y,z-micropositioner and a microscope which is complicated and time-consuming [19, 43]. A very user-friendly, end-column amperometric detection cell with an integrated guiding system for the capillary and electrode was developed by Matysik [52]. It was used in this thesis and is described in detail in section 3.5.3.

2.6 Dual detection concepts in capillary electrophoresis

The determination of analytes in complex matrices is difficult. Especially environmental, medical, and biological samples have challenging matrices and contain a broad range of analytes with different characteristics. For a single detector, it can be difficult to quantify and identify all analytes of interest. An innovative way to increase the power of an analytical method is the utilization of several detectors. The coupling of more than one detector is an ongoing trend in analytical chemistry and can be found in literature under phrases like “dual detection”, “combined detection”, “tandem detection” or “multi-detection”. Using two different detectors, their advantages can be combined and their weaknesses can be compensated in a powerful DDC. DDCs save time and costs, since several analytes with a wide range of characteristics can be determined simultaneously in one measurement [30, 53, 54]. Additionally, the selectivity could be increased by DDCs. Pairs of insufficiently separated substances can be distinguished if different detectors detect the substances individually or if both substances are detected by one detector and only one substance is detected by the second detector. If the detectors have different detection principles, it also simplifies the identification of the analytes [47].

In literature, several DDCs for CE are described and summarized in three reviews. Li et al. give a general overview of DDCs in chip electrophoresis and conventional CE [53]. Opekar and Štulík [47] focused on DDC with an emphasis on electrochemical detection methods. The latest review from Beutner et al. [30] was published in 2018 and focused on selectivity enhancement by 2D separation and DDCs. Some recent publications deal with DDCs consisting of C^4D and UV [55–57]. However, this work presents a novel DDC

consisting of an AD and a MS. Therefore, in the following some other DDCs consisting of an AD, or a MS will be discussed with special emphasis on the detector arrangement. AD is very suitable for the combination with other detection methods due to the high sensitivity, the possibility to be miniaturized, the tolerance to various BGEs and the adjustment of the detector shape to the given space. Several ADs described in literature consist of more than one working electrode. These working electrodes can be arranged in parallel for direct detection or in series for direct and indirect detection. In concepts with a serial working electrode arrangement (direct mode) usually the analyte is converted at the upstream electrode into an electroactive species, which can be detected at the downstream electrode. For this purpose, typically different potentials are applied. In the indirect detection mode, an auxiliary substance is added to the BGE, which is transferred into an active species at the upstream electrode. This electrochemically generated active species reacts with the analyte and the untreated active species is detected at the downstream electrode. This method can be used for the detection of electrochemically inactive analytes [47]. However, one can argue that only the parallel positioning of two working electrodes could be seen as real DDC, since both working electrodes provide complementary information [30]. The working electrodes can operate at different detection potentials, they can consist of different materials or have other surface modifications. The points mentioned before enhance the selectivity and sensitivity of ADs with parallel electrodes [47].

The concept of an AD with two adjacent working electrodes operating at different detection potentials was successfully used by Zhong at al. [58]. Two carbon fiber electrodes were parallel embedded in an epoxy matrix. Due to the two electrodes, it was possible to perform oxidative and reductive electrochemical detection simultaneously. This enabled the simultaneous determination of NADH and NAD^+. A detection potential of 0.85 V was used for NADH, whereas NAD^+ was detected at -0.75 V [58]. Another dual-electrode AD concept utilizing different electrode materials (carbon fiber and Au-Hg) was used for the simultaneous detection of cysteine, glutathione, ascorbic acid, and uric acid in human blood. Due to the complementary use of two different electrode materials, it was possible to enhance the selectivity of AD [59].

For AD not only DDCs with two ADs are known. There are several DDCs including one AD coupled with another detector. The combination of AD and electrochemiluminescence detection is powerful since both methods are very sensitive and provide a wide linear detection range. Additionally, the electrochemical signal and the electrochemiluminescence are generated at the same electrode, which results in a simultaneous detector response. A tris(2,2'-bipyridyl)ruthenium(II) complex is usually used as a luminescence agent for amine-containing analytes [60]. In combination with a

non-aqueous BGE the analysis times could be shortened, the electrode needed no reactivation between the measurements, and excellent reproducibility was found for both detectors [61, 62].

A DDC consisting of an UV and an AD is also described in literature [63]. UVs are the most common detectors in commercial CE systems and can be easily connected to an AD in a serial detector configuration. The standard on-column UV is thereby placed in front of the AD. The DDC (UV and AD) was successfully applied to determine various herbicide and pesticide mixtures. However, if the analytes could be detected with both detectors, the AD provides much lower LODs than the UV [64–67]. Zhang et al. [68, 69] give an example for the combination of C^4D and AD. This DDC was used for the determination of various phenylketonuria biomarkers in urine. It was technically realized by a C^4D in front of an end-column AD. The AD was predominantly used for quantifying the electroactive biomarkers, whereas the C^4D was used for non-electroactive species and to generate information about the matrix composition. So far, a detector combination of laser-introduced fluorescence detection and AD is only realized for chip electrophoresis [70]. However, both detection methods (AD and laser-induced fluorescence detection) were individually coupled with CE and compared concerning the determination of aniline derivates in water samples. It was found that the LODs were comparable between the detectors [71].

MS, as part of DDCs is mainly coupled with optical detection methods. The combination of UV and MS could be achieved by a serial detector arrangement of commercial devices. This DDC was recently used for the determination of cardiovascular biomarkers in urine [6]. However, by using commercial devices, there is always a distance between the UV and MS, resulting in a significant difference in migration times. The development of a laboratory-constructed sheath flow ESI interface with integrated UV overcame this disadvantage. Optical fibers placed close to the tip of the ESI interface allowed the detection of the analytes with UV just before entering the MS [72]. Laser-induced fluorescence detection offers very low LODs. Therefore, it is a desirable detection method that was coupled with MS. The serial arrangement of a laser-induced fluorescence detector integrated in a CE system with MS resulted in a significant shift in the migration times [73]. However, by placing the optical cell of the laser-induced fluorescence detector directly in front of the ESI interface the distance between the detection points could be reduced which resulted in minimized migration time differences [54, 74]. Szarka et al. [75] also coupled laser-induced fluorescence detection with MS. However, they performed the laser-induced fluorescence detection at the Tailor cone of the ESI interface. This enabled the simultaneous detection with both detectors. The method was successfully applied for the quantification (laser-induced fluorescence

detection) and identification (MS) of various fluorescently labeled carbohydrates. The complementary use of C^4D and MS is also described in some manuscripts. The technical realization of these DDCs was simple since a serial detector arrangement could be used. The C^4D was placed directly in front of the ESI interface of the MS [76, 77]. The challenge in combining C^4D and MS is the choice of a BGE, which is suitable for both detectors. Beutner et al. [78] used an ACN-based BGE, which showed excellent performance with both detectors (C^4D and MS).

To our knowledge, there is no DDC for CE described in literature consisting of an AD and a MS. Most of the described DDCs used a serial detector arrangement because this is easiest to implement. In the serial detector arrangement, the detectors are placed at different positions along the separation capillary, resulting in a migration time shift. Due to the different detector positions, there is also another degree of separation of the analytes. Additionally, the downstream detector can suffer from band-broadening effects [47]. In the serial detector configuration, a non-destructive detector is usually placed in front of a second detector. The second detector could be non-destructive or destructive [6, 54, 67, 77]. In some other DDCs, the detectors use the same spot for detection, resulting in identical detection times [58, 60, 75] However, with both implementation strategies for DDC (serial detector arrangement and detection at one spot), the novel DDC (CE-AD/MS) could not be implemented. The realization of this DDC is much more challenging since the CE flow must be split. To our knowledge, there is no DDC for CE described in literature for which the CE flow must be spit. In contrast to CE in gas chromatography, flow splitters have been successfully used for the combination of a flame ionization detector and MS [79, 80]. The development of the novel DDC (CE-AD/MS) is the main subject of this thesis.

References

1. Kohlrausch F. Ueber Concentrations-Verschiebungen durch Electrolyse im Inneren von Lösungen und Lösungsgemischen. Ann Phys Chem. 1897;298:209–39.
2. Kurreck J, Engels JW, Lottspeich F. Bioanalytik. 4th ed. Berlin: Springer Spektrum; 2022.
3. Skoog DA, Holler FJ, Crouch SR. Instrumentelle Analytik. 6th ed. Berlin, Heidelberg: Springer Spektrum; 2013.
4. Jorgenson JW, Lukacs KD. Zone electrophoresis in open-tubular glass capillaries. Anal Chem. 1981;53:1298–302.
5. Cammann K. Instrumentelle Analytische Chemie: Verfahren, Anwendungen, Qualitätssicherung. Heidelberg: Spektrum Akademischer Verlag; 2001.
6. Cieslarova Z, Magaldi M, Barros LA, do Lago CL, Oliveira DR, Fonseca FAH, et al. Capillary electrophoresis with dual diode array detection and tandem mass spectrometry to access cardiovascular biomarkers candidates in human urine: Trimethylamine-N-Oxide and l-carnitine. J Chromatogr A. 2019;1583:136–42.
7. Rojano-Delgado AM, Luque de Castro MD. Capillary electrophoresis and herbicide analysis: present and future perspectives. Electrophoresis. 2014;35:2509–19.
8. Arias M, Bauza R, Rodríguez J, Castañeda G, Ríos A. Rapid characterization of fatty alcohol ethoxylates by non-aqueous capillary electrophoresis. Electrophoresis. 2008;29:3060–8.
9. Simó C, Barbas C, Cifuentes A. Capillary electrophoresis-mass spectrometry in food analysis. Electrophoresis. 2005;26:1306–18.
10. Suntornsuk L. Recent advances of capillary electrophoresis in pharmaceutical analysis. Anal Bioanal Chem. 2010;398:29–52.
11. Kristoff CJ, Bwanali L, Veltri LM, Gautam GP, Rutto PK, Newton EO, et al. Challenging Bioanalyses with Capillary Electrophoresis. Anal Chem. 2020;92:49–66.
12. Furter JS, Boillat M-A, Hauser PC. Low-cost automated capillary electrophoresis instrument assembled from commercially available parts. Electrophoresis. 2020;41:2075–82.
13. Holland LA, Chetwyn NP, Perkins MD, Lunte SM. Capillary electrophoresis in pharmaceutical analysis. Pharm Res. 1997;14:372–87.
14. Ramos-Payán M, Ocaña-Gonzalez JA, Fernández-Torres RM, Llobera A, Bello-López MÁ. Recent trends in capillary electrophoresis for complex samples analysis: A review. Electrophoresis. 2018;39:111–25.

15. Voeten RLC, Ventouri IK, Haselberg R, Somsen GW. Capillary electrophoresis: trends and recent advances. Anal Chem. 2018;90:1464–81.
16. Grundmann M, Matysik F-M. Fast capillary electrophoresis-time-of-flight mass spectrometry using capillaries with inner diameters ranging from 75 to 5 µm. Anal Bioanal Chem. 2011;400:269–78.
17. Backofen U, Hoffmann W, Matysik F-M. Capillary batch injection analysis: a novel approach for analyzing nanoliter samples. Anal Chim Acta. 1998;362:213–20.
18. Walbroehl Y, Jorgenson JW. On-column UV absorption detector for open tubular capillary zone electrophoresis. J Chromatogr A. 1984;315:135–43.
19. Matysik F-M. End-column electrochemical detection for capillary electrophoresis. Electroanalysis. 2000;12:1349–55.
20. Matysik F-M. Special aspects of detection methodology in nonaqueous capillary electrophoresis. Electrophoresis. 2002;23:400–7.
21. Geiser L, Veuthey J-L. Nonaqueous capillary electrophoresis in pharmaceutical analysis. Electrophoresis. 2007;28:45–57.
22. Lauer HH, Rozing GP. High Performance Capillary Electrophoresis. 2nd ed. Germany: Agilent Technologies; 2018.
23. Kappes T, Hauser PC. Recent Developments in electrochemical detection methods for capillary electrophoresis. Electroanalysis. 2000;12:165–70.
24. Zemann AJ. Capacitively coupled contactless conductivity detection in capillary electrophoresis. Electrophoresis. 2003;24:2125–37.
25. Huang X, Pang TKJ, Gordon MJ, Zare RN. On-column conductivity detector for capillary zone electrophoresis. Anal Chem. 1987;59:2747–9.
26. Huang X, Zare RN, Sloss S, Ewing AG. End-column detection for capillary zone electrophoresis. Anal Chem. 1991;63:189–92.
27. Zemann AJ, Schnell E, Volgger D, Bonn GK. Contactless conductivity detection for capillary electrophoresis. Anal Chem. 1998;70:563–7.
28. Fracassi da Silva JA, do Lago CL. An oscillometric detector for capillary electrophoresis. Anal Chem. 1998;70:4339–43.
29. Kubán P, Hauser PC. Ten years of axial capacitively coupled contactless conductivity detection for CZE-a review. Electrophoresis. 2009;30:176–88.
30. Beutner A, Herl T, Matysik F-M. Selectivity enhancement in capillary electrophoresis by means of two-dimensional separation or dual detection concepts. Anal Chim Acta. 2019;1057:18–35.
31. Hesse M, Bienz S, Meier H, Bigler L, Fox T. Spektroskopische Methoden in der organischen Chemie. 9th ed. Stuttgart, New York: Georg Thieme Verlag; 2016.

32. Grundmann M, Matysik F-M. CE ergänzt HPLC: Kapillarelektrophorese-Massenspektrometrie. Nachrichten aus der Chemie. 2011;59:1081–3.
33. Sastre Toraño J, Ramautar R, de Jong G. Advances in capillary electrophoresis for the life sciences. J Chrom B,. 2019;1118-1119:116–36.
34. Stolz A, Jooß K, Höcker O, Römer J, Schlecht J, Neusüß C. Recent advances in capillary electrophoresis-mass spectrometry: Instrumentation, methodology and applications. Electrophoresis. 2019;40:79–112.
35. Olivares JA, Nguyen NT, Yonker CR, Smith RD. On-line mass spectrometric detection for capillary zone electrophoresis. Anal Chem. 1987;59:1230–2.
36. Maxwell EJ, Chen DDY. Twenty years of interface development for capillary electrophoresis-electrospray ionization-mass spectrometry. Anal Chim Acta. 2008;627:25–33.
37. Wang L, Li Y, Chen D, Chen DDY. Electrospray ionization stability and concentration sensitivity in capillary electrophoresis-mass spectrometry using a flow-through microvial interface. Electrophoresis. 2021;42:360–8.
38. Kubán P, Hauser PC. Fundamentals of electrochemical detection techniques for CE and MCE. Electrophoresis. 2009;30:3305–14.
39. Otto M. Analytische Chemie. 3rd ed. Weinheim: Wiley-VCH-Verlag; 2006.
40. Nagy G, Fehér Z, Pungor E. Application of silicone rubber-based graphite electrodes for continuous flow measurements. Anal Chim Acta. 1970;52:47–54.
41. Kissinger PT. The development of liquid chromatography/electrochemistry from a historical perspective. Electroanalysis. 1992;4:359–66.
42. Wallingford RA, Ewing AG. Capillary zone electrophoresis with electrochemical detection. Anal Chem. 1987;59:1762–6.
43. Pyell U. Electrokinetic chromatography. Theory, instrumentation, and applications. Hoboken, NJ: John Wiley & Sons; 2007.
44. Matysik F-M. Advances in amperometric and conductometric detection in capillary and chip-based electrophoresis. Microchim Acta. 2008;160:1–14.
45. Osboum DM, Lunte CE. Cellulose acetate decoupler for on-column electrochemical detection in capillary electrophoresis. Anal Chem. 2001;73:5961–4.
46. Matysik F-M. Improved end-column amperometric detection for capillary electrophoresis. J Chromatogr A. 1996;742:229–34.
47. Opekar F, Stulík K. Some important combinations of detection techniques for electrophoresis in capillaries and on chips with emphasis on electrochemical principles. Electrophoresis. 2011;32:795–810.
48. Matysik F-M. Elektrochemische Detektion für miniaturisierte Fließsysteme und Trennverfahren. Nachrichten aus der Chemie. 2000;48:632–5.

49. Voegel PD, Baldwin RP. Electrochemical detection in capillary electrophoresis. Electrophoresis. 1997;18:2267–78.
50. Sloss S, Ewing AG. Improved method for end-column amperometric detection for capillary electrophoresis. Anal Chem. 1993;65:577–81.
51. Matysik F-M. Experimental characterization of end-column electrochemical detection in conjunction with nonaqueous capillary electrophoresis. Anal Chem. 2000;72:2581–6.
52. Matysik F-M. Application of non-aqueous capillary electrophoresis with electrochemical detection to the determination of nicotine in tobacco. J Chromatogr A. 1999;853:27–34.
53. Li X, Tong Y-L, Liu C, Li O-L, Yang X-J, Chen Z-G. Dual detection methods for microchip and conventional capillary electrophoreses. Chinese J Anal Chem. 2009;37:1547–54.
54. Huhn C, Ruhaak LR, Mannhardt J, Wuhrer M, Neusüß C, Deelder AM, et al. Alignment of laser-induced fluorescence and mass spectrometric detection traces using electrophoretic mobility scaling in CE-LIF-MS of labeled N-glycans. Electrophoresis. 2012;33:563–6.
55. Claude B, Cutolo G, Farhat A, Zarafu I, Ionita P, Schuler M, et al. Capillary electrophoresis with dual detection UV/C4D for monitoring myrosinase-mediated hydrolysis of thiol glucosinolate designed for gold nanoparticle conjugation. Anal Chim Acta. 2019;1085:117–25.
56. Yang L, Pan G, Zhang P, Liu Q, Liu X, Li Y, et al. 3D printed two-in-one on-capillary detector: Combining contactless conductometric and photometric detection for capillary electrophoresis. Anal Chim Acta. 2021;1159:338427.
57. Zhao J, Xu Z. Capillary electrophoresis with dual C4D/UV detection for simultaneously determining major metal cations and whey proteins in milk. Anal Methods. 2021;13:801–8.
58. Zhong M, Zhou J, Lunte SM, Zhao G, Giolando DM, Kirchhoff JR. Dual-electrode detection for capillary electrophoresis/electrochemistry. Anal Chem. 1996;68:203–7.
59. Weng Q, Jin W. Carbon fiber bundle-Au-Hg dual-electrode detection for capillary electrophoresis. J Chromatogr A. 2002;971:217–23.
60. Qiu H, Yin X-B, Yan J, Zhao X, Yang X, Wang E. Simultaneous electrochemical and electrochemiluminescence detection for microchip and conventional capillary electrophoresis. Electrophoresis. 2005;26:687–93.

61. Yuan B, Huang J, Sun J, You T. A novel technique for NACE coupled with simultaneous electrochemiluminescence and electrochemical detection for fast analysis of tertiary amines. Electrophoresis. 2009;30:479–86.
62. Yuan B, Zheng C, Teng H, You T. Simultaneous determination of atropine, anisodamine, and scopolamine in plant extract by nonaqueous capillary electrophoresis coupled with electrochemiluminescence and electrochemistry dual detection. J Chromatogr A. 2010;1217:171–4.
63. Huang X, You T, Yang X, Wang E. Combination of amperometric detector & UV detector for capillary electrophoresis. Talanta. 1999;49:425–31.
64. Chicharro M, Zapardiel A, Bermejo E, Sánchez A. Simultaneous UV and electrochemical determination of the herbicide asulam in tap water samples by micellar electrokinetic capillary chromatography. Anal Chim Acta. 2002;469:243–52.
65. Chicharro M, Zapardiel A, Bermejo E, Sánchez A, González R. Multiresidue Analysis of Pesticides in Environmental Waters by Capillary Electrophoresis Using Simultaneous UV and Electrochemical Detection. Electroanalysis. 2004;16:311–8.
66. Chicharro M, Moreno M, Bermejo E, Ongay S, Zapardiel A. Determination of amitrole and urazole in water samples by capillary zone electrophoresis using simultaneous UV and amperometrical detection. J Chromatogr A. 2005;1099:191–7.
67. Chicharro M, Bermejo E, Ongay S, Zapardiel A. Determination of maleic hydrazide in potato samples using capillary electrophoresis with dual detection (UV-electrochemical). Electroanalysis. 2008;20:534–41.
68. Zhang D, Li W, Zhang J, Tang W, Qian C, Feng M, et al. Study on urinary metabolic profile of phenylketonuria by micellar electrokinetic capillary chromatography with dual electrochemical detection-potential clinical application in fast diagnosis of phenylketonuria. Anal Chim Acta. 2011;694:61–6.
69. Zhang D-L, Li W-L, Zhang J-B, Tang W-R, Chen X-F, Cao K-W, et al. Determination of unconjugated aromatic acids in urine by capillary electrophoresis with dual electrochemical detection-potential application in fast diagnosis of phenylketonuria. Electrophoresis. 2010;31:2989–96.
70. Lapos JA, Manica DP, Ewing AG. Dual fluorescence and electrochemical detection on an electrophoresis microchip. Anal Chem. 2002;74:3348–53.
71. Asthana A, Bose D, Durgbanshi A, Sanghi SK, Kok WT. Determination of aromatic amines in water samples by capillary electrophoresis with electrochemical and fluorescence detection. J Chromatogr A. 2000;895:197–203.

72. Foret F, Kirby DP, Vouros P, Karger BL. Electrospray interface for capillary electrophoresis-mass spectrometry with fiber-optic UV detection close to the electrospray tip. Electrophoresis. 1996;17:1829–32.
73. Khan S, Liu J, Szabo Z, Kunnummal B, Han X, Ouyang Y, et al. On-line capillary electrophoresis/laser-induced fluorescence/mass spectrometry analysis of glycans labeled with Teal™ fluorescent dye using an electrokinetic sheath liquid pump-based nanospray ion source. Rapid Commun Mass Spectrom. 2018;32:882–8.
74. Huhn C, Neusüß C, Pelzing M, Pyell U, Mannhardt J, Pütz M. Capillary electrophoresis-laser induced fluorescence-electrospray ionization-mass spectrometry: a case study. Electrophoresis. 2005;26:1389–97.
75. Szarka M, Szigeti M, Guttman A. Imaging laser-induced fluorescence detection at the Taylor cone of electrospray ionization mass spectrometry. Anal Chem. 2019;91:7738–43.
76. Francisco KJM, do Lago CL. A capillary electrophoresis system with dual capacitively coupled contactless conductivity detection and electrospray ionization tandem mass spectrometry. Electrophoresis. 2016;37:1718–24.
77. Beutner A, Cunha RR, Richter EM, Matysik F-M. Combining C4D and MS as a dual detection approach for capillary electrophoresis. Electrophoresis. 2016;37:931–5.
78. Beutner A, Scherer B, Matysik F-M. Dual detection for non-aqueous capillary electrophoresis combining contactless conductivity detection and mass spectrometry. Talanta. 2018;183:33–8.
79. Walters CC, Wang FC, Higgins MB, Madincea ME. Universal biomarker analysis using GC×GC with dual FID and ToF-MS (EI/FI) detection. Org Geochem. 2018;115:57–66.
80. Pillonel L, Ampuero S, Tabacchi R, Bosset JO. Analytical methods for the determination of the geographic origin of Emmental cheese: volatile compounds by GC/MS-FID and electronic nose. Eur Food Res Technol. 2003;216:179–83.

3 Experimental

This chapter gives an overview of the most important chemicals, materials, and instruments used for the measurements. Furthermore, some instrumental setups and general procedures are briefly described. The experiments, including all their details, are described in the individual chapter within the results section.

3.1 Chemicals

Ultrapure water was provided by a Milli Q Advantage A10 system from Merck (Darmstadt, Germany). The other chemicals were of analytical grade and are summarized in Table C.1.

Table C.1. List of the main chemicals

Chemicals	Abbreviation	Supplier
Acetic acid	HOAc	Sigma-Aldrich, St. Louis, USA
Acetonitrile	ACN	Merck, Darmstadt, Germany
Ammonium acetate	NH_4OAc	Merck, Darmstadt, Germany
Caffeine	Caf	ABCR, Karlsruhe, Germany
Decamethylferrocene	dMFc	ABCR, Karlsruhe, Germany
Ferrocenemethanol	FcMeOH	ABCR, Karlsruhe, Germany
(Ferrocenylmethyl)trimethylammonium iodide	[FcMTMA]I	Strem Chemicals, Newburyport, USA
Formic acid		Merck, Darmstadt, Germany
Methylene blue		Riedel-de Haën, Seelze, Germany
2-Propanol		Sigma Aldrich, St. Louis, USA
Sodium hydroxide, 0.1 M		Merck, Darmstadt, Germany
Trimetazidine	TMZ	Sigma Aldrich, St. Louis, USA

3.2 Consumables

The main consumables used for the experiments are listed in Table C.2.

Table C.2. List of the main consumables

Consumables	Supplier
CapTite Interconnect T C360 203-U-C-050	LabSmith, Livermore, USA
CapTite Interconnect Y C360-203Y-U-C-100	LabSmith, Livermore, USA
CapTite One-Piece Fitting C360-100	LabSmith, Livermore, USA
Fused silica capillary, ID 25, 50, 75 µm, outer diameter (OD) 360 µm, polyimide coating	Polymicro Technologies, Phoenix, USA
Fused silica capillary, ID 50 µm, OD 360 µm, Teflon coating	Polymicro Technologies, Phoenix, USA
Micro Tight Nuts F 125	IDEX Health & Science, Oak Harbor, USA
Micro Tight Sleeves F 184	IDEX Health & Science, Oak Harbor, USA
Micro Tight Sleeves F 185	IDEX Health & Science, Oak Harbor, USA
Union Assembly Micro Tight P 720	IDEX Health & Science, Oak Harbor, USA

3.3 Instruments

The commercially available instruments used for the experiments are listed in Table C.3.

Table C.3. List of the main instruments

Instruments	Supplier
Coaxial sheath liquid ESI interface	Agilent Technologies, Santa Clara, USA
DigiMicro Lab 5.0 microscope	dnt, Dietzenbach, Germany
Lambda 1010 UV/Vis detector	Bischoff, Leonberg, Germany
MicrOTOF mass spectrometer	Bruker Daltonics, Bremen, Germany
SP-200 potentiostat equipped with ultra-low current module	BioLogic, Seyssinet-Pariset, France
T1CP 300 304p high-voltage power supply	ISEG, Radeberg, Germany
UltraZoom Pro digital microscope	dnt, Dietzenbach, Germany

3.4 Software

The software used to operate the devices, data analysis, and presentation is listed in Table C.4.

Table C.4. List of the used software

Software	Supplier
Blender 3D Creation Suite	Blender Foundation, Amsterdam, Netherlands
DataAnalysis 4.0	Bruker Daltonics, Bremen, Germany
EC-Lab	BioLogic, Seyssinet-Pariset, France
Microsoft Office 365	Microsoft, Redmond, USA
MicrOTOF Control	Bruker Daltonics, Bremen, Germany
OriginPro 2020	OriginLab, Northampton,USA

3.5 Instrumentation and preparation procedures

3.5.1 Capillary preparation

Capillaries with IDs of 25, 50, and 75 µm were utilized for the experiments. All capillaries had an OD of 365 µm and were polyimide or Teflon coated. The capillaries were cut to the appropriate length with a ceramic cutter. A few millimeters of the polyimide respectively Teflon coating were removed at both ends of the capillaries utilizing a razor blade. The tips of the capillaries were polished at a 90° angle with a laboratory-constructed polishing machine (Fig. C.1) to get a planar surface. During the polishing step, the capillaries were permanently flushed with ultrapure water to prevent them from clogging. The capillaries were flushed by placing one capillary end in a vial with a septum and applying an excess pressure at the septum utilizing a syringe. For polishing, abrasive papers of 30 (first polishing step) and 3 µm grain size (second polishing step) were used. Before the first measurement, the capillaries were conditioned by flushing them for 10 minutes with 0.1 M sodium hydroxide solution, followed by 5 minutes with ultrapure water and at least 30 minutes with BGE. Since we performed non-aqueous CE, the capillaries were only conditioned before the first measurement. The capillaries were flushed for 5 minutes with pure ACN, followed by 5 minutes with ACN-saturated air for storage.

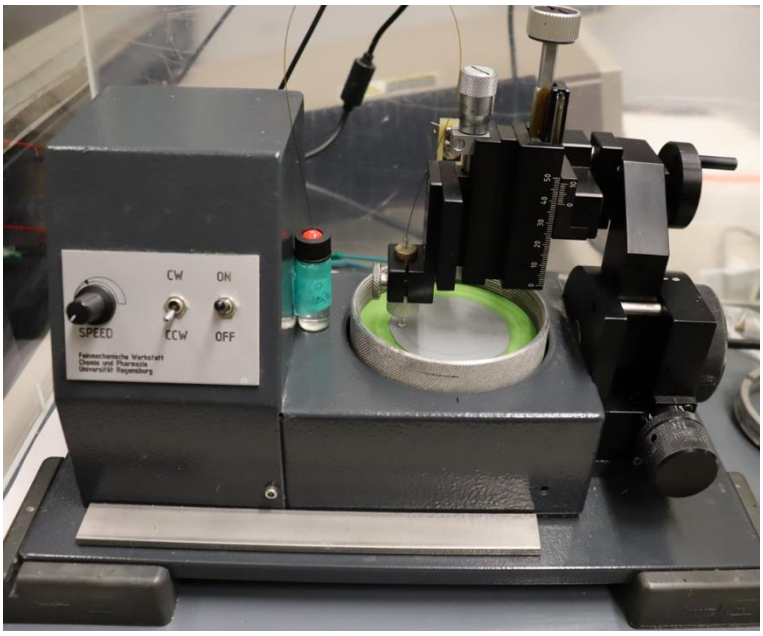

Figure C.1. Laboratory-constructed capillary polishing machine

3.5.2 Different types of flow splitters

FSs suitable for developing the novel DDC (CE-AD/MS) must fulfill certain requirements. They should have a very low dead volume to prevent peak broadening and the mixing of substance zones. Additionally, the material should be resistant to organic solvents since an ACN-based BGE was used for all experiments. Furthermore, the connection of the capillaries to the FS should be simple and robust.

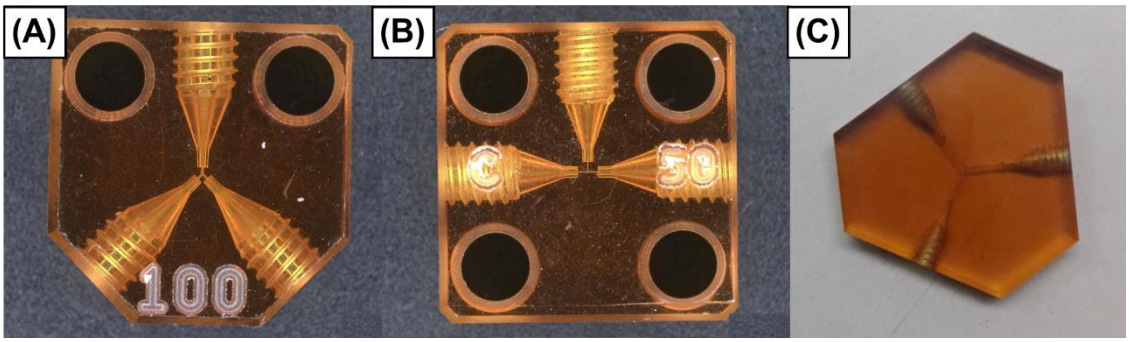

Figure C.2. Photographs of the commercially available FS: FSY (A), FST (B), and the laboratory-constructed FS (C)

Table C.5. Characteristics of the different FSs

Name	FSY	FST	laboratory-constructed FS
Shape	Y	T	Y
Dead volume [nL]	9 ±2	2.1 ±0.5	≈0
Thru-hole diameter [µm]	100	50	350
Material	PEI	PEI	PEI

Three promising FSs are shown in Fig. C.2. The details of the FSs are summarized in Table C.5. The first two FSs were commercially available. The FS CapTite Interconnect Y C360-203Y (Fig. C.2A) was called Y-shaped FS (FSY) and the FS CapTite Interconnect T C360-203U-C050 (Fig. C.2B) was called T-shaped FS (FST). Both commercially available FS had a very low dead volume in the nL rage and were made of Polyetherimide (PEI). Some preliminary experiments demonstrated that PEI was resistant to ACN for a specific time. Another advantage of this material was its transparency, allowing the view inside the FS and checking the FS for gas bubbles utilizing a microscope. The capillaries could be easily attached to the FSs by the CapTite One-Piece Fitting C360-100. For a firm connection, only 1 mm of the polyimide coating was removed at the connection side of the capillary, because otherwise the fitting could not hold the capillary in position.

The third FS (Fig. C.2C) was laboratory constructed with three drillings (thru-hole diameter 350 µm) at an 120° angle to each other. This laboratory-constructed FS allowed in principle the dead volume-free coupling of capillaries by connecting three capillaries with 120° tips. Figure C.3 shows a photograph of the capillary tips (Fig. C.3A) and a scheme of the FS with installed capillaries (Fig. C.3B). It turned out that this FS did not work in practice. Firstly, it was extremely time-consuming to fabricate the capillaries with the special tip geometry (120° tip, Fig. C.3A). Secondly, it was impossible to arrange the capillaries so that the openings of the capillaries met each other precisely in the middle. There was always a certain dead volume between the three capillary tips. Furthermore, the capillaries shifted when tightening the fittings. For these reasons, this approach was not pursued further. The project was implemented utilizing FSY and FST, which were discussed in detail in chapter 4.2.

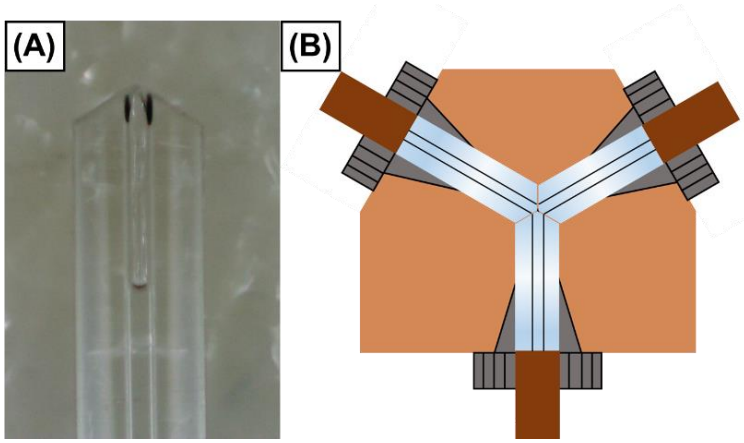

Figure C.3. Microscope image of a capillary with 120° tip (A) and a scheme of the laboratory-constructed FS with three installed capillaries with principally no dead volume (B)

3.5.3 Handling of the amperometric detector

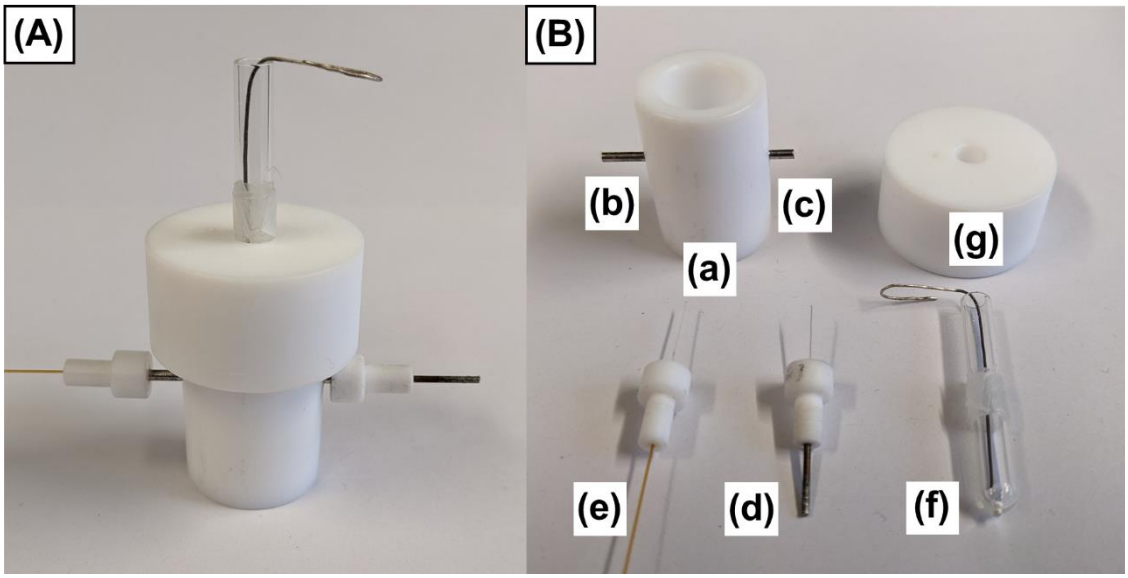

Figure C.4. Assembled AD (A) and disassembled AD (B). The AD consists of a cell body (a) with two integrated stainless steel tubes (b and c), a working electrode with adapter (d), a capillary with adapter (e), and a reference electrode (f) which is placed in a cap (g)

Figure C.4 shows an end-column AD (assembled AD, Fig. C.4A and disassembled AD, Fig. C.4B) which was developed by Matysik [1]. The AD was made of Teflon. Therefore, it could be used in combination with the ACN-based BGE. The AD had a compact design. The cell body of the AD (Fig. C.4B, a) had an OD of 2.0 cm, an ID of 1.2 cm, a height of 2.5 cm, and could hold 2.5 mL of BGE. Two stainless steel tubes (Fig. C.4B, b, and c) with an ID of 360 µm were placed in the body of the AD at exactly opposite sides. The tube on the left side (Fig. C.4B, b) served as a counter electrode for the AD, as grounding for the electrophoretic circuit of the CE, and as a guiding system for the capillary. The tube on the right side served as a guiding system for the working electrode (Fig. C.4B, c). The working electrode (Fig. C.4B, d) consisted of a 25 µm platinum wire sealed in a glass tube with an ID of 100 µm and an OD of 350 µm. One tip of the electrode was polished and served as an electrode surface. The other side of the electrode was glued into a copper tube (ID 360 µm). For electrical contact, the end of the platinum wire was soldered to the copper tube. The working electrode (Fig. C.4B, d) and the capillary (Fig. C.4B, e) were shrunken into Teflon adapters, which fit into the stainless steel tubes. The reference electrode (Fig. C.4B, f) was equipped with an Ag/AgCl wire and placed in the AD cap (Fig. C.4B, g). The cap had a small drilling for pressure exchange. The stainless steel tubes were symmetrically arranged. Therefore, the

positioning of the capillary and the working electrode was user-friendly since only the distance between the working electrode and the capillary must be aligned. The distance between the capillary and the working electrode was adjusted so that the distance corresponds to the ID of the capillary. The alignment of the capillary and the working electrode was done with the help of a microscope. Some images for the capillary-to-electrode alignment are given in Fig. C.5. After the measurement, the capillary and the working electrode could remain in their positions. Therefore, the distance between the capillary and the working electrode was adjusted before the first measurement and remained constant for all subsequent measurements. The reference electrode and the cell body of the AD were filled with BGE prior to the measurements. After finishing the measurements, the reference electrode and the cell body were flushed with pure ACN.

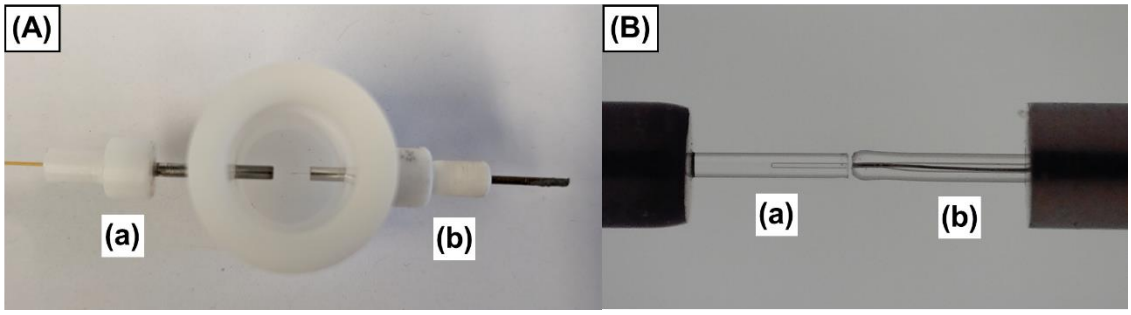

Figure C.5. Top view (A) and microscope image (B) of the capillary (a)-to-electrode (b) alignment in the AD

3.5.4 Setups

This section deals with the final setup for the DDC (CE-AD/MS). All other setups can be found in the corresponding chapters.

CE hyphenated to amperometric detection and mass spectrometry

The final DDC is depicted in Fig. C.6. It consisted of a laboratory-constructed CE device (Fig. C.6A, a), a TOF-MS equipped with a coaxial sheath liquid ESI interface (Fig. C.6A, b), and a laboratory-constructed AD (Fig. C.6B, c). The CE device was developed during the doctorate and is described in detail in the appendix. Figure C.6B shows the Y-shaped FS (Fig. C.6B, d) which was utilized for the splitting of the CE flow. The AD was placed inside a laboratory-constructed Faraday cage (Fig C.6A, e) to reduce electromagnetic interference effects. The AD was

connected to a potentiostat (Fig. C.6A, f) which was equipped with an ultra-low current module. The potentiostat worked in the floating mode. There was a permanent height difference of 6 cm between the liquid level of the vial and the tip of the coaxial sheath liquid ESI interface of the MS. The AD was variable in height due to a stand integrated into the Faraday cage. The height adjustment between the detectors was essential for synchronizing the migration times. The injection was performed hydrodynamically by the height difference between the sample vial and the detectors and was supported by the suction pressure of the ESI interface. Further experimental details are given in chapter 4.3.

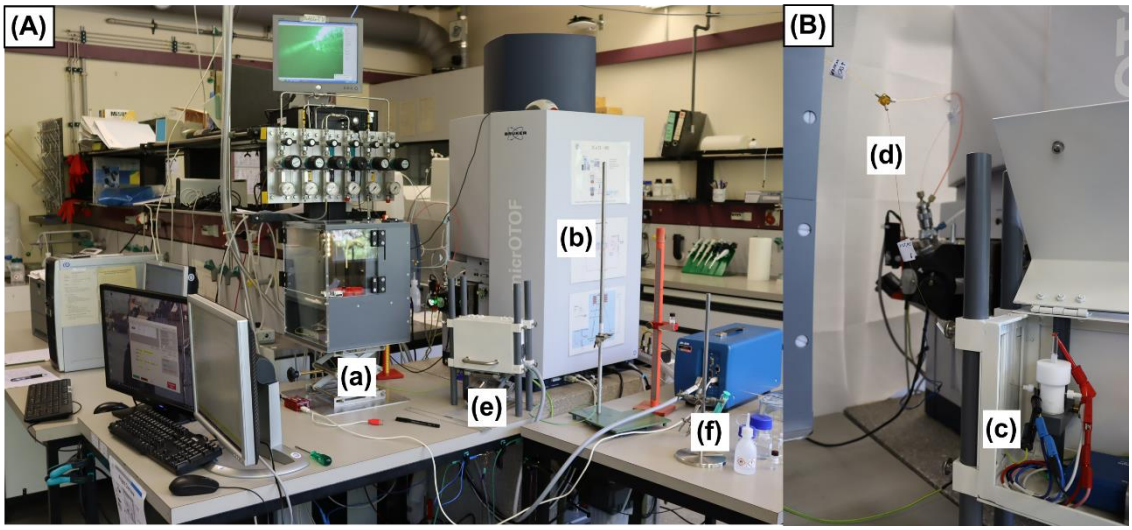

Figure C.6. Photograph (A) and close-up view (B) of the DDC (CE-AD/MS). The setup consists of a laboratory-constructed CE device (a), MS (b), AD (c), FS (d), Faraday cage (e), and potentiostat (f)

References

1. Matysik F-M. Application of non-aqueous capillary electrophoresis with electrochemical detection to the determination of nicotine in tobacco. J Chromatogr A. 1999;853:27–34.

4 Results and discussion

4.1 Characterization of linearly coupled capillaries with various inner diameters in the context of capillary electrophoresis

Böhm D, Matysik F-M. Characterization of linearly coupled capillaries with various inner diameters in the context of capillary electrophoresis. Monatsh Chem. 2021;152:1053–60.

This chapter was published in the journal Monatshefte für Chemie - Chemical Monthly. The layout specifications of the journal were changed for uniformity.

Abstract

As a result of continuous instrumental progress, capillary electrophoresis (CE) has become an established separation technique. However, the choice of the suitable capillary inner diameter (ID) is sometimes difficult due to different instrumental requirements concerning injection, separation, or detection. To overcome this problem, we assembled two capillaries with different IDs, meaning that the ID of the capillary at the injection side was different from that at the detection side. Since this was a rather uncommon approach, we focused on the associated effects in this proof-of-concept study. For the experiments, a non-aqueous model system was used, consisting of an acetonitrile-based background electrolyte and the two ferrocene derivates, ferrocenemethanol and decamethylferrocene. Utilizing capillary flow injection analysis hyphenated to capacitively coupled contactless conductivity detection, it could be shown that fragmented capillaries of the same ID had slightly lower volume flow rates than non-fragmented capillaries. With non-aqueous CE hyphenated to UV detection, it was found that the coupling of capillaries with different IDs had a much stronger effect on the CE flow than combinations with the same ID. Additionally, if the ID of the second capillary was larger than the ID of the first capillary, a higher theoretical plate number and an increased sensitivity were found. Furthermore, it was found that there was no significant peak tailing introduced by the coupling.

Graphical abstract:

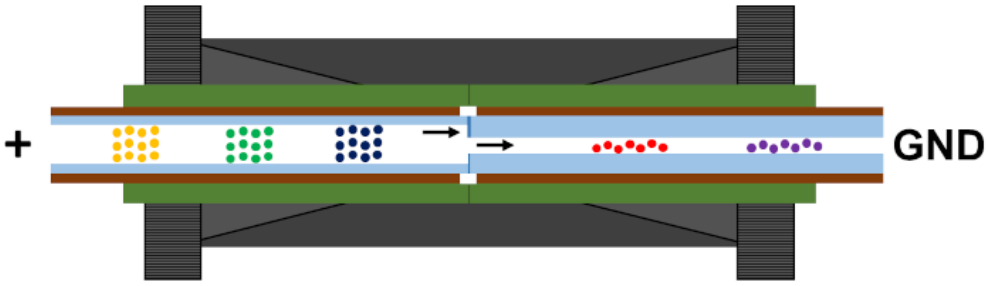

4.1.1 Introduction

Capillary electrophoresis (CE) is a powerful separation technique due to its high separation efficiency, its low sample consumption, and its high separation speed. Thus, the field of CE is still in instrumental progress [1-3]. In recent years, different injection methods were developed and CE was hyphenated to various detectors [4, 5]. However, choosing the suitable capillary inner diameter (ID) is sometimes difficult. Capillaries with small IDs are for example interesting for small amounts of sample and high separation efficiency due to lower Joule heating [4, 6, 7]. In contrast, capillaries with larger IDs are preferred for example for on-column UV/Vis photometric detection (UV) to generate a better sensitivity due to extended optical path lengths [4, 8]. These are just a few examples which show that different applications require various capillary IDs. When injection, separation, or detection aspects suggest the use of different capillary IDs, often a compromise has to be found. We tried to overcome this problem by the combination of two capillaries with various IDs.

The coupling of capillaries is already described in literature but predominately in the context of 2D separations. In these cases, the capillaries were coupled with valves or micro-structured chips [9-13]. These approaches were not suitable for our application because we intended to have a continuous CE separation without decoupling from the high-voltage field and a straightforward combination of conventional capillaries. There are other cases where capillaries with different IDs were coupled to achieve fast electrophoretic separations [14-16]. However, in these studies, injection and detection were performed in capillary segments of identical ID. Horká et al. [17] used capillaries with different IDs produced by etching for online sample pre-concentration. In most of the previously mentioned cases, the capillaries were irreversibly connected. In our approach, a commercially available capillary connector was used, which allowed for exchanging of capillaries and nearly dead volume-free coupling. Additionally, injection and detection were performed on opposite ends of the linearly coupled capillaries.

In the frame of this contribution, we investigated the linear coupling of capillaries with various IDs, meaning that the ID of the capillary at the injection side was different from that at the detection side. The resulting effects were investigated with capillary flow injection analysis hyphenated to capacitively coupled contactless conductivity detection (CFIA-C^4D) and CE hyphenated to UV (CE-UV).

4.1.2 Experimental

The following chemicals were used, all of analytical grade: ferrocenemethanol (FcMeOH) and decamethylferrocene (dMFc, purity 99%, ABCR, Karlsruhe, Germany), acetonitrile (ACN), ammonium acetate (NH_4OAc), 0.1 mM sodium hydroxide solution, ultrapure water provided by a Milli Q Advantage A10 system (Merck, Darmstadt Germany), acetic acid (HOAc, Roth, Karlsruhe, Germany), methylene blue (Riedel-de Haën, Seelze, Germany).

Capillaries

For both experiments (CFIA-C^4D and CE-UV), capillaries with IDs of 25, 50, and 75 µm, an outer diameter of 360 µm, and a total length of 70 cm were used. They were purchased from Polymicro Technologies (Phoenix, USA). Measurements were carried out with fragmented and non-fragmented capillaries. For the measurements with the fragmented capillaries, the original capillaries were cut into two pieces (20 and 50 cm), yielding a total of 9 possible capillary combinations with a total length of 70 cm (20 cm first capillary piece and 50 cm second capillary piece). These combinations are summarized in Table D.1. At both ends of the capillaries, about 2 mm of the polyimide coating was removed to avoid a dead volume introduced by polyimide swelling. To enable a nearly dead volume-free coupling, both sides of the capillary pieces were polished to receive planar capillary tips. For the linear assembling of the capillaries, both capillary pieces were placed in Micro Tight Sleeves F 185 and linearly assembled in a capillary connector called Union Assembly Micro Tight P 720 both from IDEX Health & Science (Oak Harbor, USA). The installation of the capillaries was carried out according to the user manual of the capillary connector. A detailed scheme of the two capillaries assembled in the capillary connector is shown in Fig. D.1. Before the first CE measurements, the capillaries were preconditioned by flushing them for 10 min with 0.1 M sodium hydroxide solution, afterwards for 5 min with ultrapure water, and in the end for 30 min with BGE (10 mM NH_4OAc, 1 M HOAc in ACN).

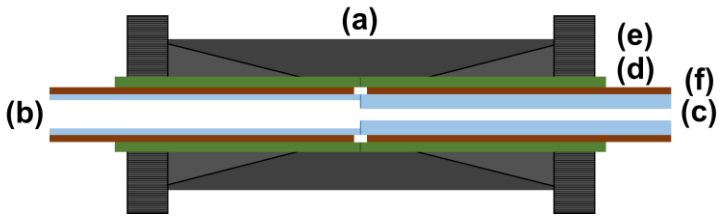

Figure D.1. Scheme of the cross-sectional view of the capillary connector (a). Two capillaries with different IDs (b and c) are coupled without dead volume. The capillaries were placed in sleeves (d) and fixed with screws (e). Additionally, about 2 mm of the polyimide (f) was removed at the connection side to avoid dead volume due to polyimide swelling

CFIA-C^{4}D setup

The volume flow rates (VFRs) for the fragmented and non-fragmented capillaries were determined with a CFIA-C^{4}D setup schematically depicted in Fig. D.2. The concept of CFIA with gravity-driven flow was first described by Matysik et al. [18]. The flow in the capillary was gravity-driven by a permanent height difference between the inlet and outlet carrier solution vials. We always used the term background electrolyte (BGE) instead of carrier solution because both solutions were identical. The injection time for all CFIA-C^{4}D experiments was 5 s. A laboratory-constructed autosampler of a CE device was used for the hydrodynamic injection. The sample solution consisted of 10 mM decamethylferrocene (dMFc) in BGE. For detection a high-resolution C^{4}D was placed after 40 cm from the injection side. The detector described elsewhere was constructed in the group of Prof. C. L. do Lago (São Paulo, Brazil) [19]. A double determination at two different heights was done for the calculation of the VFRs.

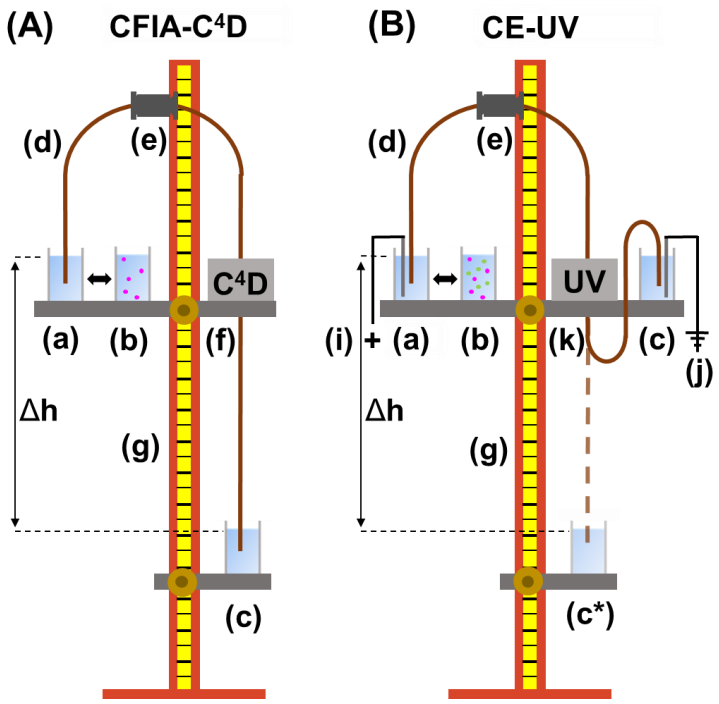

Figure D.2. Scheme of the CFIA-C^{4}D setup (A) and the CE-UV setup (B). Components of the CFIA-C^{4}D setup: inlet (a), sample (b) and outlet BGE vial (c), fused silica capillary (d), linear capillary connector (e), C^{4}D (f) and stand (g). The capillary flow was gravity-driven by a permanent height difference Δh between the inlet and outlet reservoir. Components of the CE-UV setup: High-voltage supply (i), grounding (j), and UV (k). The rest of the components were identical to the CFIA-C^{4}D setup. The outlet buffer vial was lowered for the hydrodynamic injection in the CE-UV setup (c*). During the electrophoretic separation, the liquid levels in the inlet and outlet buffer vials were at the same level, to avoid gravity-driven flow

CE-UV setup

Figure D.2 shows a scheme of the CE-UV setup on the right side. It consisted of a laboratory-constructed CE device with an integrated autosampler. This device was connected to a T1CP 300 304p high-voltage power supply from ISEG (Radeberg, Germany). The whole CE system was placed in an acrylic glass housing for safety reasons. The separations were carried out with non-fragmented 25, 50, and 75 µm capillaries and with capillary combinations implementing a 50 µm downstream capillary segment (25 + 50, 50 + 50, and 75 + 50 µm). To find an explanation for the migration behavior also, experiments with the reverse capillary combinations were performed. In these measurements, the upstream capillary piece had an ID of 50 µm and a length of 50 cm and the downstream capillaries had IDs of 25, 50, and 75 µm and a length of 20 cm. A Lambda 1010 UV/Vis detector from Bischoff (Leonberg, Germany) was used for detection at 210 nm. The detector was placed after 40 cm. A sample solution

containing 1 mM ferrocenemethanol (FcMeOH) and dMFc in BGE was utilized. The injection was performed hydrodynamically by lowering the outlet buffer vial by 20 cm. A uniform sample plug was injected to compare band-broadening effects. The injection segment had a length of 0.35 cm (0.5% of the total capillary length) and the respective injection times were determined based on the VFR of the corresponding capillary combination. For the electrophoretic separation, a separation voltage of 25 kV was applied and the inlet and the outlet BGE vials were placed at the same height so that there was no gravity-driven flow which affected the migration behavior. Each measurement was done three times.

Transparent capillary connector

To support the results from the CE-UV measurements, the behavior of a dye segment at the connection site between two capillaries with different IDs was examined utilizing a transparent capillary connector. The laboratory-constructed capillary connector was made of polyetherimide and had a 350 µm drilling. The capillary connector was additionally flattened and polished at one side for better microscope images. The laboratory-constructed capillary connector is illustrated in Fig. D.3 in comparison to the commercially available capillary connector. For the experiment, a 20 cm piece of a 25 µm and a 50 cm piece of a 75 µm capillary were used. At the connection side of each capillary, 2 cm of polyimide was removed to enable visualization of the dye plug at the connection site. Both capillary segments were coupled without dead volume by means of the transparent capillary connector. The capillaries were attached with Micro Tight Nuts F 125 and with Micro Tight Sleeves F 184 from IDEX Health & Science (Oak Harbor, USA). For the images, the connector was placed on the table of a DigiMicro Lab 5.0 microscope from dnt (Dietzenbach, Germany). A saturated methylene blue solution in BGE was used as a sample solution and BGE was used as a carrier solution. The injection was performed hydrodynamically by lowering the outlet vial and capillary flow was also generated hydrodynamically. The length of the dye segment was adjusted to about 1 cm, corresponding to the image section of the microscope.

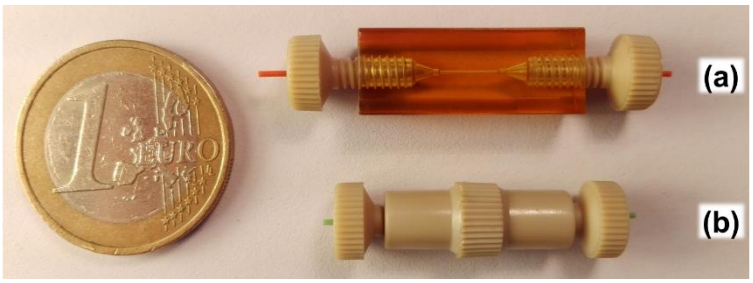

Figure D.3. Photograph of the transparent, laboratory-constructed capillary connector fabricated from polyetherimide (a) and the commercially available capillary connector fabricated from polyether ether ketone (b)

4.1.3 Results and discussion

CFIA-C^{4}D experiments

The measurements were performed with a model system containing dMFc as analyte and a non-aqueous, ACN-based BGE as carrier solution. This model system was chosen due to the good UV transparency and the stable electroosmotic flow. Additionally, in future projects, it is planned to utilize the concept of coupled capillaries in combination with an amperometric detector, where the ACN-based BGE is favorable due to the electrochemical characteristics [4, 20].

The CFIA-C^{4}D experiments in this project were performed to study the effects associated with capillary coupling under conditions of a gravity-driven flow system. The VFRs and the corresponding standard deviations (SDs) shown in Table D.1 for a height difference of 20 cm were calculated based on four CFIA-C^{4}D measurements. It should be noted that different linear flow velocities were present in different segments of the fragmented capillaries with various IDs. Therefore, we used the VFRs which were the same over the entire length of the capillary. It was found that the VFRs were slightly lower for fragmented capillaries compared to non-fragmented capillaries of the same dimension. This indicates that a small additional flow resistance arises when two capillaries are combined. Furthermore, it was found that the VFR decreases for upstream capillaries with lower IDs and vice versa. The VFR for the combination 75 + 25 µm could not be determined. We assume this was due to the formation of air bubbles at the connection site, indicated by an enormous increase in the electrical resistance. The VFRs were used for the calculations of the injection times for an 0.35 cm long injection segment in the CE-UV experiments.

Table D.1. CFIA-C^4D studies for the determination of the VFRs and the corresponding SDs (n = 4) of non-fragmented and fragmented capillaries for a height difference between inlet and outlet vial of 20 cm. Experimental conditions: sample solution 10 mM dMFc in BGE, capillary length 70 cm (40 cm to the detector, fragmented capillaries: 20 cm first part and 50 cm second part), injection time 5 s and BGE (10 mM NH_4OAc and 1 M HOAc in ACN) as carrier solution

capillary combination [µm]	VFR [10^{-9} dm^3/s]
25	0.0577 ±0.0005
25+25	0.057 ±0.001
50+25	0.0775 ±0.0007
75+25	- [a]
25+50	0.137 ±0.005
50	0.865 ±0.002
50+50	0.80 ±0.05
75+50	1.05 ±0.06
25+75	0.187 ±0.002
50+75	1.941 ±0.003
75	4.56 ±0.02
75+75	4.2 ±0.1

[a] For the capillary combination 75+25 µm, no VFR could be determined due to bubble formation

CE-UV experiments

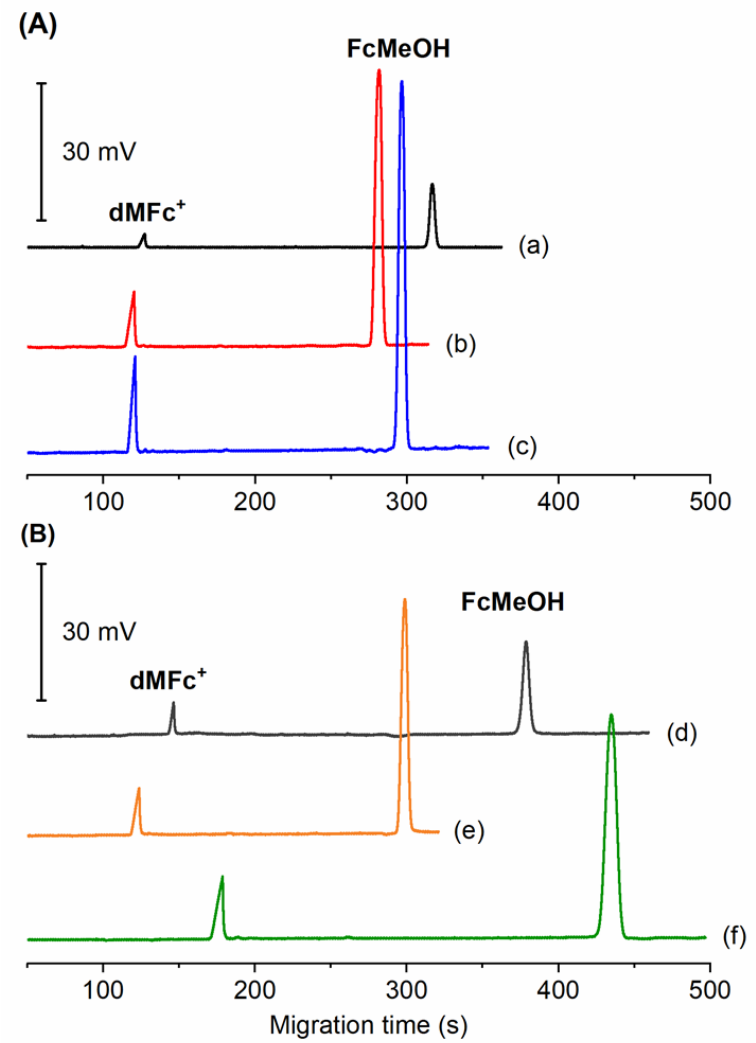

Figure D.4. Electropherograms of the model mixture FcMeOH/dMFc measured with non-fragmented (A) and fragmented capillaries (B) of different IDs: 25 (a), 50 (b), 75 (c), 25+50 (d), 50+50 (e), and 75+50 µm (f). Experimental parameters: 1 mM FcMeOH and dMFc in BGE (10 mM NH_4OAc and 1 mM HOAc in ACN). Injection segment 0.35 cm, separation voltage 25 kV, capillary length 70 cm (40 cm to the detector, fragmented capillaries: 20 cm first part and 50 cm second part), UV detection at 210 nm. The BGE levels in the inlet and outlet vial were at the same height

Figure D.4 shows the electropherograms of the non-fragmented capillaries with IDs of 25, 50, and 75 µm in the upper part and the electropherograms of the capillary combinations with a downstream 50 µm capillary segment (25 + 50, 50 + 50, and 75 + 50 µm) in the lower part. Prior to the detailed discussion, it has to be mentioned that the neutral FcMeOH served as electroosmotic flow (EOF) marker while dMFc served as cationic model analyte since it is easily oxidized by dissolved oxygen in solution [21]. The BGE levels in the inlet and outlet reservoirs were at the same height. Therefore, there

was no gravity-driven flow. The measurements performed with non-fragmented capillaries had nearly the same migration times for the cationic ($dMFc^+$) and the neutral species (FcMeOH), independent of the ID. The averaged migration times and the corresponding SDs for the non-fragmented and fragmented capillaries are listed in Table D.2. Since the electrophoretic and the EOF migration contribute to the overall migration time of the $dMFc^+$, we calculated the apparent mobility of $dMFc^+$ (μ_a), the EOF mobility of FcMeOH (μ_{EOF}), and the effective mobility of $dMFc^+$ (μ_{eff}) to separate these effects. Due to the very similar migration times for the non-fragmented capillaries (25, 50, and 75 µm), the mobilities were nearly the same. The relative standard deviations for the mobilities of the non-fragmented capillaries with different IDs were 3% for μ_a, 6% for μ_{EOF} and 2% for μ_{eff} (n = 9). The calculated mobilities (μ_a, μ_{EOF}, and μ_{eff}) and the corresponding SDs for the different capillary combinations are summarized in Table D.3.

Table D.2. CE-UV studies for the determination of the migration times for $dMFc^+$ and FcMeOH, the measured electrophoretic currents, and the corresponding SDs (n = 3) of non-fragmented and fragmented capillaries. Experimental conditions: 1 mM FcMeOH and dMFc in BGE (10 mM NH_4OAc and 1 mM HOAc in ACN), injection segment 0.35 cm, separation voltage 25 kV, capillary length 70 cm (40 cm to the detector, fragmented capillaries: 20 cm first part and 50 cm second part), UV detection at 210 nm

capillary combination [µm]	migration time $dMFc^+$ [s]	migration time FcMeOH [s]	electrophoretic current [µA]
25	128 ±1	319 ±2	1.42 ±0.01
50	120.1 ±0.9	281 ±3	3.98 ±0.09
75	120.7 ±0.2	295 ±1	9.7 ±0.1
25+50	146.3 ±0.3	379 ±1	2.92 ±0.08
50+50	124 ±2	300 ±3	4.02 ±0.01
75+50	180 ±1	439 ±4	4.84 ±0.08

Table D.3. Calculated mobilities μ_a for $dMFc^+$, μ_{EOF} for FcMeOH, μ_{eff} for $dMeFc^+$, and the corresponding SDs (n = 3) of non-fragmented and fragmented capillaries based on the CE-UV experiments

capillary combination [µm]	μ_a $dMFc^+$ [$cm^2 \cdot kV^{-1} \cdot s^{-1}$][a]	μ_{EOF} FcMeOH [$cm^2 \cdot kV^{-1} \cdot s^{-1}$][b]	μ_{eff} $dMFc^+$ [$cm^2 \cdot kV^{-1} \cdot s^{-1}$][c]
25	0.873 ±0.008	0.351 ±0.002	0.522 ±0.006
50	0.933 ±0.007	0.398 ±0.005	0.535 ±0.002
75	0.928 ±0.001	0.380 ±0.002	0.5484 ±0.0006
25+50	0.765 ±0.002	0.295 ±0.001	0.4701 ±0.0008
50+50	0.90 ±0.01	0.374 ±0.004	0.527 ±0.007
75+50	0.623 ±0.004	0.255 ±0.003	0.368 ±0.001

[a] μ_a was calculated according to the equation $\mu_a = (l \cdot L)/(t_a \cdot V)$, where l was the effective capillary length to the detector, L was the total capillary length, t_a the migration time of the analyte ion, and V the applied voltage [22]

[b] μ_{EOF} was calculated according to the equation $\mu_{EOF} = (l \cdot L)/(t_{EOF} \cdot V)$, where t_{EOF} was the migration time of the EOF marker [22]

[c] μ_{eff} was calculated according to the equation $\mu_{eff} = \mu_a - \mu_{EOF}$ [22]

The electropherograms for the capillary combinations with a downstream 50 µm capillary segment (25 + 50, 50 + 50, and 75 + 50 µm) are presented in the lower part of Fig. D.4. For the combination 50 + 50 µm, the migration times were 4% higher for the cationic ($dMFc^+$) and 7% higher for the neutral species (FcMeOH) compared to the non-fragmented 50 µm capillary. Looking at the mobilities, it was found that μ_{EOF} was 8% and μ_{eff} was 1% lower for the fragmented capillary (50 + 50 µm). Therefore, the coupling of two identical capillaries predominately affected the EOF. The reduction of the EOF was probably due to a flow resistance at the connection site, which was also found for the CFIA-C^4D experiments.

In contrast to the combination of capillaries with the same ID, a considerable shift of the migration times and the corresponding mobilities was found for the fragmented capillaries with different IDs (25 + 50 and 75 + 50 µm). Since μ_{EOF} and μ_{eff} were significantly lower for fragmented capillaries with different IDs, it can be concluded that the coupling influenced the EOF and the migration of the cationic species. It is important to note that in the present case, μ_{eff} does not represent the conventional electrophoretic mobility but includes a contribution which can be attributed to influences of the flow due to the coupling. In our opinion, the lower mobilities were related to the disturbance of the CE flow at the connection site. The CE flow was slightly affected by the coupling of capillaries with the same ID (50 + 50 µm) which resulted in no significant changes in the

mobilities, especially for μ_{eff}. However, the CE flow was strongly influenced by the coupling of capillaries with different IDs which resulted in a significant change in the mobilities.

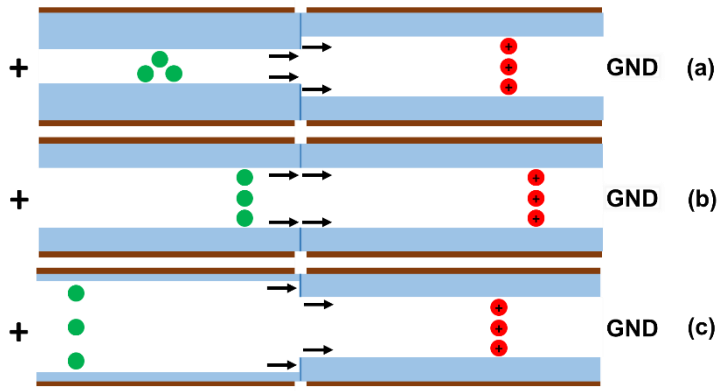

Figure D.5 Scheme of the capillary combinations with a downstream 50 µm capillary at the connection site: 25+50 (a), 50+50 (b), and 75+50 µm (c). Especially for the capillary combination 75+50 µm, the CE flow was hindered by the downstream smaller capillary

Figure D.5 illustrates the connection region of the capillary combinations (25 + 50, 50 + 50, and 75 + 50 µm). Comparing the capillary combinations 25 + 50 µm and 50 + 50 µm, it was found that the former yielded μ_a, μ_{EOF}, and μ_{eff} that were 15, 21, and 11% lower, respectively. However, for the capillary combination 75 + 50 µm, μ_a, μ_{EOF}, and μ_{eff} were 31, 32, and 30% lower compared to the capillary combination 50 + 50 µm. Figure D.5 shows the hindrance of the CE flow for the combination 75 + 50 µm by the narrower downstream capillary. This explains why the species for the combination 75 + 50 µm showed lower mobilities in comparison to the capillary combination 25 + 50 µm.

To prove this hypothesis, CE-UV experiments with the inverted capillaries (upstream 50 µm capillary and downstream 25, 50, or 75 µm capillary) were carried out. According to the hypothesis, the capillary combination 50 + 25 µm should have the lowest mobilities, because in this configuration, the CE flow hits the front surface of the 25 µm capillary. The CE-UV experiments with the reverse capillary combinations confirmed this assumption because the lowest mobilities were found for the capillary combination 50 + 25 µm (electropherograms not shown). Based on these experiments, it can be concluded that the coupling influenced the CE flow due to a mechanical hindrance at the connection site. Especially for capillary combinations starting from a larger capillary ID and going to a smaller ID, a decrease of the mobilities was found.

Another striking point was that the peak areas for the combination 25 + 50 µm were about 2 times higher than the peak areas for the non-fragmented 25 µm capillary, although the same injection volume was applied in both cases (electropherograms shown in Fig. D.4). This can be explained by Lambert–Beer law because with a downstream 50 µm capillary the layer thickness is two times higher than with a 25 µm capillary. Additionally, the lower linear flow velocity in the downstream 50 µm capillary compared to the upstream 25 µm capillary contributed to the increased peak areas. Due to the slower linear flow velocity, the analytes spent more time in the detection window, which led to higher peak areas.
Furthermore, it was demonstrated that all peaks showed nearly Gaussian shape and for all combinations there was only negligible peak tailing. Additionally, there was an increase of the theoretical plate number found for the capillary combinations starting from a smaller ID and going to a larger ID. The theoretical plate numbers for the $dMFc^+$ and FcMeOH peak were $27 \times 10^3 \pm 3 \times 10^3$ and $28 \times 10^3 \pm 5 \times 10^3$ for the capillary combination 25 + 50 µm while the theoretical plate numbers for the non-fragmented 50 µm capillary were $81 \times 10^2 \pm 3 \times 10^2$ for $dMFc^+$ and $206 \times 10^2 \pm 9 \times 10^2$ for FcMeOH. This resulted from a compression of the peaks at the transition between a capillary starting with a smaller ID and going to a capillary with a larger ID. This effect could be explained by the different linear flow velocities in the capillary combination 25 + 50 µm. The linear flow rate in the upstream 25 µm capillary was higher than the linear flow velocity in the downstream 50 µm capillary, which led to the compression of the peaks at the connection site.

Figure D.6. Subsequently recorded microscopic images (A-E) showing the behavior of a dye plug at the connection site between a 25 (left side) and a 75 µm (right side) capillary. The photos show the compression of the dye plug at the transition between a capillary with a smaller and a capillary with a larger ID. Experimental parameters: dye solution (methylene blue in BGE), the flow was gravity-driven by BGE (10 mM NH_4OAc and 1 mM HOAc in ACN)

We tried to visualize this by the behavior of a dye plug at the connection site between a capillary with a smaller and a larger ID. For this purpose, a transparent capillary connector was fabricated. Figure D.6 shows a series of microscopic images of a dye plug at the connection site between a 25 and 75 µm capillary. Figure D.6C shows the long dye segment in the 25 µm capillary, which shortens at the transition to the 75 µm capillary. The microscopic image D.6E shows the compressed dye plug in the 75 µm capillary piece. Even if this experiment was performed by a simple CFIA setup, it could explain the increase of the theoretical plate number by the compression of the peaks at the connection site.

4.1.4 Conclusion

To overcome the problem of choosing the best-suited capillary ID for injection, separation, or detection in CE, the concept of fragmented capillaries with various IDs was introduced and a proof-of-concept study was carried out. With this approach, it is possible to select the ideal capillary ID combination for the respective application.
With the findings listed in this manuscript, the questions pointed out in the introduction could be clarified. It could be shown that CE measurements with linearly coupled

capillaries of various IDs could be realized. Additionally, an increased sensitivity was found for on-column UV detection for the capillary combination 25 + 50 µm, due to the extended optical path length. The same capillary combination (25 + 50 µm) showed also a higher theoretical plate number than a non-fragmented 50 µm capillary. Contrary to expectations, no significant changes in the peak shape or peak tailing were found for capillary combinations with the same or different IDs. From the CFIA and the CE measurements, it could be concluded that there was a mechanical disturbance of the flow due to the coupling. Unlike the capillary combination with the same ID, a shift towards lower mobilities was found for capillary combinations starting from a larger ID and going to a smaller ID which was a drawback of fragmented capillaries.

Based on the results described in this manuscript, it can be concluded that the concept of linearly coupled capillaries with various IDs could be established. Therefore, it is possible to combine two capillaries with different IDs to adapt capillary dimensions to the respective injection, separation, or detection requirements.

References

1. Ramos-Payán M, Ocaña-Gonzalez JA, Fernández-Torres RM, Llobera A, Bello-López MÁ. Recent trends in capillary electrophoresis for complex samples analysis: A review. Electrophoresis. 2018;39:111–25.
2. Voeten RLC, Ventouri IK, Haselberg R, Somsen GW. Capillary electrophoresis: trends and recent advances. Anal Chem. 2018;90:1464–81.
3. Beutner A, Scherer B, Matysik F-M. Dual detection for non-aqueous capillary electrophoresis combining contactless conductivity detection and mass spectrometry. Talanta. 2018;183:33–8.
4. Blasco S, Kortz L, Matysik F-M. Comparison of detection performance of UV and electrochemical detection in NACE for a range of different capillary inner diameters. Electrophoresis. 2009;30:3355–60.
5. Beutner A, Herl T, Matysik F-M. Selectivity enhancement in capillary electrophoresis by means of two-dimensional separation or dual detection concepts. Anal Chim Acta. 2019;1057:18–35.
6. Lapainis T, Sweedler JV. Contributions of capillary electrophoresis to neuroscience. J Chromatogr A. 2008;1184:144–58.
7. Grundmann M, Matysik F-M. Analyzing small samples with high efficiency: capillary batch injection-capillary electrophoresis-mass spectrometry. Anal Bioanal Chem. 2012;404:1713–21.
8. Deyl Z, Mikšík I, Charvátová J, Eckhardt A. Comparison of the electrophoretic separation of proteins in capillaries with different inner diameter. J Chromatogr A. 2003;1013:233–8.
9. Jooß K, Hühner J, Kiessig S, Moritz B, Neusüß C. Two-dimensional capillary zone electrophoresis-mass spectrometry for the characterization of intact monoclonal antibody charge variants, including deamidation products. Anal Bioanal Chem. 2017;409:6057–67.
10. Kler PA, Posch TN, Pattky M, Tiggelaar RM, Huhn C. Column coupling isotachophoresis-capillary electrophoresis with mass spectrometric detection: characterization and optimization of microfluidic interfaces. J Chromatogr A. 2013;1297:204–12.
11. Sydes D, Kler PA, Hermans M, Huhn C. Zero-dead-volume interfaces for two-dimensional electrophoretic separations. Electrophoresis. 2016;37:3020–4.

12. Wei J, Gu X, Wang Y, Wu Y, Yan C. Two-dimensional separation system by on-line hyphenation of capillary isoelectric focusing with pressurized capillary electrochromatography for peptide and protein mapping. Electrophoresis. 2011;32:230–7.
13. Kohl FJ, Sánchez-Hernández L, Neusüß C. Capillary electrophoresis in two-dimensional separation systems: Techniques and applications. Electrophoresis. 2015;36:144–58.
14. Pavlíček V, Tůma P, Matějčková J, Samcová E. Very fast electrophoretic determination of creatinine and uric acid in human urine using a combination of two capillaries with different internal diameters. Electrophoresis. 2014;35:956–61.
15. Šebestová A, Petr J. Fast separation of enantiomers by capillary electrophoresis using a combination of two capillaries with different internal diameters. Electrophoresis. 2017;38:3124–9.
16. Tůma P, Opekar F, Samcová E. Very fast electrophoretic separation on commercial instruments using a combination of two capillaries with different internal diameters. Electrophoresis. 2013;34:552–6.
17. Horká M, Karásek P, Roth M, Šlais K. Fused silica capillaries with two segments of different internal diameters and inner surface roughnesses prepared by etching with supercritical water and used for volume coupling electrophoresis. Electrophoresis. 2017;38:1260–7.
18. Matysik F-M, Werner G. Trace metal determination in tears by anodic stripping voltammetry in a capillary flow injection system. Analyst. 1993;118:1523–6.
19. Francisco KJM, do Lago CL. A compact and high-resolution version of a capacitively coupled contactless conductivity detector. Electrophoresis. 2009;30:3458–64.
20. Matysik F-M. Non-aqueous capillary electrophoresis with electrochemical detection. J Chromatogr A. 1998;802:349–54.
21. Scholz R, Matysik F-M. A novel approach for the separation of neutral analytes by means of electrochemically assisted injection coupled to capillary electrophoresis-mass spectrometry. Analyst. 2011;136:1562–5.
22. Lauer HH, Rozing GP. High Performance Capillary Electrophoresis. 2nd ed. Germany: Agilent Technologies; 2018.

4.2 Dead volume–free flow splitting in capillary electrophoresis

This chapter was published in the journal ELECTROPHORESIS. The layout specifications of the journal were changed for uniformity.

Böhm D, Koall M, Matysik F-M. Dead volume-free flow splitting in capillary electrophoresis. Electrophoresis. 2022;43:1438–45.

Abstract

In recent years, several dual detection concepts (DDCs) for capillary electrophoresis (CE) were developed, which consisted of at least one non-destructive detector. For these DDCs, a linear detector arrangement could be used, which is not possible when both detectors are destructive. To overcome this problem, we developed a concept for the splitting of the CE stream utilizing commercially available flow splitters (FSs) that allow the parallel positioning of two destructive detectors. In this proof-of-concept study, T- and Y-shaped FSs were characterized regarding their suitability for DDCs. To keep it simple, an UV/Vis photometric detector (UV) and a capacitively coupled contactless conductivity detector (C^4D) were used for the characterization. The model system consisted of an acetonitrile-based background electrolyte and two model substances (ferrocenylmethyl)trimethylammonium iodide and caffeine. CE hyphenated to UV measurements revealed that the split ratio was about 50% for both FSs. CE hyphenated to C^4D was used to evaluate the peak shape in front of and behind the FSs. These measurements showed that there was no significant peak broadening introduced by the FSs. Additionally, there were no changes in the limits of detection in front of and behind the FSs. Furthermore, the flexibility of the new FS approach allowed the usage of capillaries with different inner diameters (25–75 µm) for injection and detection.

Front Cover

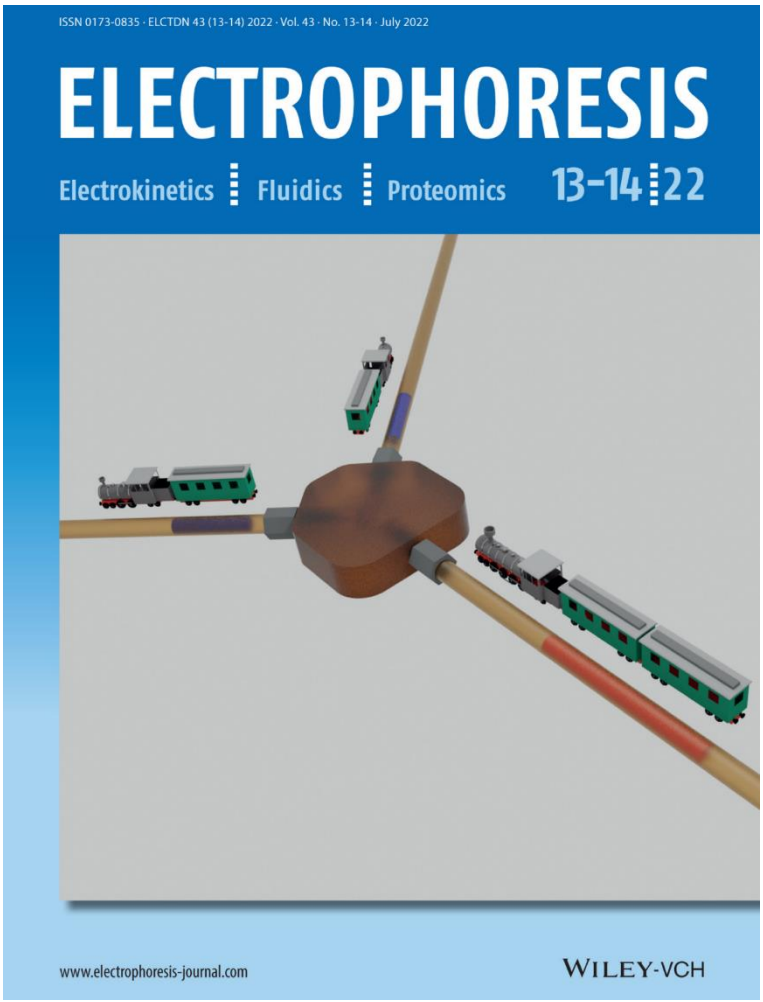

Abstract front cover

The cover picture shows a flow splitter which enables the splitting of the capillary electrophoresis (CE) stream in conventional fused silica capillaries into two parts. It was found that the analyte zones (red and blue plugs) were split symmetrically inside the flow splitter. Therefore, the individual zones had only half of the original length after the splitting. Additionally, the flow rates of the analyte zones were halved. The behavior of the analyte zones is illustrated by the trains. The splitting of the CE stream was investigated to develop new dual detection concepts for CE consisting of two destructive detectors.

4.2.1 Introduction

There is a need for powerful analytical methods as the number of samples, the sample complexity, and the amount of substances that need to be analyzed is steadily increasing [1]. In recent years, capillary electrophoresis (CE) was established as a potent separation technique due to its high separation efficiency, the simplicity of the instrumental setup, the small sample and reagent consumption, and its high separation speed [2-5]. An ongoing trend is also the coupling of a separation technique like CE with more than one detector. These dual detection concepts (DDCs) are especially interesting when both detectors provide complementary information [1, 6]. Several DDCs for CE are described in the literature [7-12]. Most DDCs consist of at least one non-destructive detector that allows a serial detector arrangement [6]. However, some analytical problems would require a combination of two destructive detectors. To our knowledge, such a DDC was not realized so far as a linear detector arrangement is not possible. One of these DDCs would be the combination of an amperometric detector (AD) and a mass spectrometer (MS). This is a very powerful DDC because the AD is one of the most sensitive detection methods for electroactive analytes and therefore ideal for the quantification of low concentrations, whereas MS is perfect for the identification of substances [7, 13, 14]. Another interesting DDC that was also not realized so far is the combination of electrospray ionization (ESI) MS and inductively coupled plasma MS. Karst and coworkers [15] already described the potential of CE hyphenated to both techniques but have not linked the methods with each other. The instrumental implementation of these DDCs is complicated as both detectors are destructive. To overcome these problems, we introduced a new concept for the development of DDCs consisting of two destructive detectors by splitting the CE stream utilizing commercially available flow splitters (FSs). With this approach, it would be possible to place the detectors in parallel to each other. For some applications, it is challenging to find the best suitable capillary inner diameter (ID), due to the different requirements of injection, separation, and detection [16]. For trace analysis capillaries with bigger IDs at the injection side are favorable to achieve higher sample loads. Additionally, for DDCs, the detectors could have different requirements concerning the capillary ID. Due to the flexibility of the FS approach, the IDs of the capillaries could be adjusted individually to the requirements of injection and of each detector. However, capillary combinations with different IDs could also be used for generating higher electrical field strengths [17]. The splitting of the CE flow is already described in the literature, but this was predominately in the context of 2D separations or for the concurrent analysis of cations and anions [18-20]. In the frame of this contribution, we

describe the splitting of the CE stream for the usage in DDCs. Special attention was paid to a low dead volume, easy handling, and the material of the FSs. During the project, we characterized two commercially available FSs (Y- and T-shaped) regarding their suitability for DDCs. Since in a future project, it is planned to develop a novel DDC consisting of an AD and a MS, an acetonitrile (ACN)-based background electrolyte (BGE) was used, which is favorable for both detectors (AD and MS) [21, 22]. To keep it simple, CE hyphenated to a UV/Vis photometric detection (CE-UV) and CE hyphenated to capacitively coupled contactless conductivity detection (CE-C^4D) were utilized for the characterization of the FSs.

4.2.2 Experimental

Chemicals, materials, and samples

The following chemicals of analytical grade were used: ACN, ammonium acetate, 0.1 M sodium hydroxide solution, and ultrapure water (Milli Q Advantage A10 system) were obtained from Merck (Darmstadt, Germany). Acetic acid was purchased from Carl Roth (Karlsruhe, Germany). (Ferrocenylmethyl)trimethylammonium iodide ([FcMTMA]I) was bought from Strem Chemicals (Newburyport, USA). Caffeine (Caf) was obtained from ABCR (Karlsruhe, Germany). Fused silica capillaries (25, 50, and 75 µm ID, 365 µm outer diameter (OD); polyimide- and Teflon-coated) were purchased from Polymicro Technologies (Phoenix, USA). The FSs CapTite Interconnect T C360 203U C050 (FST), CapTite Interconnect Y C360 203Y (FSY), and the corresponding fitting CapTite One-Piece Fitting C360-100 were purchased from LabSmith (Livermore, USA). All experiments (CE-UV and CE-C^4D) were performed with a non-aqueous BGE consisting of 10 mM ammonium acetate and 1 M acetic acid in ACN. The sample solution for the CE-UV experiments consisted of 0.5 mM ferrocenylmethyl)trimethylammonium ion ($[FcMTMA]^+$) and Caf in BGE. For the CE-C^4D experiments, the sample solutions consisted of 0.1 mM $[FcMTMA]^+$ in BGE. The data analysis was performed with OriginPro 2020 (Northampton, USA).

Properties of the FSs and capillary preparation

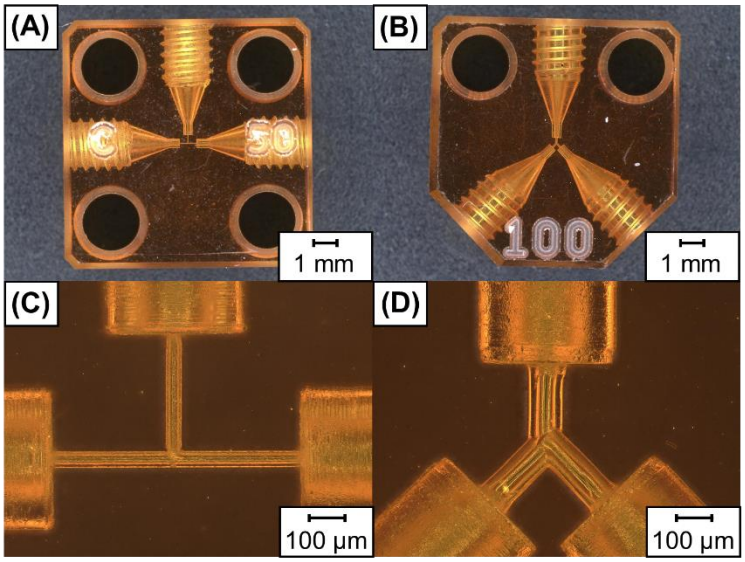

Figure E.1. Microscope images of FST (A), FSY (B), and the corresponding close-up images of FST (C) and FSY (D)

The two commercially available FSs, which were used in this project, are shown in Fig. E.1. The T-shaped FS (FST, Fig. E.1A and C) had a thru-hole diameter of 50 µm, which resulted in a dead volume of 2.1 ± 0.5 nL. According to technical reasons the Y-shaped FS (FSY, Fig. E.1B and D) had a thru-hole diameter of 100 µm, which resulted in a dead volume of 9 ± 2 nL. Both FSs were fabricated from polyetherimide, also known by the trade name Ultem. The FSs did not show any swelling or other visual changes when they came into contact with the ACN-based BGE. Capillaries were connected to the FSs with commercially available fittings, which were suitable for 365 µm OD capillaries. These fittings were fabricated from polyether ether ketone and were therefore also resistant to ACN.

Three capillary pieces were connected to the FS, a 20 cm long capillary piece was assembled to the injection side (P1) of the FS. At the two other sides of the FS (detection sides, P2 and P3), capillary pieces with a length of 40 cm were placed. To avoid any dead volume introduced by polyimide swelling, about 2 mm of the outer polymer coating of the capillary was removed. Additionally, both sides of each capillary were polished to receive planar capillary tips that enable a dead volume–free coupling with the FS. Before the first CE measurements, the capillaries were conditioned by flushing with 0.1 M sodium hydroxide solution (10 min), ultrapure water (5 min), and finally BGE (30 min).

CE-UV setup

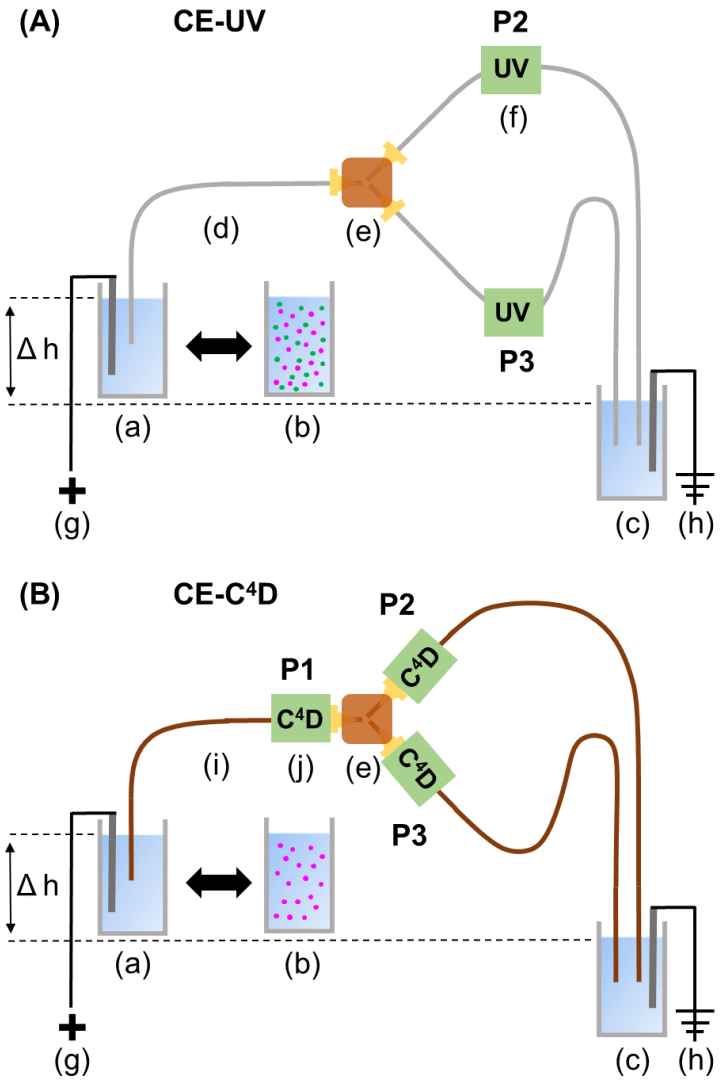

Figure E.2. Scheme of the CE-UV setup (A) and the CE-C^4D setup (B). Components of the CE-UV setup: inlet (a), sample (b), and outlet BGE vial (c), Teflon-coated fused silica capillaries (d), FST or FSY (e), UV (f), positive high-voltage source (g), and grounding (h). Components of the CE-C^4D setup: polyimide-coated fused silica capillaries (i) and C^4D (j). For both setups, there was a permanent height difference between the injection and detection side of 15 cm. The position of the detectors (UV and C^4D) was changed without disassembling the capillary pieces from the FS

Figure E.2A shows a scheme of the CE-UV setup. It consisted of a laboratory-constructed CE device with an integrated autosampler that was connected to a positive high-voltage power supply from ISEG (Radeberg, Germany). Experiments were carried out with FST and FSY. Each FS was connected to three capillaries (50 µm ID and 365 µm OD). Both capillary ends were placed in a grounded outlet vial. There

was a permanent height difference between the inlet and outlet vials of 15 cm. The injection was performed hydrodynamically for 5 s. The UV was placed after a capillary length of 40 cm (20 cm behind the FS). A Lambda 1010 UV/Vis detector from Bischoff (Leonberg, Germany) was used for detection at 265 nm. For calculating the split ratio and other parameters, measurement data were needed for both detection sides behind the FS (P2 and P3, highlighted in Fig. E.2A). As only one UV was available, a simultaneous detection at both sides (P2 and P3) was not possible. Therefore, the position of the UV was changed between P2 and P3. To minimize potential errors, during the position change of the detector, the capillary pieces were not disassembled from the FS. Thus, for each set of measurements, there was the same capillary to FS alignment because only the position of the detector was swapped. To simplify the detector change, Teflon-coated capillaries were used. Due to the transparent Teflon coating, no coating must be removed at the detection point of the UV, which makes the capillary less brittle. Five consecutive measurements were performed at P2 and P3. The sample solution consisted of 0.5 mM $[FcMTMA]^+$ as a cationic model analyte and 0.5 mM Caf as an EOF marker. The separations were performed at 25 kV. Special attention is needed when experiments are performed with high-voltage. Hence, the whole setup was placed in a safety housing made of acrylic glass. Additionally, the device was equipped with safety switches and warning signs.

CE-C^4D setup

CE-C^4D was used to evaluate the peak shape in front of and behind the FS. The CE-C^4D setup is depicted in Fig. E.2B. For detection, a C^4D was used, which was constructed in the group of Prof. C. L. do Lago and is described elsewhere [23]. Due to its compact design, the C^4D could be placed directly in front of (P1) and behind the FSs (P2 and P3). The detector positions are highlighted in Fig. E.2B. As described for the CE-UV setup, the position of the C^4D was changed after five measurements without disassembling the capillary pieces from the FSs. Experiments were carried out with FST and FSY. In contrast to the CE-UV setup, capillaries (50 µm ID and 365 µm OD) with polyimide coating were used. The sample solution consisted of 0.1 mM $[FcMTMA]^+$ in BGE. The other parameters were identical to the CE-UV setup.

The LODs were determined in front of (P1) and behind FSY (P2). Sample solutions ranging from 0.01 to 0.25 mM $[FcMTMA]^+$ in BGE were used. Each measurement was performed five times and the LODs were calculated for a signal-to-noise ratio (S/N) of 3. The effect of different FS geometries was investigated by measurements with a reversed FST (FST rev.). In this case, the injection capillary (P1) and one outlet capillary (P2) were arranged linearly, whereas the other outlet capillary (P3) was arranged perpendicularly.

To achieve higher sample loads and to show the flexibility of the FSs regarding different capillary IDs, FSY was connected at P1 with two capillary pieces of different IDs (50 and 75 µm). At P2 and P3, there were still capillaries with an ID of 50 µm. To compare the effects, we injected a sample plug of the same length (2.8 mm) in each capillary combination. The corresponding injection times were calculated based on capillary flow injection experiments. The injection of the sample solution (0.1 mM $[FcMTMA]^+$ in BGE) was performed hydrodynamically by a height difference of 10 cm between the inlet and outlet BGE vials. During the electrophoretic separation, the BGE levels in the vials were at the same height to avoid gravity-driven flow. For each capillary combination, the detector was placed at P1, P2, and P3.

4.2.3 Results and discussion

Characterization of the FSs

As the FS would be the central component for the realization of new DDCs, it must fulfill certain requirements: (i) The FS should have a low dead volume to prevent peak broadening or mixing of already separated analyte zones. (ii) The material of the FS should be resistant against organic solvents especially ACN, because we used an ACN-based BGE. (iii) The connection of the capillaries to the FS should be easy, robust, and flexible.

We chose commercially available FSs (FST and FSY, depicted in Fig. E.1) instead of expensive and time-consuming laboratory-constructed FSs. Both FSs fulfill the abovementioned requirements. Additionally, the transparency of the material simplified the troubleshooting as air bubbles inside the FS could be easily recognized. As they were commercially available, they also showed very good reproducibility contrary to laboratory-constructed items.

Characterization of the FSs utilizing UV detection

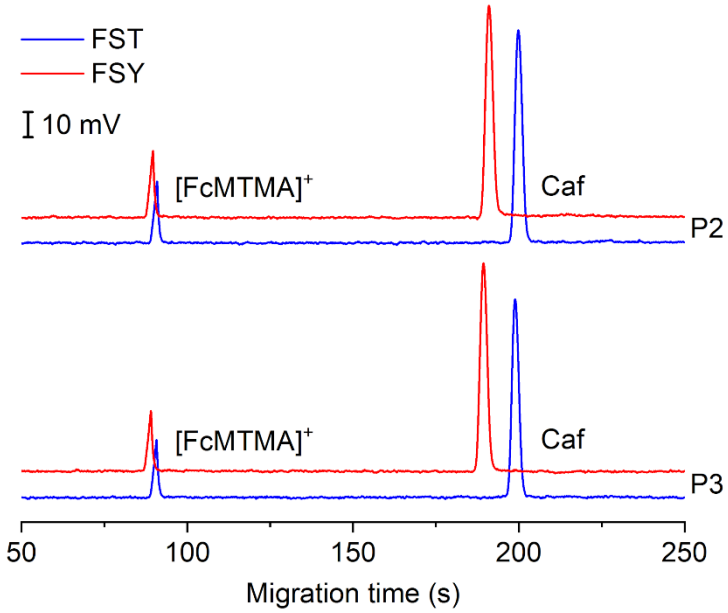

Figure E.3. Electropherograms of the model mixture $[FcMTMA]^+$/Caf were measured with CE-UV. The UV was placed at P2 (top) and P3 (bottom) of FST and FSY. Experimental parameters: 0.5 mM $[FcMTMA]^+$ and Caf in BGE, injection time 5 s, separation voltage 25 kV, current 6.7 µA (FST) and 6.9 µA (FSY), UV detection at 265 nm. The UV detector was placed after a capillary length of 40 cm (20 cm behind the FS)

The electropherograms for FST and FSY with parallel UV detection at different sides (P2 and P3) are depicted in Fig. E.3. The measurements showed that the splitting of the CE flow with the FSs worked because the model analytes were detected at both capillary sides. Regarding the peak shape, it was found that all peaks showed nearly Gaussian shape with negligible peak tailing for both FSs. For the development of new DDCs, the split ratio and its reproducibility are of special importance. The parameters were calculated based on the peak areas of the cationic and neutral model analytes at both sides (P2 and P3) and are summarized in Table S.E.1. For FST, the split ratio was a little closer to 50% than for FSY, but the reproducibility of the splitting was better for FSY. In our opinion, the reproducibility of the splitting is more important than the split ratio because it is mandatory for the reliable quantification of the analytes that the split ratio is stable throughout the measurements. The theoretical plate numbers (summarized in Table S.E.1) were slightly higher for FST, which indicated better separation efficiency due to the smaller dead volume of FST. For both FSs, the migration times were approximately the same at both capillary sides (P2 and P3). Slight differences were only found between the FSs. For FST, the cationic model analyte ($[FcMTMA]^+$) migrated 2 s and the EOF marker (Caf) 9 s later than for FSY. The reproducibility of the migration

times was better for FSY than for FST. We think this resulted from disturbances of the CE flow at the connection side between FST and the capillary pieces. For FST, the thru-hole diameter was 50 µm that was also the ID of the capillary pieces. Consequently, slight shifts at the connection side could influence the CE flow, which affected the migration times. This phenomenon was intensively discussed in some of our previous works, where we coupled capillaries with different IDs linearly [16]. For FSY, the robustness of the connection was better due to the thru-hole diameter of 100 µm.

From the CE experiments with parallel UV detection, one can conclude that the separation efficiency was slightly better for FST, but the reproducibility of the splitting and the robustness of the capillary coupling to the FS were better for FSY.

Characterization of the FSs utilizing C^4D detection

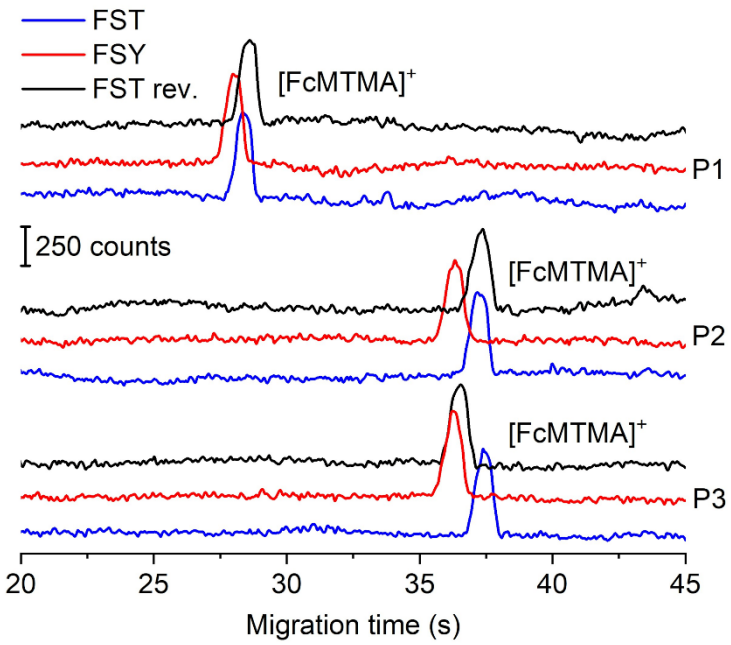

Figure E.4. CE-C^4D measurements of FST, FSY, and FST rev. In contrast to FST for FST rev., the inlet capillary (P1) and one outlet capillary (P2) were arranged linearly, and the second outlet capillary (P3) was arranged perpendicular to them. The C^4D was placed directly in front of (P1) and behind the FSs (P2 and P3). Experimental parameters: 0.1 mM $[FcMTMA]^+$ in BGE, injection time 5 s, separation voltage 25 kV, current 6.0 µA (FST), 6.1 µA (FSY) and 6.1 µA (FST rev.)

The effects of the flow splitting on the peak shape were characterized by CE-C^4D. Due to its compact design, the C^4D could be placed directly in front of (P1) and behind the FS (P2 and P3). The corresponding electropherograms of the different FSs are depicted in Fig. E.4. The investigated sample solution consisted only of the cationic model

analyte ([FcMTMA]$^+$) due to the detection characteristics of the C^{4}D. As observed for the CE-UV experiments, the cationic model analyte ([FcMTMA]$^+$) migrated at each side (P2 and P3) nearly simultaneously. From the electropherograms shown in Fig. E.4, we found that for both types of FSs, the peaks look almost identical in front of and behind the FS. The corresponding figures of merit for the peaks at P1, P2, and P3 are summarized in Table S.E.2. It was found that the full widths at half maximum (FWHMs) were the same for FSY at P1, P2, and P3. The FWHMs of the peaks for FST were slightly larger behind the FS (P2 and P3). We suggest that this was also a disturbance effect from the connection side. Nevertheless, the FWHMs were almost the same in front of and behind both FSs. The sample zones were split simultaneously inside of the FS without dilution effects. Therefore, the sample zones have only half of the length after the splitting, but the peak width behind the FS was almost identical to the peak width in front of the FS. A possible explanation for the very similar peak widths could be given by the different flow rates in front of and behind the FS. We calculated the flow rates for the different sections of the FSs based on the migration times and the positions of the detectors. For FST, we determined a flow rate of 6.21 ±0.06 mm/s at P1, 3.00 ±0.04 mm/s at P2, and 3.1 ±0.1 mm/s at P3. Very similar results were obtained for the flow rate of FSY. For both FSs, the flow rates prior to the FS were about twice as high as the flow rates afterward. Thus, after passing the FS the sample zones needed twice the time to pass the detector. Compared to the peak widths in front of the FS, the combination of halved sample zones and halved flow rates behind the FS leads to nearly identical peak widths behind the FS. As the sample zones were not diluted during the splitting process and the fact that the C^{4}D is a concentration-related detector, also the peak heights were identical in front of and behind the FS. As the peaks looked nearly the same in front of and behind the FS, also the LODs should be the same. Therefore, we determined the LODs in front of and behind FSY and we found that the LODs were 13 ±6 µM in front of the FS and 15 ±8 µM behind the FS. Within the scope of measurement precision, the LODs could be considered identical. As our experiments did not reveal any peak broadening effects introduced by the FSs, we consider the splitting as nearly dead volume free.

As FST and FSY had different thru-hole diameters, we investigated the effect on the geometry of the FS by changing the direction of FST, so that P1 and P2 were arranged linearly. However, the other outlet capillary (P3) was arranged perpendicular to P1 and P2. The corresponding electropherograms of the reversed FST are also depicted in Figure E.4. For both arrangements of FST, no significant difference was detectable. Hence, we concluded that the geometry of the FS had no measurable effect on the splitting of the CE flow.

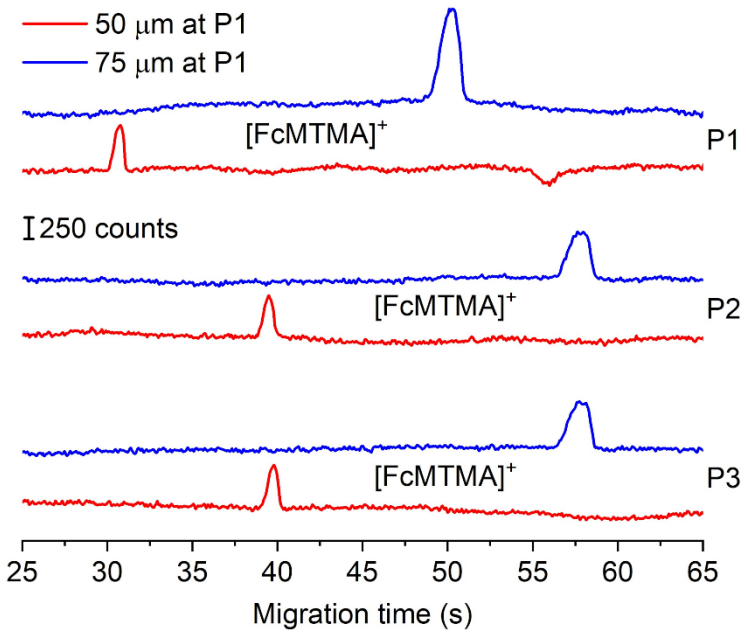

Figure E.5. CE-C^4D measurements of an $[FcMTMA]^+$ sample solution with a 50 and 75 µm capillary in front of FSY (P1) and two 50 µm capillaries behind the FSY (P2 and P3). The C^4D was placed directly in front of (P1) and behind the FS (P2 and P3). Experimental parameters: 0.1 mM $[FcMTMA]^+$ in BGE, separation voltage 25 kV, current 6.2 µA (50 µm at P1) and 9.0 µA (75 µm at P1), sample plug length 2.8 mm. The sample plug length was calculated based on capillary flow injection experiments

For trace analysis, usually larger sample amounts are required. To achieve higher sample loads, by similar sample plug length, we placed a 75 µm instead of a 50 µm capillary in front of FSY (P1). Figure E.5 shows the corresponding electropherograms with a 50 and 75 µm capillary at P1 for identical sample plug lengths. For the measurements using a 75 µm capillary at P1, the cationic model substance migrated at P1 20 s later compared to the configuration using the 50 µm capillary, which could be explained by the smaller electrical field strength in the 75 µm capillary. The plateau formation of the peaks at P2 and P3 for the configuration with the 75 µm capillary approved the higher amount of injected sample compared to the configuration using the 50 µm capillary at P1. Furthermore, the peaks recorded using the 75 µm capillary at P1 were about twice as high as in the 50 µm capillary. This was predominantly an effect of the higher sensitivity of the C^4D for capillaries with a larger ID and not due to the higher sample volume. Table S.E.3 depicts the dependence of the sensitivity of the C^4D on the ID of the capillary for our used model system. The data in Table S.E.3 show that the sensitivity of the C^4D was about twice as high for the 75 µm than for the 50 µm capillary. Overall, these measurements showed the flexibility of the FS concept regarding different capillary IDs and were not limited to the injection position (P1). At P2 and P3, also

capillaries with different IDs could be used, which allows the individual adjustment of the capillary ID to the requirements of injection and of each detector.

4.2.4 Conclusion

For the development of novel DDCs, including more than one destructive detector at the capillary end, we have introduced a simple concept for the splitting of the CE stream utilizing commercially available FSs. With this approach, it was possible to place two detectors in parallel to each other.

In this manuscript, we performed some proof-of-concept experiments where we could show that the splitting of the CE flow with commercially available FSs is promising for detection concepts using two destructive detectors. Both FSs provided very good performance. Additionally, they were very simple in handling and user-friendly. The split ratio was about 50% for both types of FSs. We found that it was favorable for the reproducibility of the measurements when the thru-hole diameter of the FS was 50 µm larger than the ID of the capillary. CE-C^4D measurements showed no significant peak broadening due to the implementation of the FSs. Additionally, the LODs in front of and behind the FS were the same. Consequently, the splitting can be considered almost dead volume free. Additionally, we found that the shape of the FS had no measurable effect on the splitting. The FSs were also successfully tested in combination with capillaries of various IDs. Therefore, it was possible to choose the best suitable capillary ID for injection and each detector individually. In contrast to conventional DDCs with a linear detector arrangement, the concept with the FSs has, in combination with capillaries of identical IDs, the potential to synchronize the detector responses.

Based on the results described in this article, it can be pointed out that utilizing commercially available FSs, the concept of CE flow splitting is a powerful and simple approach that could be used for the implementation of novel DDCs consisting of two destructive detectors. Moreover, the FSs hold great potential to be used in other, more sophisticated applications of capillary-based analytical systems.

4.2.5 Supporting information

Table S.E.1. CE-UV studies with FST and FSY for the determination of the migration time (t), split ratio (SR), theoretical plate number (TPN), and the corresponding error (n = 5). The detector was placed at two different positions (P2 and P3)

species	**[FcMTMA]$^+$**		**Caf**	
position	**P2**	**P3**	**P2**	**P3**
t (FST) [s]	90.9 ±0.3	90.5 ±0.2	200 ±1	198 ±1
t (FSY) [s]	89.6 ±0.1	88.8 ±0.2	191 ±0.2	189.2 ±0.2
SR (FST) [%]	51 ± 3	49 ±3	52 ± 2	48 ± 2
SR (FSY) [%]	54 ± 2	46 ± 2	52 ±1	48 ±1
TPN (FST)	$25 \cdot 10^3 \pm 1 \cdot 10^3$	$269 \cdot 10^2 \pm 9 \cdot 10^2$	$34 \cdot 10^3 \pm 1 \cdot 10^3$	$38 \cdot 10^3 \pm 2 \cdot 10^3$
TPN (FSY)	$232 \cdot 10^2 \pm 4 \cdot 10^2$	$251 \cdot 10^2 \pm 8 \cdot 10^2$	$313 \cdot 10^2 \pm 5 \cdot 10^2$	$35 \cdot 10^3 \pm 1 \cdot 10^3$

Table S.E.2. CE-C^{4}D studies with FST and FSY for the determination of the migration time (t), the peak height (H), the peak width at half maximum (FWHM), the peak area (A) and the corresponding error (n = 5). The detector was placed directly in front of the FS (P1) and behind the FS (P2 and P3)

species	**[FcMTMA]$^+$**		
position	**P1**	**P2**	**P3**
t (FST) [s]	28.42 ±0.06	37.2 ±0.2	37.2 ±0.2
t (FSY) [s]	27.91 ±0.04	36.20 ±0.09	36.3 ±0.2
H (FST) [counts]	$54 \cdot 10^1 \pm 1 \cdot 10^1$	$54 \cdot 10^1 \pm 3 \cdot 10^1$	$55 \cdot 10^1 \pm 3 \cdot 10^1$
H (FSY) [counts]	$57 \cdot 10^1 \pm 2 \cdot 10^1$	$53 \cdot 10^1 \pm 1 \cdot 10^1$	$56 \cdot 10^1 \pm 1 \cdot 10^1$
FWHM (FST) [s]	0.62 ±0.02	0.73 ±0.04	0.78 ±0.04
FWHM (FSY) [s]	0.71 ±0.01	0.71 ±0.02	0.71 ±0.02
A (FST) [counts·s]	$34 \cdot 10^1 \pm 1 \cdot 10^1$	$39 \cdot 10^1 \pm 2 \cdot 10^1$	$42 \cdot 10^1 \pm 1 \cdot 10^1$
A (FSY) [counts·s]	$40 \cdot 10^1 \pm 2 \cdot 10^1$	$37 \cdot 10^1 \pm 1 \cdot 10^1$	$40 \cdot 10^1 \pm 1 \cdot 10^1$

Table S.E.3. CE-C^{4}D studies with single capillaries for the determination of the peak height (H) and the corresponding error (n = 5) in dependence of different IDs (25, 50 and 75 µm)

species	**[FcMTMAM]$^+$**		
capillary ID [µm]	**25**	**50**	**75**
H [counts]	$17 \cdot 10^1 \pm 1 \cdot 10^1$	556 ±8	$119 \cdot 10^1 \pm 3 \cdot 10^1$

References

1. Beutner A, Herl T, Matysik F-M. Selectivity enhancement in capillary electrophoresis by means of two-dimensional separation or dual detection concepts. Anal Chim Acta. 2019;1057:18–35.
2. Furter JS, Boillat M-A, Hauser PC. Low-cost automated capillary electrophoresis instrument assembled from commercially available parts. Electrophoresis. 2020;41:2075–82.
3. Holland LA, Chetwyn NP, Perkins MD, Lunte SM. Capillary electrophoresis in pharmaceutical analysis. Pharm Res. 1997;14:372–87.
4. Ramos-Payán M, Ocaña-Gonzalez JA, Fernández-Torres RM, Llobera A, Bello-López MÁ. Recent trends in capillary electrophoresis for complex samples analysis: a review. Electrophoresis. 2018;39:111–25.
5. Voeten RLC, Ventouri IK, Haselberg R, Somsen GW. Capillary electrophoresis: trends and recent advances. Anal Chem. 2018;90:1464–81.
6. Opekar F, Stulík K. Some important combinations of detection techniques for electrophoresis in capillaries and on chips with emphasis on electrochemical principles. Electrophoresis. 2011;32:795–810.
7. Beutner A, Scherer B, Matysik F-M. Dual detection for nonaqueous capillary electrophoresis combining contactless conductivity detection and mass spectrometry. Talanta. 2018;183:33–8.
8. Francisco KJM, do Lago CL. A capillary electrophoresis system with dual capacitively coupled contactless conductivity detection and electrospray ionization tandem mass spectrometry. Electrophoresis. 2016;37:1718–24.
9. Mironov GG, Clouthier CM, Akbar A, Keillor JW, Berezovski MV. Simultaneous analysis of enzyme structure and activity by kinetic capillary electrophoresis-MS. Nat Chem Biol. 2016;12:918–22.
10. Szarka M, Szigeti M, Guttman A. Imaging laser-induced fluorescence detection at the Taylor cone of electrospray ionization mass spectrometry. Anal Chem. 2019;91:7738–43.
11. Zhang D, Li W, Zhang J, Tang W, Qian C, Feng M, et al. Study on urinary metabolic profile of phenylketonuria by micellar electrokinetic capillary chromatography with dual electrochemical detection–potential clinical application in fast diagnosis of phenylketonuria. Anal Chim Acta. 2011;694:61–6.

12. Huhn C, Ruhaak LR, Mannhardt J, Wuhrer M, Neusüß C, Deelder AM, et al. Alignment of laser-induced fluorescence and mass spectrometric detection traces using electrophoretic mobility scaling in CE-LIF-MS of labeled N-glycans. Electrophoresis. 2012;33:563–6.
13. Holland LA, Lunte SM. Capillary electrophoresis coupled to electrochemical detection: a review of recent advances. Anal Commun. 1998;35:1–4.
14. Matysik F-M. End-column electrochemical detection for capillary electrophoresis. Electroanalysis. 2000;12:1349–55.
15. Meermann B, Bartel M, Scheffer A, Trümpler S, Karst U. Capillary electrophoresis with inductively coupled plasma-mass spectrometric and electrospray time of flight mass spectrometric detection for the determination of arsenic species in fish samples. Electrophoresis. 2008;29:2731–7.
16. Böhm D, Matysik F-M. Characterization of linearly coupled capillaries with various inner diameters in the context of capillary electrophoresis. Monatsh Chem. 2021;152:1053–60.
17. Tůma P, Opekar F, Samcová E. Very fast electrophoretic separation on commercial instruments using a combination of two capillaries with different internal diameters. Electrophoresis. 2013;34:552–6.
18. Jooß K, Scholz N, Meixner J, Neusüß C. Heart-cut nano-LC-CZE-MS for the characterization of proteins on the intact level. Electrophoresis. 2019;40:1061–5.
19. Sydes D, Kler PA, Hermans M, Huhn C. Zero-dead-volume interfaces for two-dimensional electrophoretic separations. Electrophoresis. 2016;37:3020–4.
20. Pham TTT, Mai TD, Nguyen TD, Sáiz J, Pham HV, Hauser PC. Automated dual capillary electrophoresis system with hydrodynamic injection for the concurrent determination of cations and anions. Anal Chim Acta. 2014;841:77–83.
21. Matysik F-M. Non-aqueous capillary electrophoresis with electrochemical detection. J Chromatogr A. 1998;802:349–54.
22. Riekkola M-L. Recent advances in nonaqueous capillary electrophoresis. Electrophoresis. 2002;23:3865–83.
23. Francisco KJM, do Lago CL. A compact and high-resolution version of a capacitively coupled contactless conductivity detector. Electrophoresis. 2009;30:3458–64.

4.3 Combining amperometry and mass spectrometry as a dual detection approach for capillary electrophoresis

Böhm D, Koall M, Matysik F-M. Combining amperometry and mass spectrometry as a dual detection approach for capillary electrophoresis. Electrophoresis. 2023;44:492-500.

Abstract

Dual detection concepts (DDCs) are becoming more and more popular in analytical chemistry. In this work, we describe a novel DDC for capillary electrophoresis (CE) consisting of an amperometric detector (AD) and a mass spectrometer (MS). This detector combination has a good complementarity as the AD exhibits high sensitivity, whereas the MS provides excellent selectivity. Both detectors are based on a destructive detection principle, making a serial detector arrangement impossible. Thus, for the realization of the DDC, the CE flow was divided into two parts with a flow splitter. The DDC was characterized in a proof-of-concept study with ferrocene derivates and a non-aqueous background electrolyte. We could show that splitting the CE flow was a suitable method for the instrumental realization of the DDC consisting of two destructive detectors. By lowering the height of the AD compared to the MS, it was possible to synchronize the detector responses. Additionally, for the chosen model system, we confirmed that the AD was much more reproducible and had lower limits of detection (LODs) than the MS. The LODs were identical for the DDC and the single-detection arrangements, indicating no sensitivity decrease due to the CE flow splitting. The DDC was successfully applied to determine the drug and doping agent trimetazidine.

4.3.1 Introduction

The number of complex samples in fields like medicine or environmental research is steadily increasing. Therefore, powerful separation and detection methods are required [1, 2]. After its invention by Jorgenson and Lukacs [3] in the early 1980s, capillary electrophoresis (CE) became an established separation method due to its high separation efficiency, short analysis times, and low sample consumption [4-6]. Due to the minimal amount of injected sample and the small dimensions in CE, the sensitivity of the detection technique plays an important role. A detection method that copes very well with these conditions is amperometric detection (AD). AD was first applied with CE by Wallingford and Ewing [7] in 1987 by a porous joint as an electrical field decoupler. A few years later Ewing's group also introduced the first hyphenation of CE with AD without an electrical field decoupler termed end-column AD [8]. For electroactive analytes, AD is considered as a very sensitive detection method [9-11]. In combination with a non-aqueous background electrolyte (BGE), the long-term stability of AD is excellent, allowing the quantification utilizing external calibration or standard addition method [12, 13]. Nevertheless, one drawback of AD is the limited selectivity. With AD, it is usually impossible to identify unknown substances or to examine the peak purity.

In contrast to AD, mass spectrometry (MS) is the detection method of choice when it comes to selectivity because it is possible to determine molecular weight and structural information [14]. Smith and coworkers [15] described the combination of electrospray ionization (ESI) and MS as a detection method for CE in 1987. The sensitivity of ESI-MS depends strongly on the ionization efficiency of the analyte. Additionally, the sensitivity of ESI-MS is negatively affected by the dilution of the CE effluent with sheath liquid of the sheath-flow interface. Thus, the limits of detection (LODs) of ESI-MS are usually higher than the ones determined with AD [11, 16–18]. Moreover, the long-term stability of ESI-MS signals is typically relatively poor. Therefore, the quantification with ESI-MS is often achieved with isotope-labeled internal standards, but these are expensive and not available for every analyte [16-19].

A dual detection concept (DDC) combines the power of different single-detection techniques and overcomes their limitations. Both detectors (AD and MS) have an excellent complementarity. Therefore, they provide a powerful DDC, which is to the best of our knowledge not described in literature so far. According to the features of the detectors, the AD is perfect for quantifying substances, and the MS is ideal for identifying substances. In recent years, many DDCs for CE have been developed [20-25]. These DDCs consist of at least one non-destructive detector. This simplifies the instrumental realization because a serial detector arrangement could be used [2]. The development

of the novel DDC (CE-AD/MS) is much more challenging because both detectors are destructive and must be decoupled from the high-voltage field of the CE. For the realization of this concept, the CE flow has to be split into two parts. Thereby, it is possible to arrange the detectors in parallel to each other. The splitting of the CE flow is already described in literature but predominately in the context of 2D separations or for the concurrent analysis of cations and anions [26-28]. In a previous work we presented a user-friendly flow splitter (FS) that could be used for flow splitting in CE [29]. Different types of FSs were characterized. Additionally, it was demonstrated that the FSs introduced no peak broadening wherefore the splitting was considered to be dead volume-free. Based on these results, we used this FS for the realization of the new DDC. In principle, an approach with two capillaries (both capillaries starting from the inlet vial and one capillary going to the AD and the other to the MS) would also be possible. This approach was not used to implement the DDC because each capillary has its characteristics, which leads to different migration behavior, making a synchronization of the migration times difficult. Additionally, a two capillary approach cannot be implemented with most of the commercially available CE devices.

In this proof-of-concept study, we describe the development of a DDC for CE combining AD and MS. For the characterization of the new DDC ferrocene derivates dissolved in a non-aqueous BGE were used. The non-aqueous BGE was favorable for both detectors. On the one hand, it has a wide potential window and an excellent long-term stability in terms of AD. On the other hand, the non-aqueous BGE is very volatile, which is good for ESI-MS [30]. Finally, we determined trimetazidine (TMZ), which was recently discussed in the context of doping, demonstrating the complementary action of AD/MS.

4.3.2 Experimental

Chemicals and materials

The following chemicals were used, all of analytical grade: acetonitrile (ACN), ammonium acetate, 0.1 M sodium hydroxide solution, formic acid, and ultrapure water provided by a Milli-Q Advantage A10 system, were acquired from Merck (Darmstadt, Germany). Ferrocenemethanol (FcMeOH) was purchased from ABCR (Karlsruhe, Germany). (Ferrocenylmethyl)trimethylammonium iodide ([FcMTMA]I) was obtained from Strem Chemicals (Newburyport, USA). Acetic acid was purchased from Carl Roth (Karlsruhe, Germany). Trimetazidine dihydrochloride (TMZ) and 2-propanol were purchased from Sigma-Aldrich (St. Louis, USA). Fused silica capillaries (50 µm inner diameter (ID), 365 µm outer diameter, polyimide coated) were received from Polymicro Technologies (Phoenix, USA). The FS CapTite Interconnect Y C360-203Y-U-C100 and

the corresponding fitting CapTite One-Piece Fitting C360-100 were obtained from LabSmith (Livermore, USA).

Instrumentation CE-AD/MS

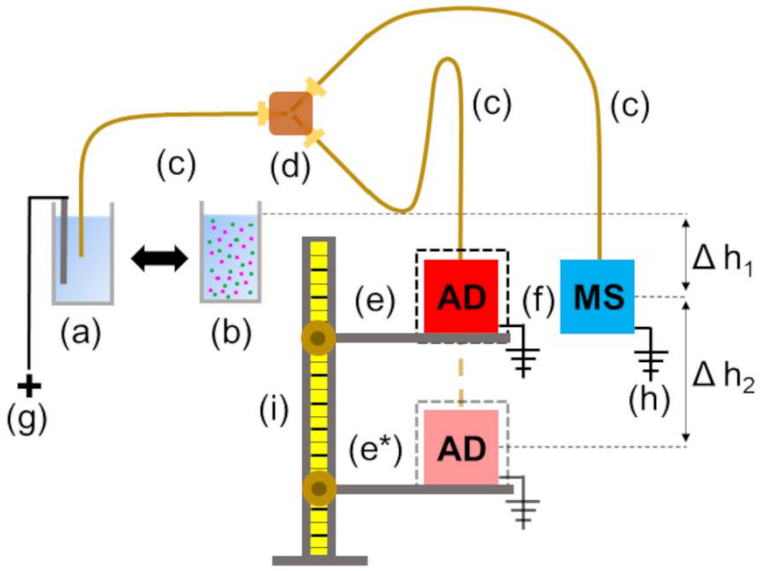

Figure F.1. Scheme of the CE-AD/MS setup showing the main components: Inlet vial (a), sample vial (b), fused silica capillaries (c), FS (d), AD (e), MS (f), positive high-voltage power source (g), grounding (h), and Faraday cage with integrated stand (i). There was a permanent height difference Δh_1 between the inlet vial and the MS of 6 cm. The height difference Δh_2 between AD and MS was variable. The height difference Δh_2 was adjusted by lowering the AD (e*)

Figure F.1 shows a scheme of the DDC (CE-AD/MS), consisting of a CE device connected to an AD and a MS via a Y-shaped FS. For a better illustration, a photograph of the DDC is shown in Fig. S.F.1. The laboratory-constructed CE system was connected to a positive high-voltage power supply from ISEG (Radeberg, Germany). Special caution is required when experiments are performed with high-voltage. The CE device was placed in a safety housing that was equipped with safety switches and warning signs.

The end-column AD was laboratory-constructed and is described in detail elsewhere [13]. Briefly, the AD was made of polytetrafluoroethylene, which allowed the usage in combination with the ACN-based BGE. For the user-friendly positioning of the capillary and the working electrode, the AD was equipped with two symmetrically arranged stainless steel tubes which served as a guiding system. The separation capillary and the working electrode were placed at a distance of 50 µm from each other. The positioning was done utilizing an UltraZoom Pro digital microscope from

dnt (Dietzenbach, Germany). The working electrode consisted of a 25 µm platinum wire sealed in a glass tube and the Ag/AgCl reference electrode (filled with BGE) was placed in the cap of the AD. A stainless steel tube served additionally as counter electrode for the AD and as grounding for the electrophoretic circuit of the CE. The electrodes were connected to an SP-200 potentiostat equipped with an ultralow current module from BioLogic (Seyssinet-Pariset, France). The AD cell was filled with BGE and placed in a Faraday cage to reduce electromagnetic interference effects. As in this work an AD with an end-column design was used, the potential shift at the working electrode was determined at the beginning of each measurement day by performing cyclic voltammograms without and with 25 kV separation voltage. The potentials of the electrode pretreatment protocol and the detection potential were corrected by the potential shift. The determination of the potential shift for NACE in combination with an end-column AD is described in detail elsewhere [31]. Simultaneously with each CE measurement, an electrode pretreatment protocol (2.5 V for 10 s followed by −0.5 V for 10 s) was started to avoid electrode fouling. Subsequently, the detection potential (0.8 V for the ferrocene derivates and 1.3 V for the TMZ) was applied at the working electrode. A micrOTOF-MS from Bruker Daltonics (Bremen, Germany) with a coaxial sheath liquid ESI interface from Agilent Technologies (Santa Clara, USA) was used as a second detector. Due to the properties of the analytes, all measurements were performed in the positive MS mode. For the measurements, the following MS parameters were used: nebulizer gas pressure 1 bar, electrospray voltage 4 kV, dry gas (N_2) flow 4 L/min, dry gas temperature 190°C, end plate offset −500 V, capillary exit 85 V, skimmer 1 29 V, skimmer 2 23 V, hexapole 1 23 V, hexapole RF 80 Vpp, lens 1 transfer 35 µs, lens 1 pre pulse storage 6 µs, m/z 50–400, and spectra acquisition rate 5 Hz. The sheath liquid had a flow rate of 8 µl/min and consisted of water, 2-propanol, and formic acid (49.9:49.9:0.2, v/v/v).

A Y-shaped FS (material polyetherimide, dead volume 9 nL, and thru-hole diameter 100 µm) was used to split the CE flow. A microscopic image and a detailed description of the FS can be found in our previous manuscript [29]. The FS was connected to three capillary pieces. The capillary piece on the injection side had a length of 30 cm, and the two capillary pieces on the detection side had a length of 35 cm. On both sides of the capillary pieces, about 3 mm of the polyimide coating was removed with a razor blade to avoid any dead volume introduced by polyimide swelling. To prevent a dead volume introduced by nonplanar capillary tips, all capillary edges were polished at a 90° angle with abrasive papers of 30 and 3 µm grid size. Before the first CE measurements, the capillaries were conditioned by flushing them for 10 min with 0.1 mM sodium hydroxide solution, followed by 5 min with ultrapure water and at least 30 min with BGE.

There was a fixed height difference of 6 cm between the capillary inlet and the tip of the coaxial sheath liquid ESI interface of the MS. The AD was variable in height. For some measurements, it was located at the same height as the tip of the coaxial sheath liquid interface of the MS, but for synchronizing the detector responses the AD was placed at a lower height level. To simplify the height adjustment, the AD was placed in a stand that was integrated into the Faraday cage. The Faraday cage with an integrated stand is shown in Fig. S.F.1. The injection was performed hydrodynamically by the height difference between the injection side and the detectors. The suction pressure of the ESI source also supported the injection. The optimized injection time was 20 s. For all measurements, a separation voltage of 25 kV was applied.

Experimental parameters and sample preparation

All experiments were performed with a non-aqueous BGE consisting of 10 mM ammonium acetate and 1 M acetic acid in ACN. If not indicated differently, a sample solution containing 0.1 mM $[FcMTMA]^+$ and 0.5 mM FcMeOH in BGE was used to characterize the DDC. The effect of the height difference between AD and MS was investigated to achieve similar migration times for both detectors. For the very first measurements, both detectors were at the same level, defined as a height difference of 0 cm. As the height of the MS was not adjustable, the height of the AD was systematically decreased by 2 cm steps compared to the tip of the coaxial sheath liquid interface of the MS. The height difference was adjusted for all subsequent measurements to get a simultaneous detector response. The reproducibility of the most important parameters like migration time, peak areas, and peak heights was tested by performing 11 consecutive measurements of the sample solution. To evaluate a possible decrease in detectability due to the flow splitting, the LODs for the DDC and the single-detection arrangements were determined. For the single-detection measurements, each detector (AD and MS) was separately coupled with the CE device. For these measurements, almost all parameters were retained. Only the capillary length and the injection times for the measurements with the single-detection arrangements were adjusted. The CE device was coupled to the single detectors via a continuous capillary with a length of 65 cm. The injection times were optimized for each single-detection arrangement to ensure maximum sensitivity. The optimized injection times for the DDC (CE-AD/MS) and the single-detection arrangement (CE-AD) were 20 s, for the other single-detection arrangement (CE-MS) the injection time was 15 s.

In the second set of experiments, TMZ was used as an analyte. The electrochemical behavior of TMZ was characterized by cyclic voltammetry. The cyclic voltammograms were performed in a batch cell with identical electrodes to the AD. A solution of 0.1 mM

TMZ in bare BGE was used for the cyclic voltammograms. The cyclic voltammograms were measured between 0 and 1.5 V with a scan rate of 50 mV/s. For the CE-AD/MS measurements, a sample solution containing 1.25 µg/ml TMZ in BGE, including 10% MeOH was used. The MeOH was added to increase the solubility of the TMZ in BGE.
All LODs (ferrocene derivates and TMZ) were determined by measuring the detector signals within a concentration range near the LOD. The LODs were determined for a signal-to-noise ratio (S/N) of three, and each measurement was performed three times.

Data evaluation

The measurement data were evaluated with Origin 2020 SR 1 from OriginLab (Northampton, USA), Excel 2016 from Microsoft (Redmond, USA), Data Analysis 4.0 SP1 from Bruker Daltonics (Bremen, Germany), and EC-Lab V11.43 from BioLogic (Seyssinet-Pariset, France).

4.3.3 Results and Discussion

Synchronization of the detector responses

For the first proof-of-concept measurements with the new DDC, we used a model system consisting of $[FcMTMA]^+$ as cationic model analyte and FcMeOH as electroosmotic flow (EOF) marker. These analytes were very favorable for the characterization of the DDC because they could be detected with both detectors (AD and MS). The mass-to-charge ratio (m/z) 199 was used for the MS as it was the most sensitive signal for both model analytes ($[FcMTMA]^+$ and FcMeOH).
For the first measurements, the detectors were placed at the same height. This means the AD and the tip of the coaxial sheath liquid interface of the MS were at the same height level. The corresponding electropherograms measured with the AD are shown on top, and the MS measurements are shown in Fig. F.2A. The model analytes could be detected at both detectors. This shows that the splitting of the CE flow for the implementation of a new DDC worked. For no height difference between the detectors, it was found that the model substances migrated earlier at the side of the MS than at the side of the AD. The reason for this finding was the suction pressure of the ESI interface, which accelerated the flow towards the MS. In order to utilize the full potential of the DDC, it is desirable to synchronize the migration times as it is planned to identify the substances via MS and simultaneously quantify the substances via AD. It would be ideal if the detector responses could be synchronized without internal standards and mathematical calculations. Therefore, we tried to synchronize the detector responses by adjusting the height difference between the two detectors. By lowering the AD, the

hydrodynamic flow towards the AD was increased, which could compensate the suction pressure of the ESI interface at the MS. The effect on the migration time for a reduction of the height level of the AD compared to the MS is depicted in Fig. F.2A. For a height difference of −2 cm, the substances migrated earlier at the side of the AD and later at the side of the MS compared to the first measurements where the detectors were at the same height. This trend continued with increasing height differences. For a height difference of −6 cm, the substances migrated even earlier on the side of the AD than on the MS side. Due to these findings, there should be a height difference where the substances migrate simultaneously at both detectors. We plotted the migration times against the height differences for both model analytes to find the ideal height difference for simultaneous detection. The corresponding chart for the cationic model analyte ($[FcMTMA]^+$) is depicted on top and for the EOF marker (FcMeOH) at the bottom of Fig. F.2B. It was found that there was a linear correlation between migration times and height differences. There was an intercept between the linear trend curves of the AD and the MS at about −4 cm, indicating that for this height difference, the substances migrated simultaneously at both detectors. The synchronization of the migration times was stable throughout the whole measurement day. When the capillaries were not disassembled from the detectors overnight, no or only minimal adjustments had to be done before the next measurements session. The height difference for all subsequent measurements was adjusted to get a simultaneous detector response.

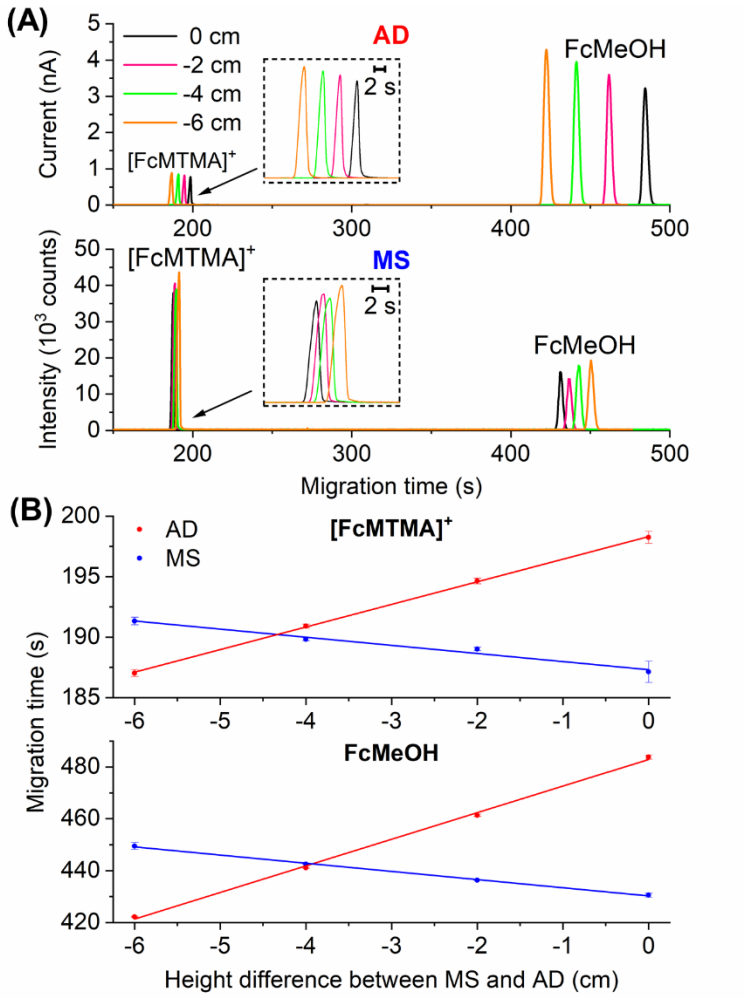

Figure F.2. CE-AD/MS measurements (A) of the model mixture $[FcMTMA]^+$/FcMeOH for different height differences (0, −2, −4, and −6 cm) between AD and MS. The electropherograms were recorded with AD (top) and with MS (bottom). Corresponding electropherograms for the AD and the MS have the same color. Development of the migration times (B) for $[FcMTMA]^+$ (top) and FcMeOH (bottom) depending on the height difference between AD and MS. Experimental parameters: 0.1 mM $[FcMTMA]^+$ and 0.5 mM FcMeOH in BGE, injection time 20 s, separation voltage 25 kV, detection potential AD 0.8 V (vs. Ag/AgCl), and extracted ion electropherograms for both model analytes (m/z 199). The detectors were placed after a respective total capillary length of 65 cm (30 cm in front of the FS and 35 cm behind the FS)

Reproducibility of the DDC (CE-AD/MS)

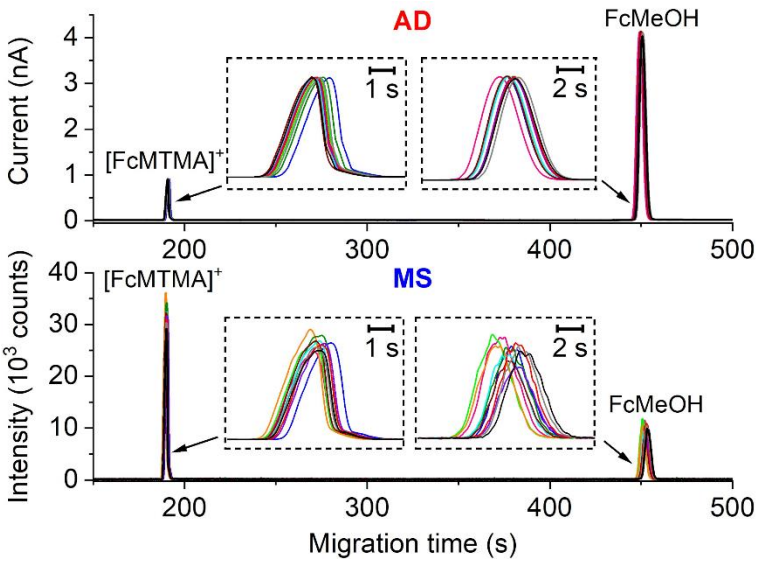

Figure F.3. CE-AD/MS measurements of the model mixture $[FcMTMA]^+$/FcMeOH for 11 consecutive measurements. The electropherograms on top were recorded with AD and at the bottom with MS. Corresponding electropherograms for the AD and the MS have the same color. Experimental parameters: The conditions are as in Fig. F.2

As it was possible to synchronize the detectors by a simple adjustment of the height difference between AD and MS, as a next step we looked at the reproducibility of the new DDC. The reproducibility was tested by performing 11 consecutive measurements. The corresponding electropherograms are shown in Fig. F.3. It could be seen that the substances migrated nearly simultaneously at both detectors due to the height adjustment carried out at the beginning of the measurements. For both detectors, it was found that all peaks showed a nearly Gaussian shape with negligible peak tailing. For the AD one peak looked like the other, whereas for the MS some differences in the peak shape were detectable. To substantiate this finding, we determined the peak areas and heights for the two different detectors and summarized the figures of merit in Table F.1. It was found that the relative standard deviations (RSDs) of the peak areas were in a range of 1.2%–1.3% for the AD and 6.9%–10.8% for the MS. A similar result was found for the peak heights, where the RSDs were in the range of 0.4%–0.7% for the AD and between 6.3% and 10.0% for the MS. Both results showed that the reproducibility was better for the AD than for the MS. As the reproducibility of the detector response is especially important for the quantification of analytes, we concluded that the AD was better suited for quantification purposes than the MS. Due to the excellent reproducibility of the AD, it could be used in combination with external calibration or standard addition methods. There is no need for an internal standard that is often used in combination with

MS. Summing up, if the analytes can be detected with both detectors, the AD should be used for quantification and the MS for identification. Furthermore, the small RSDs of the AD also showed the good reproducibility of the CE flow splitting. This was an essential point, because for the quantification, it was important that the split ratio was stable throughout the measurements. In one of our previous works, we also found a good reproducibility of the CE flow splitting for the used FS [29].

Table F.1 CE-AD/MS studies of 0.1 mM $[FcMTMA]^+$ and 0.5 mM FcMeOH for the determination of the reproducibility of the migration time (t), the peak area (A), the peak height (H), and the corresponding SDs at the different detectors (n = 11)

species	**$[FcMTMA]^+$**		**FcMeOH**	
detector	**AD**	**MS**	**AD**	**MS**
t [s]	191.1 ±0.2	190.2 ±0.3	450.2 ±0.5	452.3 ±0.8
A [pA·s or counts·s]	$156 \cdot 10^1 \pm 2 \cdot 10^1$	$58 \cdot 10^3 \pm 4 \cdot 10^3$	$163 \cdot 10^2 \pm 2 \cdot 10^2$	$37 \cdot 10^3 \pm 4 \cdot 10^3$
H [pA or counts]	893 ±4	$32 \cdot 10^3 \pm 2 \cdot 10^3$	$409 \cdot 10^1 \pm 3 \cdot 10^1$	$10 \cdot 10^3 \pm 1 \cdot 10^3$

Detectability characteristics of the DDC (CE-AD/MS)

Another point addressed in this study was the detectability within the new DDC. Before the first measurements, the injection time was optimized to get the maximum peak height with no plateau formation for the lowest LODs. The LODs of the dual detection method (CE-AD/MS) were determined for an S/N of 3 and are listed in Table F.2. The LODs were up to a factor of 60 for $[FcMTMA]^+$ and 1357 for FcMeOH lower for the AD than for the MS. It was striking that the differences in LODs between the two detectors were higher for FcMeOH than for $[FcMTMA]^+$. This finding was because $[FcMTMA]^+$ was already positively charged and can therefore be easily detected by MS. Therefore, for $[FcMTMA]^+$ the differences between the LODs of the AD and the MS were smaller. In contrast, the LODs for FcMeOH were much lower for the AD compared to the MS, as FcMeOH has a poor ionization efficiency. If the substances can be detected with MS and AD, the AD has usually the lower LODs. To illustrate the excellent detectability of the AD in comparison to the MS, we performed measurements with model analyte concentrations near the LODs of the MS. The corresponding electropherograms are depicted in Fig. F.4. From the electropherograms, one could see that the S/Ns were relatively low for the MS and much higher for the AD. Nevertheless, it was possible to identify the substances using MS.

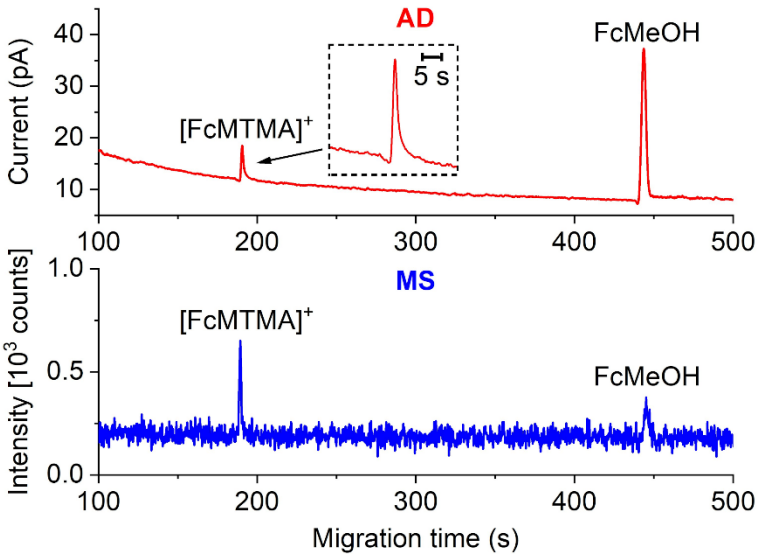

Figure F.4. CE-AD/MS measurement of the model mixture containing 1 µM $[FcMTMA]^+$ and 10 µM FcMeOH in BGE. The electropherograms on top were recorded with AD (red) and at the bottom with MS (blue). Experimental parameters: the conditions are as in Fig. F.2

To see if there was a decrease in detectability for the DDC (CE-AD/MS) due to the CE flow splitting, we determined the LODs for the single-detection arrangements (CE-AD and CE-MS) as well. For a fair comparison, we optimized the injection times of the single-detection measurements to get maximum sensitivity. The other experimental parameters were identical to the DDC. The calculated LODs for the single-detection arrangements are also listed in Table F.2. Within the scope of measurement precision, the LODs of the single-detection arrangements and the DDC could be considered identical. From this, it can be concluded that there was no loss in detectability for the DDC due to the CE flow splitting.

Table F.2. CE-AD/MS, CE-AD, and CE-MS studies for the determination of the LODs and the corresponding error for $[FcMTMA]^+$ and FcMeOH (n = 3)

species	**[FcMTMA]+**		**FcMeOH**	
detector	**AD**	**MS**	**AD**	**MS**
LODs (CE-AD/MS) [nM]	10 ±2	$6 \cdot 10^2 \pm 1 \cdot 10^2$	14 ±3	$19 \cdot 10^3 \pm 5 \cdot 10^3$
LODs (CE-AD) [nM]	9 ±3	-	14 ±4	-
LODs (CE-MS) [nM]	-	$5 \cdot 10^2 \pm 2 \cdot 10^2$	-	$13 \cdot 10^3 \pm 4 \cdot 10^3$

[a] The LODs were calculated for an S/N of 3

Determination of trimetazidine

To convict doping offenders, powerful analytical methods are needed to identify and quantify doping agents. Our new DDC has the potential to be used for that purpose as it has high sensitivity due to AD and excellent selectivity due to MS. A possible practical application for the complementary use of AD and MS is the determination of TMZ, which is usually used as a heart medication. However, its performance-enhancing effect is sometimes misused as a doping agent in competitive sports. Before the first measurement with the DDC, the electrochemical behavior of TMZ was characterized by utilizing cyclic voltammetry. The corresponding cyclic voltammograms are shown in Fig. S.F.2. For TMZ, an oxidative current was detectable above 0.8 V. According to the cyclic voltammogram, a detection potential of 1.3 V was chosen for the AD of TMZ. Additionally, the cyclic voltammogram showed the huge potential window of the ACN-based BGE. The electropherograms for the measurements with the DDC are shown in Fig. F.5.

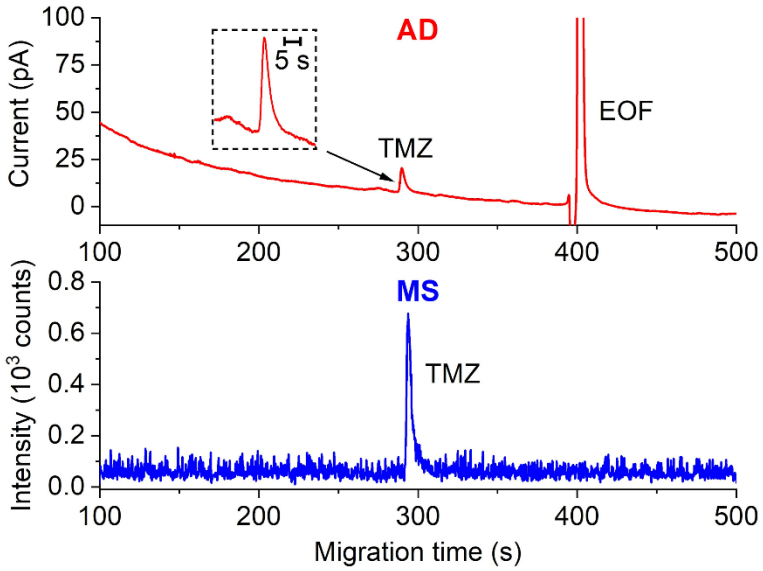

Figure F.5. CE-AD/MS measurements of 1.25 µg/ml trimetazidine (TMZ) in BGE with 10% MeOH as sample solution. The electropherograms on top were recorded with AD (red) and at the bottom with MS (blue). Experimental parameters: detection potential AD 1.3 V (vs. Ag/AgCl) and extracted ion electropherograms for TMZ (m/z 267). The other conditions are as in Fig. F.2

It was found that TMZ could be detected with both detectors. TMZ could be identified with MS, and the m/z 267 of the protonated TMZ species was used for the data evaluation. Furthermore, under the used conditions TMZ was positively charged because it migrated before the EOF. In these experiments, MeOH was used as an EOF marker, which was added to the sample solution to increase the solubility of TMZ.

However, only the AD was able to detect the added MeOH because it showed an anodic signal. The time-of-flight MS showed a too low sensitivity for m/z below 50. The depicted electropherograms (Fig. F.5) were recorded for a TMZ concentration of 1.25 µg/ml. It could be derived from the measurements that the S/Ns for the AD were higher than for the MS. This finding was supported by the LODs, which were 0.022 ±0.004 µg/ml for the AD and 0.6 ±0.2 µg/ml for the MS. Therefore, the AD had about 27 times lower LODs than the MS. As TMZ belongs to the list of prohibited substances by the World Anti-Doping Agency categorized under section S 4.4, the minimum required performance limit for the analytical method is 10 ng/ml in urine [32]. This is already in the order of magnitude of the LODs of the DDC. The DDC (CE-AD/MS) should reach the required performance limit with an appropriate preconcentration step included in a sample pretreatment protocol.

4.3.4 Conclusion

In this manuscript, a novel DDC for CE consisting of an AD and a MS was described for the first time. For this detector combination with two destructive detectors, a serial detector arrangement was not possible. Hence, the CE flow was split with a FS so that the detectors could be placed in parallel to each other.

In a proof-of-concept study, we could show that the new DDC worked as the model substances could be detected at both detectors. By adjusting the height difference between AD and MS, it was possible to synchronize the detector responses. The simultaneous detection of the analytes was also an advantage over traditional DDCs with a serial detector arrangement that usually has a time offset between the detectors. It could be shown that the weaknesses of the individual detectors (AD and MS) were compensated by the complementary use of AD and MS. The AD was the method of choice for the quantification as it was found that the reproducibility of the peak areas and heights was much better for the AD than for the MS. The RSDs of both parameters were in the range of about 1% for the AD and about 10% for the MS (concentration level 0.1 mM $[FcMTMA]^+$ and 0.5 mM FcMeOH). Additionally, for our used model system, it was found that the LODs for the AD were more than three orders of magnitude lower than for the MS (calculated from the DDC LODs of FcMeOH, listed in Table F.2). It has to be mentioned that the LODs of the AD depend very much on the electrochemical properties of the analyte. In contrast, the MS was the method of choice for identifying the compounds by means of the mass spectra. Furthermore, no loss in detectability was found due to the splitting as the LODs for the DDC and the single detection arrangements were identical.

Provided that the analytes are electrochemically active and detectable with MS, the DDC has the potential to solve many analytical problems. The DDC is especially interesting for applications in fields like pharmacy, environmental research, and medicine because low amounts of analytes could be precisely quantified and identified due to the complementary use of AD and MS. The practical application of the method was demonstrated by determining the doping agent TMZ. It was possible to quantify TMZ with AD and to identify the substance with MS. Overall, in this study, the potentials of the two destructive detectors (AD and MS) could be combined in an attractive DDC.

4.3.5 Supporting Information

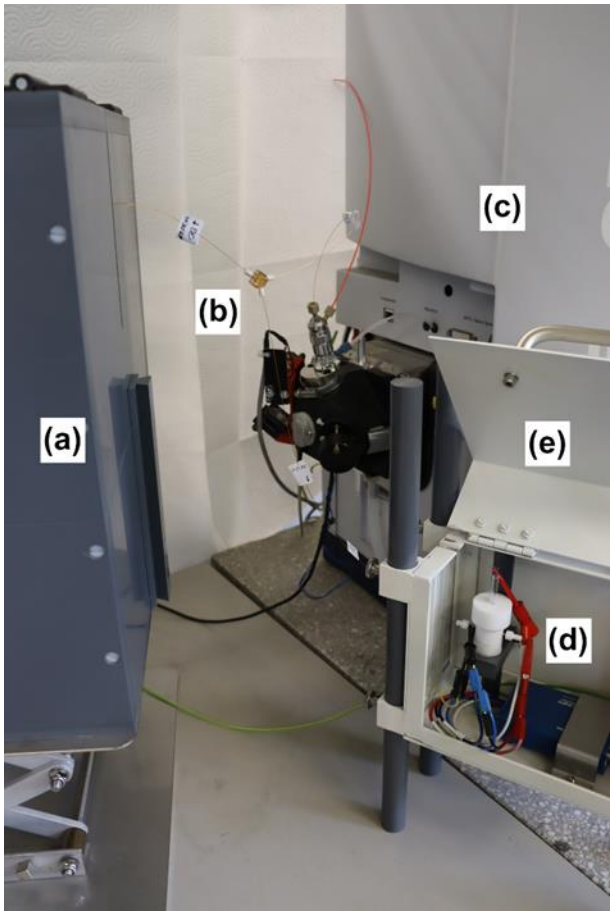

Figure S.F.1. Close-up view showing the main components of the CE-AD/MS setup: Backside of the laboratory-constructed CE device (a), flow splitter (b), MS (c), AD (d), and Faraday cage with integrated stand (e)

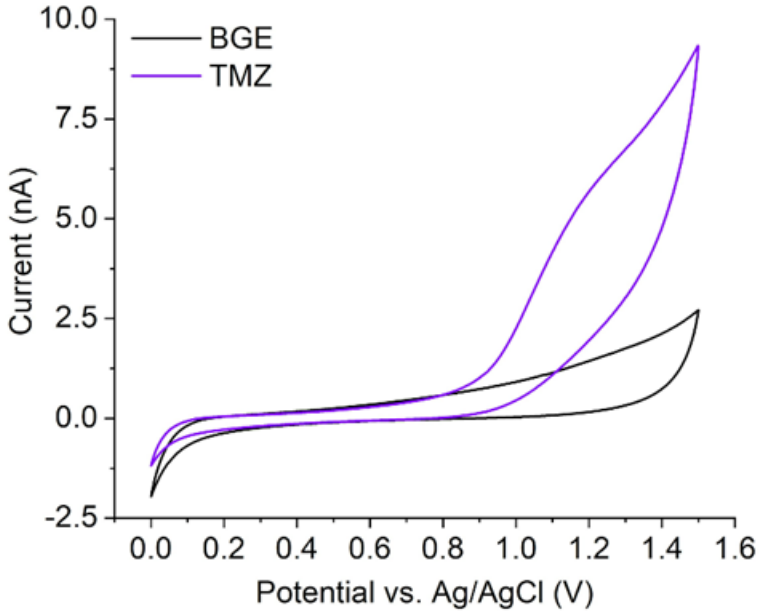

Figure S.F.2. Cyclic voltammograms of BGE (black) and 0.1 mM TMZ in BGE (purple). Experimental parameters: same electrodes as for AD, scan rate 50 mV/s

References

1. Beutner A, Herl T, Matysik F-M. Selectivity enhancement in capillary electrophoresis by means of two-dimensional separation or dual detection concepts. Anal Chim Acta. 2019;1057:18–35.
2. Opekar F, Stulík K. Some important combinations of detection techniques for electrophoresis in capillaries and on chips with emphasis on electrochemical principles. Electrophoresis. 2011;32:795–810.
3. Jorgenson JW, Lukacs KD. Zone electrophoresis in open-tubular glass capillaries. Anal Chem. 1981;53:1298–302.
4. Furter JS, Boillat M-A, Hauser PC. Low-cost automated capillary electrophoresis instrument assembled from commercially available parts. Electrophoresis. 2020;41:2075–82.
5. Ramos-Payán M, Ocaña-Gonzalez JA, Fernández-Torres RM, Llobera A, Bello-López MÁ. Recent trends in capillary electrophoresis for complex samples analysis: A review. Electrophoresis. 2018;39:111–25.
6. Voeten RLC, Ventouri IK, Haselberg R, Somsen GW. Capillary electrophoresis: trends and recent advances. Anal Chem. 2018;90:1464–81.
7. Wallingford RA, Ewing AG. Capillary zone electrophoresis with electrochemical detection. Anal Chem. 1987;59:1762–6.
8. Sloss S, Ewing AG. Improved method for end-column amperometric detection for capillary electrophoresis. Anal Chem. 1993;65:577–81.
9. Holland LA, Lunte SM. Capillary electrophoresis coupled to electrochemical detection: a review of recent advances. Anal Commun. 1998;35:1–4.
10. Matysik F-M. End-Column Electrochemical Detection for Capillary Electrophoresis. Electroanalysis. 2000;12:1349–55.
11. Holland LA, Chetwyn NP, Perkins MD, Lunte SM. Capillary Electrophoresis in Pharmaceutical Analysis. Pharm Res. 1997;14:372–87.
12. Riekkola M-L. Recent advances in nonaqueous capillary electrophoresis. Electrophoresis. 2002;23:3865–83.
13. Matysik F-M. Application of non-aqueous capillary electrophoresis with electrochemical detection to the determination of nicotine in tobacco. J Chromatogr A. 1999;853:27–34.
14. Beutner A, Scherer B, Matysik F-M. Dual detection for non-aqueous capillary electrophoresis combining contactless conductivity detection and mass spectrometry. Talanta. 2018;183:33–8.

15. Olivares JA, Nguyen NT, Yonker CR, Smith RD. On-line mass spectrometric detection for capillary zone electrophoresis. Anal. Chem. 1987;59:1230–2.
16. Maxwell EJ, Chen DDY. Twenty years of interface development for capillary electrophoresis-electrospray ionization-mass spectrometry. Anal Chim Acta. 2008;627:25–33.
17. Issaq HJ, Janini GM, Chan KC, Veenstra TD. Sheathless electrospray ionization interfaces for capillary electrophoresis–mass spectrometric detection. J Chromatogr A. 2004;1053:37–42.
18. Wang L, Li Y, Chen D, Da Chen DY. Electrospray ionization stability and concentration sensitivity in capillary electrophoresis-mass spectrometry using a flow-through microvial interface. Electrophoresis. 2021;42:360–8.
19. Samskog J, Wetterhall M, Jacobsson S, Markides K. Optimization of capillary electrophoresis conditions for coupling to a mass spectrometer via a sheathless interface. J Mass Spectrom. 2000;35:919–24.
20. Beutner A, Cunha RR, Richter EM, Matysik F-M. Combining C4D and MS as a dual detection approach for capillary electrophoresis. Electrophoresis. 2016;37:931-5.
21. Francisco KJM, do Lago CL. A capillary electrophoresis system with dual capacitively coupled contactless conductivity detection and electrospray ionization tandem mass spectrometry. Electrophoresis. 2016;37:1718–24.
22. Huhn C, Ruhaak LR, Mannhardt J, Wuhrer M, Neusüß C, Deelder AM, et al. Alignment of laser-induced fluorescence and mass spectrometric detection traces using electrophoretic mobility scaling in CE-LIF-MS of labeled N-glycans. Electrophoresis. 2012;33:563–6.
23. Mironov GG, Clouthier CM, Akbar A, Keillor JW, Berezovski MV. Simultaneous analysis of enzyme structure and activity by kinetic capillary electrophoresis-MS. Nat Chem Biol. 2016;12:918–22.
24. Szarka M, Szigeti M, Guttman A. Imaging Laser-Induced Fluorescence Detection at the Taylor Cone of Electrospray Ionization Mass Spectrometry. Anal Chem. 2019;91:7738–43.
25. Zhang D, Li W, Zhang J, Tang W, Qian C, Feng M, et al. Study on urinary metabolic profile of phenylketonuria by micellar electrokinetic capillary chromatography with dual electrochemical detection-potential clinical application in fast diagnosis of phenylketonuria. Anal Chim Acta. 2011;694:61–6.
26. Jooß K, Scholz N, Meixner J, Neusüß C. Heart-cut nano-LC-CZE-MS for the characterization of proteins on the intact level. Electrophoresis. 2019;40:1061–5.

27. Pham TTT, Mai TD, Nguyen TD, Sáiz J, Pham HV, Hauser PC. Automated dual capillary electrophoresis system with hydrodynamic injection for the concurrent determination of cations and anions. Anal Chim Acta. 2014;841:77–83.
28. Sydes D, Kler PA, Hermans M, Huhn C. Zero-dead-volume interfaces for two-dimensional electrophoretic separations. Electrophoresis. 2016;37:3020–4.
29. Böhm D, Koall M, Matysik F-M. Dead volume-free flow splitting in capillary electrophoresis. Electrophoresis. 2022;43:1438–45.
30. Matysik F-M. Special aspects of detection methodology in nonaqueous capillary electrophoresis. Electrophoresis. 2002;23:400–7.
31. Matysik F-M. Experimental characterization of end-column electrochemical detection in conjunction with nonaqueous capillary electrophoresis. Anal Chem. 2000;72:2581–6.
32. WADA Science, MRPL Working Group. Technical Document – TD2022MRPL [Internet]. World Anti-Doping Agency; 2021 [updated 2021 October 6; cited 2022 October 25]. Available from: https://www.wada-ama.org/sites/default/files/ resources/files/td2022 mrpl_v1.0_final_eng.pdf

5 Summary

In this thesis, a novel DDC for CE consisting of an AD and a MS was developed. The presented DDC has an excellent complementarity because it combines the sensitivity of AD and the selectivity of MS in one method. Due to the destructive detection principle of both detectors (AD and MS), their serial arrangement was impossible. Therefore, the CE stream was divided into two parts utilizing a FS. This allowed the parallel positioning of the detectors. A model system consisting of an ACN-based BGE and different ferrocene derivatives was used for the whole project.

The development of the DDC was divided into three subprojects:

- Coupling of capillaries with various IDs
- Comparison of different FSs
- Characterization of the DDC and its practical application

For the realization of the new DDC, three capillaries had to be combined without dead volume. Since this is very complex, the linear coupling of two capillaries was investigated in the first subproject. A total of nine capillary combinations with partly different IDs (25, 50, and 75 µm) were tested. A commercially available capillary connector was used, whereby the injection and detection were performed at different sides of the capillary connector. Within this work, differences between non-fragmented and fragmented capillaries were predominately examined. With CFIA-C^4D, it could be shown that a flow resistance arose when two capillaries with identical ID were coupled. The flow resistance was particularly distinct for capillary combinations going from a larger to a smaller ID. The same effect was found with CE-UV. The migration behavior of the EOF marker was more affected by the coupling than the migration of the cationic species. It was concluded that this effect resulted from a mechanical resistance at the connection site. Furthermore, the peaks were compressed at the transition from a smaller to a larger ID, resulting in increased TPNs. The peak compression was visualized with a dye solution and a transparent capillary connector. For the capillary combination 25+50 µm, the signal intensity at the UV doubled due to the larger ID (doubled optical path length). In addition to the first experiences for the coupling of capillaries in the DDC, the linear coupling of capillaries had another advantage. It is often difficult to choose the best suitable capillary ID because injection, separation, and detection could have different requirements. Due to the approach with the capillary connector, it was possible to select the best suitable ID for each application individually.

In the second subproject, the continuous flow splitting, which was required for the technical implementation of the DDC, was investigated. For this purpose, two FSs with different geometry (T- and Y-shaped) were compared. Both FSs were commercially

available, user-friendly, resistant to ACN, and had a dead volume of just a few nL. The split ratio was approximately 50% for both FSs, whereby the reproducibility was slightly better for FSY. The split ratios were determined by CE-UV. By placing a C^4D directly in front of and behind the FS, it could be shown that there was no significant peak broadening due to the flow splitting. Additionally, the LODs in front of and behind the FS were identical. Therefore, the flow splitting was considered as almost dead volume free. Contrary to expectations, the geometry of the FS had no measurable influence on flow splitting. A capillary with an ID of 75 µm instead of 50 µm at the injection side (in front of the FS) achieved a higher sample loading of the capillary by similar sample zone lengths. This is especially interesting for trace analysis. In summary, it could be shown that flow splitting using commercially available FSs was a suitable method for establishing a DDC consisting of two destructive detectors.

In the third subproject, the final DDC (CE-AD/MS) was characterized using the two model substances, $[FcMTMA]^+$ and FcMeOH. The model substances could be detected at both detectors (AD and MS). By a simple adjustment of the height difference between AD and MS, it was possible to synchronize the migration times. This was an advantage over traditional DDCs with serial detector arrangement, where usually a time offset between the detectors occurs. Reproducibility measurements demonstrated that the RSDs for the peak area and peak height were approximately 1% for the AD. In comparison, the RSDs for both parameters were about 10% for MS. The LODs were up to three orders of magnitude lower for AD than for MS. The better reproducibility and lower LODs illustrated that the AD was much better suited for quantification than the MS. However, in contrast to AD it was possible to identify the substances with MS. There was no loss of detection power due to flow splitting as the LODs for the DDC were identical to the detectors coupled to CE individually. The practicability of the new dual detection method was demonstrated by determining the doping agent trimetazidine.

Overall, a new DDC for CE with a unique, parallel detector positioning was developed. Due to the excellent complementarity, the weaknesses of the MS could be compensated by the strengths of AD and vice versa. The new DDC is particularly interesting for pharmacy, environmental analysis, or medicine, as it can be used to quantify (AD) and identify (MS) minimal amounts of analytes simultaneously. In addition, complex sample mixtures can be separated by CE. The approach of continuous flow splitting using a FS could be also used to establish other dual detection concepts or for more sophisticated applications in CE.

Parallel to the development of the DDC, a user-friendly, miniaturized CE system was developed. Due to a compact design and several capillary passages, the CE device could be connected to different detectors. It had a novel capillary positioning system that

allowed the variable positioning of the capillary at the injection side. Injections could be carried out from sealed vials with micro inserts, which enabled the handling of very small sample volumes. Due to its flexibility, the new system is particularly interesting for research institutions.

6 Zusammenfassung in deutscher Sprache

Im Rahmen der Promotion wurde ein neues DDC bestehend aus einem AD und einem MS für die CE entwickelt. Dieses DDC hat eine hervorragende Komplementarität, da es die Sensitivität des AD und die Selektivität des MS in einer Methode vereint. Aufgrund des destruktiven Detektionsprinzips der beiden Detektoren war deren serielle Anordnung nicht möglich, weswegen der Fluss der Kapillarelektrophorese mittels eines FS geteilt werden musste. Für das gesamte Projekt wurde ein Modellsystem bestehend aus einem ACN basierten BGE und verschiedenen Ferrocen-Derivaten verwendet.
Die Entwicklung des DDC wurde in drei Teilprojekte unterteilt:

- Kopplung von Kapillaren mit verschiedenen IDs
- Vergleich verschiedener FSs
- Charakterisierung des DDC und dessen praktische Anwendung

Für die Realisierung des neuen DDC mussten drei Kapillaren totvolumenfrei gekoppelt werden. Aufgrund der Komplexität wurde in einem ersten Teilprojekt die lineare Kopplung von zwei Kapillaren betrachtet. Hierbei wurden im Speziellen die Unterschiede zwischen durchgehenden und gekoppelten Kapillaren untersucht. Für die Untersuchung wurden neun Kapillar-Kombinationen mit teils unterschiedlichen IDs (25, 50 und 75 µm) betrachtet. Für die Kopplung wurde ein kommerziell erhältlicher Kapillarverbinder verwendet, wobei Injektion und Detektion an unterschiedlichen Seiten des Kapillarverbinders stattfanden. Mittels CFIA-C^4D konnte gezeigt werden, dass bei der Kopplung von zwei Kapillaren mit identischem ID ein Fließwiderstand entsteht. Dieser Fließwiderstand war besonders ausgeprägt beim Übergang von einem größeren auf einen kleineren ID. Der gleiche Effekt konnte mittels CE-UV nachgewiesen werden. Das Migrationsverhalten des EOF Markers wurde dabei wesentlich stärker beeinträchtigt als das des Kations. Es wurde geschlussfolgert, dass dieser Effekt aus einer mechanischen Hinderung an der Verbindungsstelle resultiert. Im Gegensatz dazu trat bei Übergang von einem kleineren auf einen größeren ID eine Kompression der Peaks auf, welche mittels einer Farbstofflösung visualisiert wurde und zu einer Erhöhung der TPN führte. Ebenfalls kam es beim Übergang von einer 25 µm auf eine 50 µm Kapillare zu einer Verdopplung des Signalintensität am UV-Detektor aufgrund des größeren ID. In diesem Teilprojekt konnten erste Erkenntnisse für das DDC gewonnen werden. Darüber hinaus wurde ein weiterer Anwendungsbereich für die Kapillarverbinder gefunden. Häufig ist es schwierig, den richtigen ID zu wählen, da Injektion, Trennung und Detektion unterschiedliche Anforderungen an den ID haben. Durch den Ansatz mit den Kapillarverbindern war es möglich, den jeweils passenden ID zu wählen.

Im zweiten Teilprojekt wurde die kontinuierliche Flusssplittung, welche für die technische Umsetzung des DDC benötigt wurde, untersucht. Hierzu wurden zwei FSs mit unterschiedlicher Geometrie (T- und Y-förmig) verglichen. Beide FSs waren kommerziell erhältlich, sehr einfach in der Handhabung, beständig gegenüber ACN und hatten ein sehr geringes Totvolumen von nur wenigen nL. Mittels CE-UV wurde das Split-Verhältnis bestimmt. Dieses betrug für beide FSs annähernd 50%, wobei die Reproduzierbarkeit für FSY etwas besser war. Durch die Platzierung eines C^4D unmittelbar vor und nach dem FS konnte gezeigt werden, dass es aufgrund der Flusssplittung zu keiner signifikanten Bandenverbreitung kam. Auch die LODs vor und nach dem FS waren identisch, weswegen die Flusssplittung als nahezu totvolumenfrei bezeichnet wurde. Entgegen den Erwartungen hatte die Geometrie des FS keinen nachweisbaren Einfluss auf die Flusssplittung. Durch die Verwendung einer Kapillare mit einem ID von 75 µm anstelle von 50 µm auf der Injektionsseite (vor dem FS) konnte bei gleicher Probenzonenlänge eine höhere Beladung der Kapillare erreicht werden. Zusammengefasst konnte im zweiten Teilprojekt gezeigt werden, dass die Flusssplittung mittels kommerziell erhältlicher FS für die Etablierung eines DDCs bestehend aus zwei destruktiven Detektoren geeignet ist.

Im dritten Teilprojekt wurde das finale DDC (CE-AD/MS) mittels zweier Modelsubstanzen ($[FcMTMA]^+$ und FcMeOH) charakterisiert. Die Modellsubstanzen konnten an beiden Detektoren (AD und MS) detektiert werden. Durch eine Absenkung des AD gegenüber des MS war es möglich, die Migrationszeiten auf einfache Weise zu synchronisieren. Dies war ein Vorteil gegenüber den etablierten DDC mit serieller Detektoranordnung, wo zwangsläufig ein Zeitversatz zwischen den Detektoren auftritt. Aus Reproduzierbarkeitsmessungen ging hervor, dass die RSD für die Peakfläche und Peakhöhe für den AD ungefähr 1% betrug, wohingegen die RSD für das MS bei circa 10% lag. Die LODs waren für den AD um bis zu drei Größenordnungen geringer als für das MS. Die bessere Reproduzierbarkeit und die niedrigeren Nachweisgrenzen zeigten, dass der AD wesentlich besser für die Quantifizierung geeignet war als das MS. Mit dem MS war es im Gegensatz zum AD allerdings möglich, die Substanzen zu identifizieren. Aufgrund der Flusssplittung kam es zu keinem Verlust der Nachweisstärke, da die LODs für das DDC und die einzeln mittels CE gekoppelten Detektoren identisch waren. Die Praxistauglichkeit der neuen Dualdetektionsmethode wurde durch die Bestimmung des Dopingmittels Trimetazidin gezeigt.

Zusammengefasst konnte im Rahmen der Promotion eine neue Dualdetektionsmethode für die CE mit einer bisher einmaligen, parallelen Anordnung der Detektoren entwickelt werden. Aufgrund der hervorragenden Komplementarität konnten die Schwächen des einen Detektors durch die Stärken des anderen Detektors ausgeglichen werden. Das

neue DDC ist besonders für die Pharmazie, Umweltanalytik oder Medizin interessant, da mit ihm sehr geringe Analytmengen hochpräzise quantifiziert (AD) und gleichzeitig identifiziert (MS) werden können. Zudem können durch die vorgeschaltete CE komplexe Probengemische getrennt werden. Der Ansatz der kontinuierlichen Flusssplittung mittels eines FS kann auch für die Etablierung weiterer DDCs oder für andere Anwendungen in der CE verwendet werden.

Parallel zur Entwicklung des DDCs wurde ein benutzerfreundliches, miniaturisiertes Kapillarelektrophorese-System entwickelt, welches ein neuartiges Kapillarpositionierungssystem besitzt. Aufgrund der kompakten Bauweise und den zahlreichen Kapillarausgängen war es möglich das CE System mit den unterschiedlichsten Detektoren zu koppeln. Durch die variable Positionierung der Kapillare konnten Injektionen aus verschlossenen Injektionsgefäßen mit Mikroeinsätzen durchgeführt werden, was die Handhabung kleiner Probenmengen ermöglichte. Das neue System ist aufgrund seiner Flexibilität besonders für Forschungseinrichtungen interessant.

7 Appendix

Development of a user-friendly, miniaturized CE device with a novel capillary positioning concept for research purposes

General remarks

The CE device was developed by the author based on previous versions of miniaturized CE devices [1, 2]. The project was technically implemented by the mechanical and electronic workshops of the Faculty of Chemistry and Pharmacy of the University of Regensburg. Andreas Graf, Thomas Meyer, Eva Piendl, Matthias Kainz, and Thomas Höfele (mechanical workshop) manufactured most of the mechanical parts of the CE device. Peter Fuchs and Achim Stark (electronic workshop) built the electronic components and programmed the software for the CE device. The project was done under the supervision of Prof. Dr. Frank-Michael Matysik. The CE device was repeatedly tested by the author and revised by the workshops. In this thesis, the final version of the CE device is described.

Motivation

Commercial CE systems are often not suitable for the individual requirements of research institutes. Due to their closed design, permanently installed detectors, large dimensions, predefined injection positions, and a software with only few variation parameters regarding the hardware, it is often difficult to realize new projects or ideas. However, most laboratory-constructed devices have a lack of user-friendliness and reproducibility. Therefore, in this thesis a user-friendly and miniaturized CE system with a novel capillary positioning concept for research purposes was developed, based on the experiences with different CE systems (commercially available and laboratory-constructed). The CE device was already used for the development of the novel DDC (CE-AD/MS). The CE system is described in detail in the next sections.

Overall setup

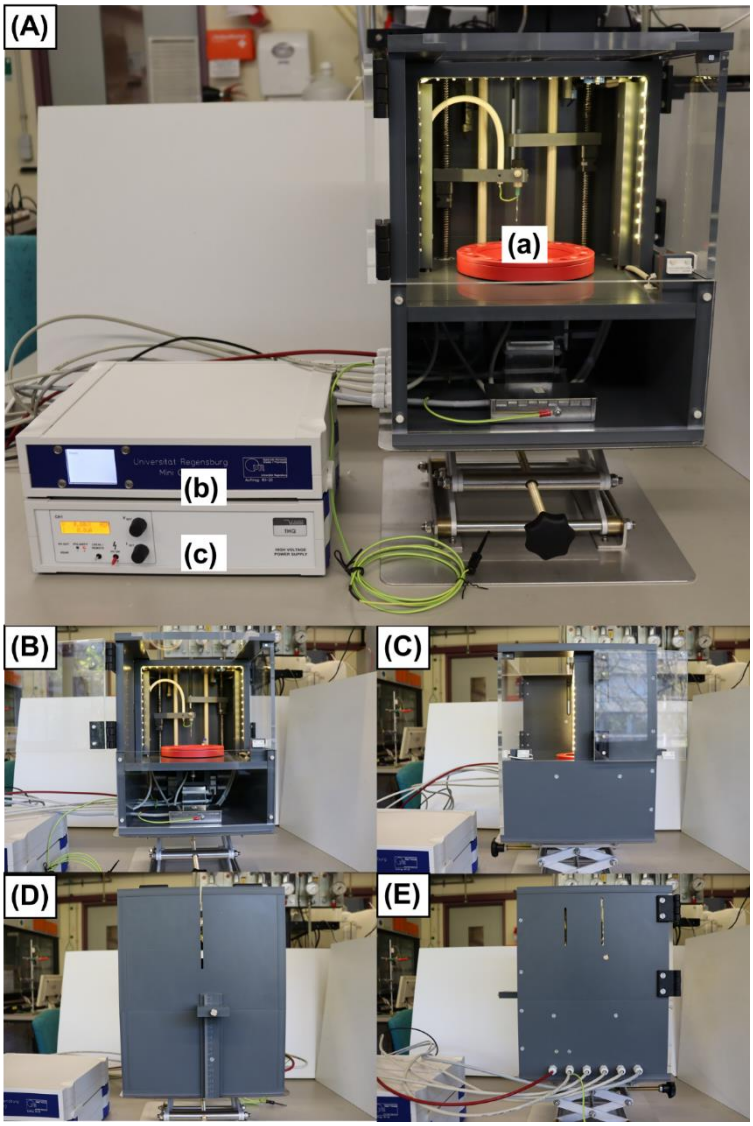

Figure G.1. Photograph (A) of the laboratory-constructed CE device showing the main components: Autosampler (a), electronics (b), and the high-voltage power supply (c). Photographs (B-E) showing the CE device from different perspectives: Front view (B), view from the right side (C), back view (D), and view from the left side (E)

Figure G.1 shows the laboratory-constructed CE device. The overall setup consisted basically of three components, an autosampler (Fig. G.1A, a), a box containing the control electronics (Fig. G.1A, b), and a high-voltage power supply (Fig. G.1A, c). The autosampler unit was the central component. It is shown from different perspectives in Fig. G.1B-E. The autosampler had dimensions of 30/30/37.5 cm (length/width/height). The housing of the CE device was made of 1 cm thick polyvinyl chloride plates. The device had three doors made of polymethyl methacrylate (front, right side, and top)

enabling an excellent accessibility. All doors were equipped with safety switches that immediately stopped the high-voltage source when the door was opened. The housing of the CE device was additionally provided with four capillary passages (left, right, back, and top) to guide the capillary to the detector and to achieve the highest possible flexibility in detector alignment. For safety reasons, the slits were very tight, that nobody could grab inside the CE system. In the upper part of the autosampler, all moveable parts of the CE device were located. In the lower part only the engines for the propulsion of the arms were placed. The CE device was equipped with LED illumination, which simplifies the working within the CE system. A holder for the outlet vial was located at its backside (Fig. G.2A). The holder was variable in height. The zero point of the graduation refers to the height of the sample tray. The CE device was also equipped with a separate grounding cable for the outlet vial to close the electrophoretic circuit. The purpose-made circuit boards to control the CE system were placed in a separate box (Fig. G.1A, b) to protect the sensitive electronics from voltage flashovers. The positive high-voltage source T1CP 300 304p (Fig. G.1A, c) was purchased from ISEG (Radeberg, Germany). With this, it was possible to apply high-voltages up to 30 kV.

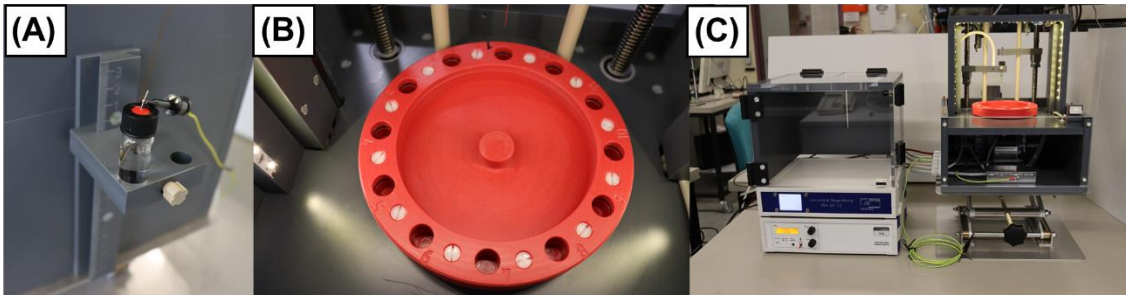

Figure G.2. Close-up views showing the holder for the outlet reservoir (A), the sample tray (B), and the removable autosampler cover (C)

The sample tray is depicted in Fig. G.2B. It has an outer diameter of 15 cm and a capacity for twelve ND 11 vials (1.5 mL, 11.6/32.0 mm, radius/height). These vials are standard for liquid chromatography and gas chromatography. The vials were held in position by rubber seals placed inside the sample tray. By tightening the screws in the sample tray, the rubber seals were pressed against the vials. Figure G.2C illustrates the removeable cover of the autosampler with the three doors. This feature was very useful for the installation of capillaries or for the exchange of wearing parts.

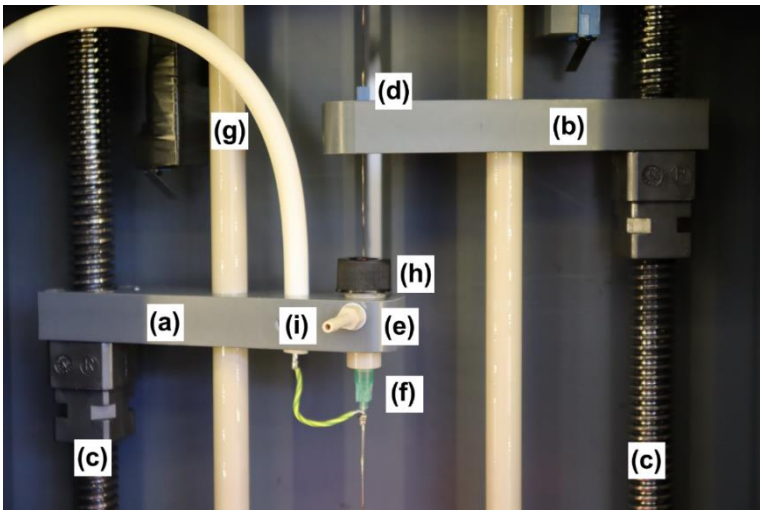

Figure G.3. Close-up view showing the most important parts of the autosampler: cannula arm (a), capillary arm (b), threaded rods for the movement of the arms (c), fitting for the fixation of the capillary (d), funnel-shaped capillary holder (e), cannula (f), high-voltage cable (g), screw cap with integrated septum (h), and gas connection (i)

The most innovative part of the CE device was the autosampler which is depicted in Fig. G.3. The cannula arm (Fig. G.3, a) and the capillary arm (Fig. G.3, b) were connected to different threaded rods (Fig. G.3, c) driven by motors placed in the lower part of the CE device. Both arms were moveable up and down and could be controlled individually. The capillary arm (Fig. G.3, b) was used to move the capillary. The capillary was guided through a Union Assy MicroTight P-720 made of polyether ether ketone, which was placed inside the capillary arm. The capillary was fixed in position by a screw with integrated fitting (NanoPort Nut 6-32 360 µm F-124HX, Fig. G.3, d) from IDEX Health & Science (Oak Harbor, USA). The cannula arm was positioned below the capillary arm to the threaded rod on the left side. A funnel-shaped and gas-tight holder for the cannula (Fig. G.3, e) was attached to the cannula arm. The cannula 0.80/40 mm (diameter/lengths, Fig. G.3, f) from B. Braun (Melsungen, Germany) was connected to the holder via a bayonet lock which was milled into the lower part of the cannula holder. Due to this bayonet lock, the cannula could easily be replaced by a new one. The cannula was used to pierce the silicone septum, as a guiding system for the capillary, and as an electrode for the high-voltage power supply. The cannula was connected to the high-voltage source via a specially insulated cable (Fig. G.3, g). On top, the cannula holder was equipped with a screw cap ND 13 LC41.1 with integrated silicone septum E158.1 from Carl Roth (Karlsruhe, Germany, Fig. G.3, h). The capillary was guided through the middle of the septum, into the funnel-shaped cannula holder, and through the attached cannula. The disassembled cannula holder is depicted in Fig. G.4. An excess pressure could be applied via the gas connection at the cannula

holder (Fig. G.3, i). Due to the screw cap with integrated septum, the cannula holder was sealed at the top. Therefore, the end of the cannula was the only opening for the gas, which allowed the flushing of the capillaries or the hydrodynamic injection when the end of the cannula was immersed in a vial equipped with septum. A nitrogen gas bottle with a reducing valve was used for the application of gas. The application of excess pressure at the injection site for the flushing of the CE system, the capillary installation, and the functionality of the autosampler are described in detail in separate chapters.

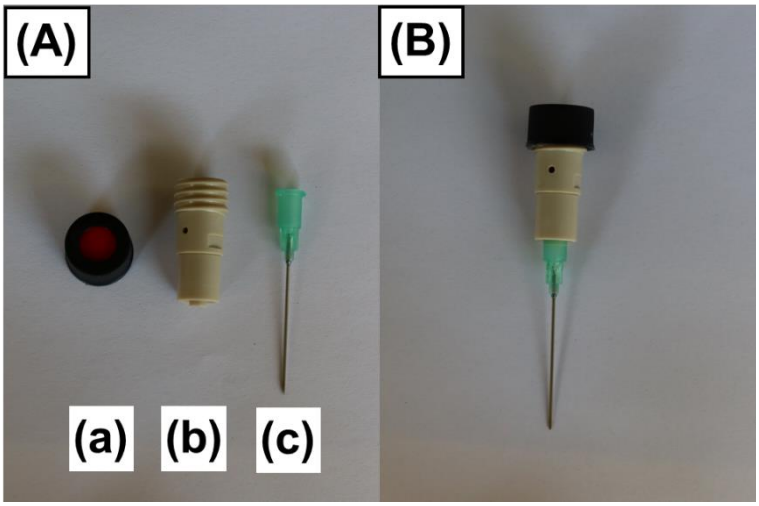

Figure G.4. Disassembled (A) and assembled (B) cannula holder, consisting of a screw cap with integrated septum (a), funnel-shaped cannula holder (b), and cannula (c)

Software

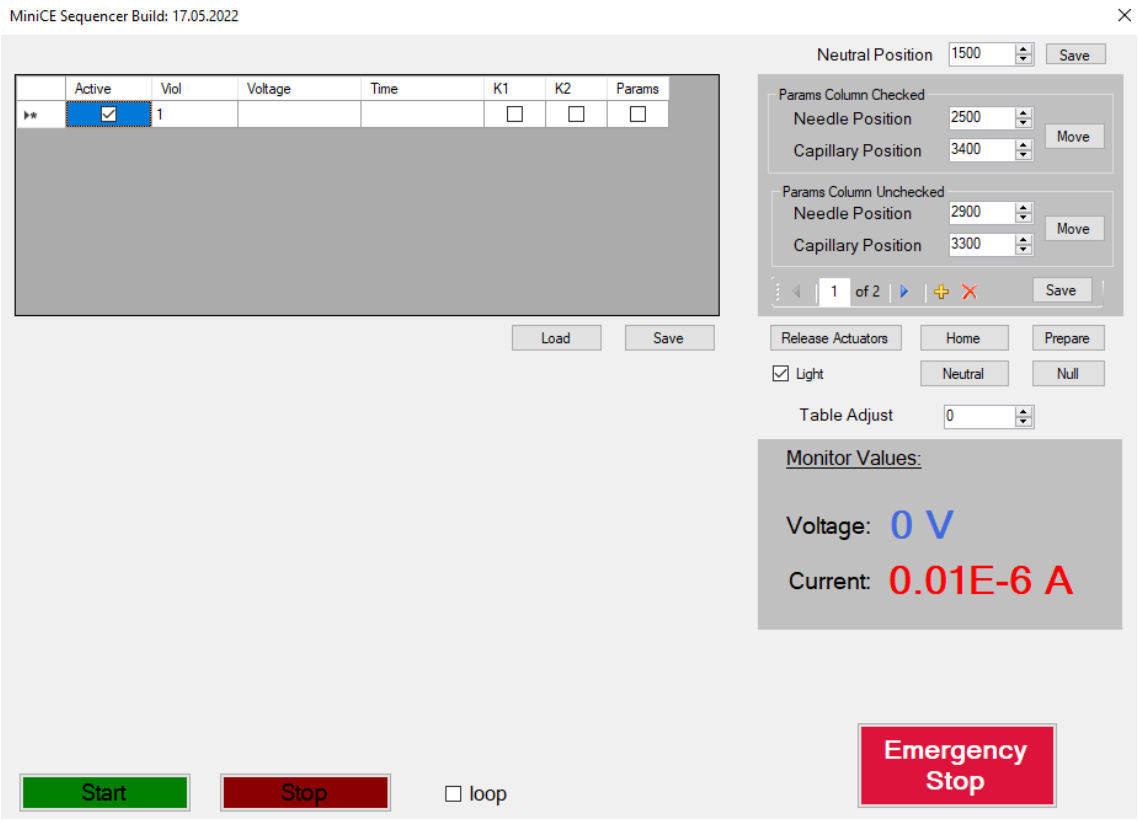

Figure G.5. User interface of the laboratory-constructed CE-device

The whole CE device was controlled by a Visual Basic-based software. The corresponding user interface is shown in Fig. G.5. The software worked through the run sequence line by line, from the top to the bottom. For injection and separation, two separate lines were needed. Due to the individual programming of the run sequence, it was possible to implement rinsing steps. In this section, the details of the software and its utilization are described.

Table G.1. Description of the different software functions

Symbol/Button	Comment
Active	Checked: The line of the run sequence was processed. Unchecked: The line was bypassed, and the software continued with the next activated line of the run sequence.
Vial	Position of the vial in the sample tray (1 – 12), which was approached by the autosampler.
Voltage	Applied high-voltage (0 – 30 kV)
Time	Duration of the respective line.
K1 and K2	Checked: The remote start of external detectors was triggered. Unchecked: The external detectors must be started manually.
Params	Checked: The arms for the cannula and capillary moved to the position “Params Column Checked” (injection position). Unchecked: The arms moved to the position “Params Column unchecked” (separation position).
Load and Save	The run sequence could be saved and loaded.
Neutral Position	The neutral position (position of the arms when the sample tray rotates) could be adjusted individually to the height of the used vials. The position could be adjusted by entering numerical values in the respective field. For higher values, both arms (capillary and cannula) moved down and vice versa. The height difference between the two arms was for all neutral positions 2.5 cm.
Params Column Checked	The position “Params Column Checked” was used for the injection. The positions of the capillary and cannula arm could be adjusted individually by entering numerical values in the respective fields. For higher values the arms moved down and vice versa.
Params Column Unchecked	The position “Params Column Unchecked” was used for the separation. The positions of the capillary and cannula arm could be adjusted individually by entering numerical values in the respective fields. For higher values the arms moved down and vice versa.
Move	The capillary and cannula arm moved to the position “Params Column Checked” (injection) or to the position “Params Column Unchecked” (separation).
Release Actuators	The capillary and cannula arms moved up until they reached the stop switches.
Home	The capillary arm, cannula arm, and sample tray were readjusted.
Prepare	Between both arms a space (4 cm) was created, which simplified the installation of a new capillary.
Neutral	The capillary and cannula arms moved to the neutral position (position of the arms when the sample tray rotated). The distance between both arms was 2.5 cm.
Null	Starting from the prepare position the cannula arm moved upwards until the distance of 2.5 cm between the arms was reached.
Light	Checked: The light was on. Unchecked: The light was off.

Table Adjust	The table position could be adjusted individually so that the cannula pierced exactly through the middle of the septum. The position could be adjusted by entering numerical values in the respective field.
Monitor Values	Displayed the applied voltage and the current. The values were also shown on the display of the high-voltage source.
Start	The run sequence started with the first activated line.
Stop	The actual processed line of the run sequence was finished, and the next line was not started.
loop	Checked: The run sequence was restarted after completion. Unchecked: The run sequence was stopped after completion.
Emergency Stop	The high-voltage and the run sequence were immediately stopped.

Installation and flushing of the capillary

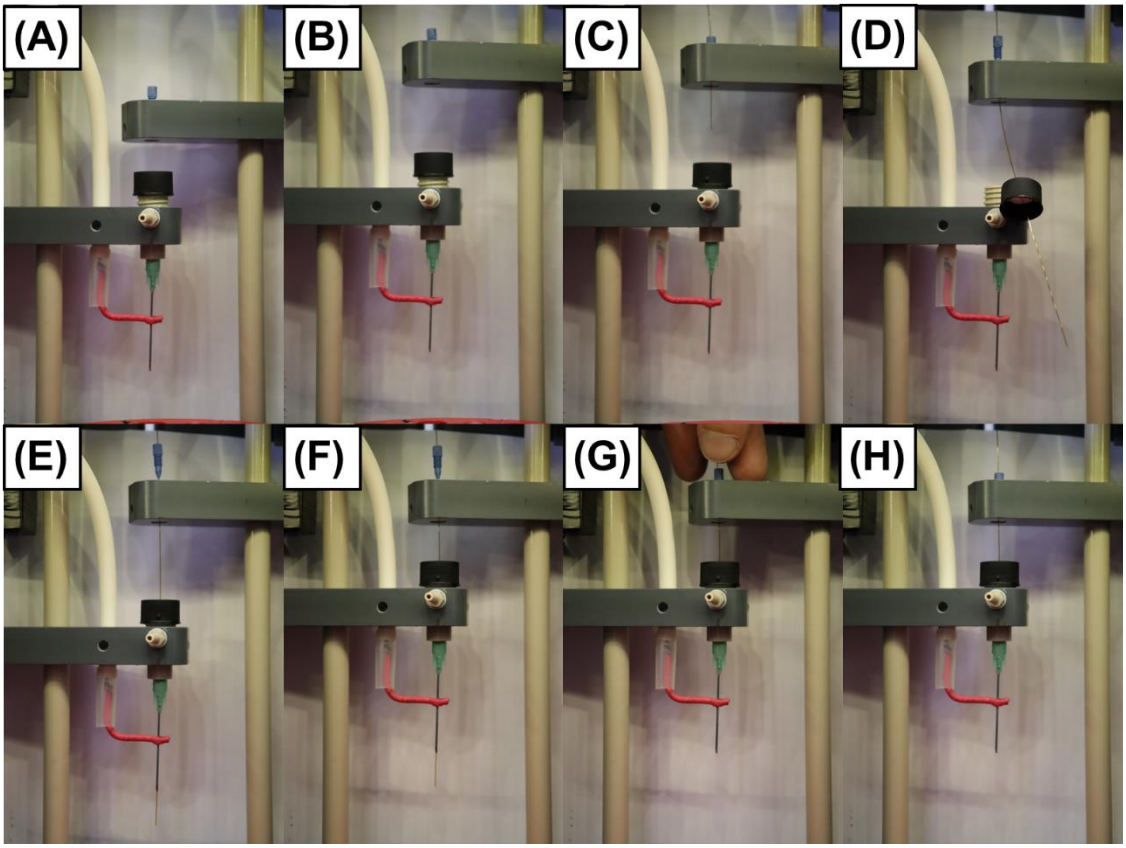

Figure G.6. Photo series (A – H) showing the capillary installation procedure

Figure G.6A shows the starting point without capillary. For the capillary installation, the button “Prepare” was pressed in the software and the capillary arm moved up. The resulting gap (4 cm) between the arms facilitated the installation of the capillary (Fig. G.6B). First, the capillary was guided through the NanoPort Nut and Union

Assy MicroTight attached to the capillary arm (Fig. G.6C). Then the capillary was guided through the silicon septum placed in a screw cap into the cannula holder (Fig. G.6D). Due to the funnel-shape of the cannula holder, the capillary was also guided directly through the attached cannula until the capillary protruded a few millimeters from the tip of the cannula (Fig. G.6E). Afterward, the button “Null” was pressed and the cannula arm moved up until the distance of the neutral position (2.5 cm) was reached (Fig. G.6F). The screw cap with the septum was tightened, and the capillary was pulled upwards until it was about 2 mm deep inside the cannula. The capillary was fixed by tightening the NanoPort Nut at the capillary arm (Fig. G.6G). Since the capillary arm was the only point where the capillary was fixed, the capillary was moveable up and down independently of the cannula arm. The distance (2.5 cm) between the capillary and cannula holder was kept constant during the injection process. Therefore, the capillary was protected inside the cannula (Fig. G.6H).

For flushing the capillary, the autosampler was placed at the injection position (the capillary tip was immersed into the BGE, and the cannula pierced the septum but was still in the gas phase above the BGE) and an excess pressure was applied at the cannula holder (Fig. G.7, a). Due to the gas-tight cannula holder, the gas (nitrogen) went through the tip of the cannula into the gas phase of the closed vial and pushed the solution through the capillary. This feature allowed the flushing of the capillary without disassembling the capillary from the autosampler or the detector.

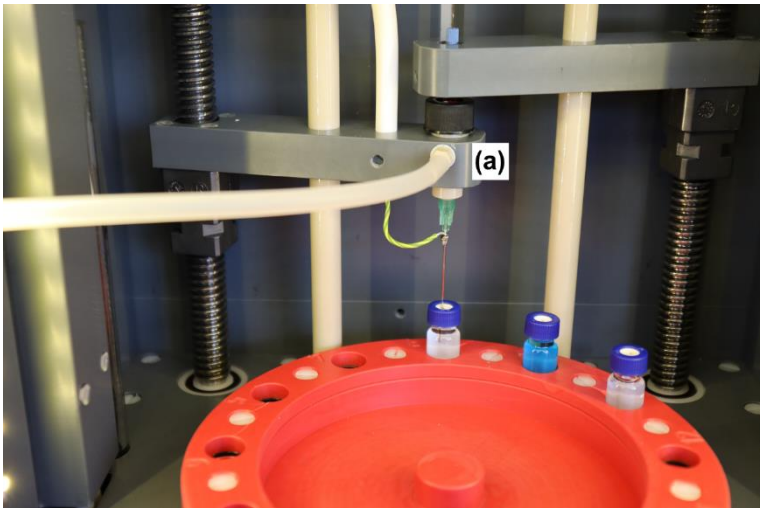

Figure G.7. Photograph showing the flushing of a capillary via the application of an excess pressure at the gas connection at the funnel-shaped cannula holder (a). The gas (nitrogen) flowed through the cannula into the gas phase of the vial and pressed the BGE through the capillary

Innovative capillary positioning concept

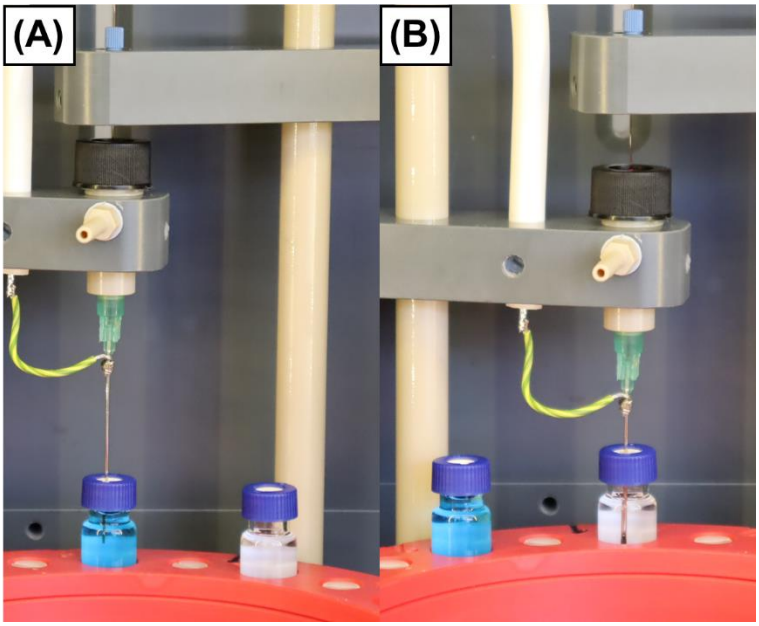

Figure G.8. Photographs showing the different positions for injection and separation. At the injection position (A), only the capillary touched the sample solution (blue colored) and the cannula stopped in the gas phase beyond the sample solution to minimize sample carryover. At the separation position (B), the cannula was immersed into the BGE for electrical contact and the capillary protruded a few millimeters from the cannula tip

The innovative capillary positioning concept was based on a capillary arm and a cannula arm that could be positioned independently of each other. It was possible to set a position for the injection ("Params Column Checked") and a different position for the separation ("Params Column Unchecked"). For the injection from a standard sample vial, the cannula pierced the septum but stopped inside the gas phase above the sample solution. Only the capillary was immersed into the sample solution (colored blue, Fig. G.8A). Since the cannula did not come into contact with the sample solution, the risk of sample carryover was minimized. In the separation position, the cannula dipped into the BGE to establish electrical contact with the BGE. The capillary protruded about 2 mm from the tip of the cannula (Fig. G.8B). Both positions (capillary and cannula arm) could be programmed by entering numbers at the appropriate places in the user interface. The capillary and cannula arms were lifted for smaller numbers, and vice versa. Usually, for the injection from standard ND 11 vials (neutral position 1500), the positions of the arms were 2800 (capillary) and 2000 (cannula). The standard positions for the separation were 3300 (capillary) and 3000 (cannula). Small adjustments of the parameters were in some cases necessary, because the exact position of the capillary after installation

sometimes varies. According to the variable adjustment of the autosampler, it was also possible to do injections directly from vials with micro inserts. A detailed description of the injection from vials with micro inserts is given in the next section.

Injection from a vial with micro insert

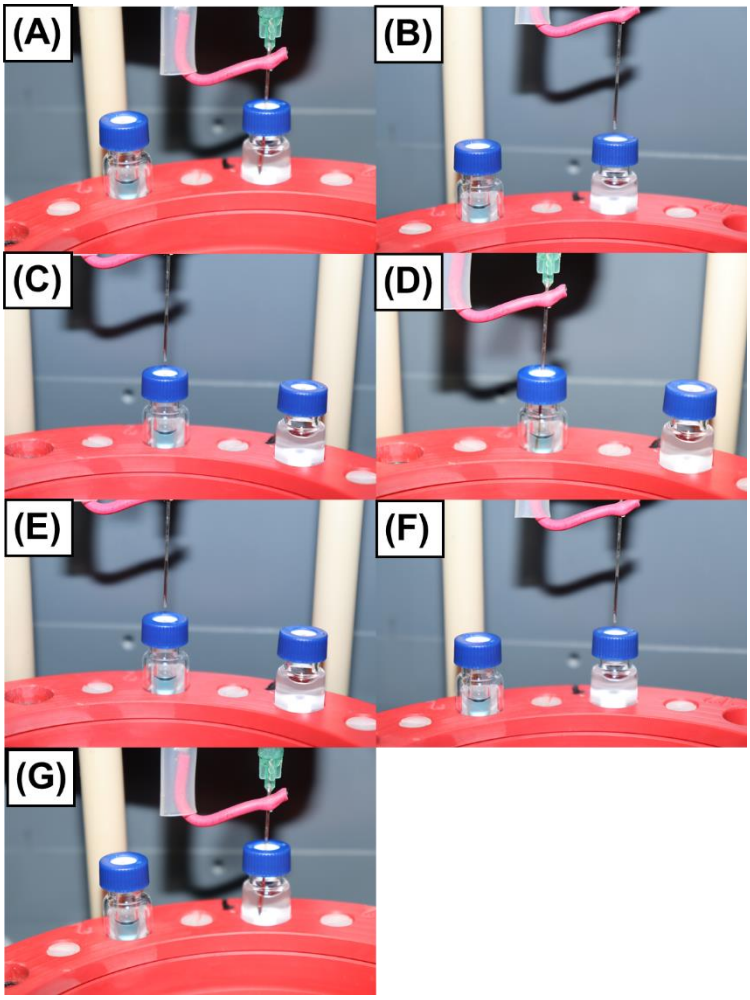

Figure G.9. Photo series (A – G) showing the injection from a vial with micro insert. For a better visibility, the sample solution was colored blue

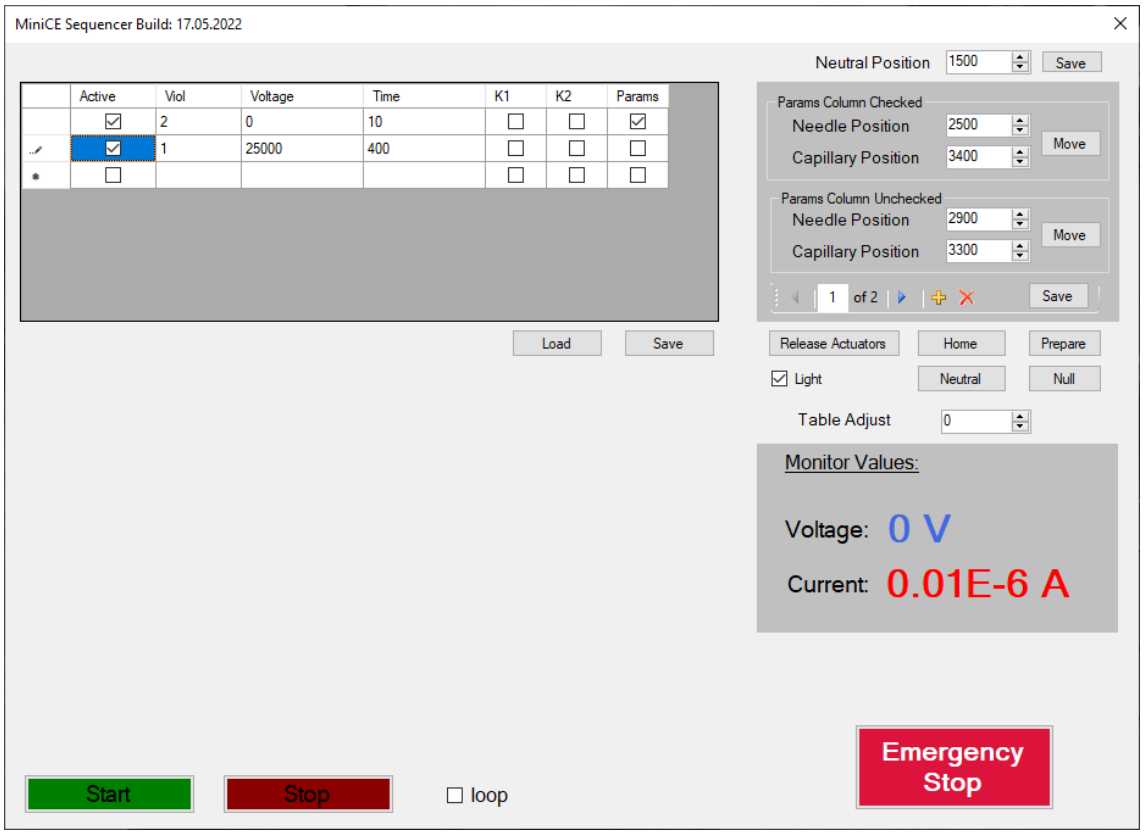

Figure G.10 User interface with example parameters for the injection from a vial with micro insert and subsequent separation

This chapter describes the injection from a vial with micro insert. A series of photos (Fig. G.9) shows each step of the autosampler during the injection process in detail. The corresponding run sequence of the user interface is illustrated in Fig. G.10. The starting point was the BGE vial at position 1 of the sample tray (Fig. G.9A). The arms of the autosampler were in the separation position and the corresponding position parameters were 3300 for the capillary and 2900 for the cannula (Fig. G.10, “Params Column Unchecked”). After pressing the “Start” button, the software processed the run sequence. In the first step, the arm of the capillary moved upwards until the capillary was protected inside the cannula (distance between both arms 2.5 cm, same distance as for the “Null” position during the installation of the capillary). Afterwards both arms (capillary and cannula) moved upwards with a constant distance (2.5 cm) until they reached the “Neutral” position (Fig. G.9B). In the next step, the sample tray turned to position 2, where the sample vial with micro insert was placed (Fig. G.9C). Both holders moved with a constant distance (2.5 cm, capillary protected inside the cannula) into the sample vial. During this step, the cannula pierced the septum of the sample vial while the capillary was protected inside the cannula. After the cannula arm reached its final position, the capillary arm moved to its position. In Fig. G.9D, the arms of the autosampler were in the injection position, the corresponding position parameter for the capillary arm were 3400

and 2500 for the cannula arm (Fig. G.10, “Params Column Checked”). The autosampler held the injection position for 10 s (Fig. G.10, “Time”). After finishing the first line of the run sequence, the capillary arm moved up until the capillary was protected inside the cannula. Then both arms moved with a constant distance (2.5 cm) to the “Neutral” position (Fig. G.9E). Due to the command from the next line of the run sequence, the sample tray turned from position 2 to position 1 (Fig. G.9F).

Both arms moved with a constant distance (2.5 cm) into the BGE (same procedure as previously described). Fig. G.9G shows the autosampler in the separation position. The cannula was placed inside the BGE and the capillary protruded about 2 mm from the cannula tip. The separation positions for both arms are shown in Fig. G.10 (“Params Column unchecked”). According to the commands in the second line of the run sequence, a separation voltage of 25 kV was applied for 400 s. After the time had expired, the autosampler remained in its last position and the high-voltage was turned off. It was found that injections from vials with micro inserts down to a sample volume of 15 µL could be performed.

Advantages

The laboratory constructed CE device has several advantages and is a reasonable basis for further innovations. The greatest advantages of the new CE device are shortly summarized in this chapter:

- Due to a compact design and several capillary passages, the CE device could be connected to a wide variety of detectors (AD, MS, UV, and C^4D).
- All components of the CE device were easily accessible and interchangeable. Additionally, the installation of the capillary was very user-friendly.
- The capillary tip could be positioned individually to enable injections from different sample containers, including standard vials and vials with micro inserts. This enabled the handling of very small sample volumes (15 µL). Theoretically, also injections from electrode surfaces should be possible.
- The new CE device was able to perform injections from vials covered with a septum. This was especially useful for measurements with non-aqueous BGE to avoid solvent evaporation.
- The CE system could be flushed with BGE by applying an excess pressure at the injection site without disassembling the capillary from the CE device or the detector. For storage, the capillary could remain installed, which enhanced the reproducibility.

References

1. Mark J. Analytical approaches to the analysis of small samples and hyphenation of fast capillary electrophoresis to other instrumental techniques [dissertation]. Regensburg (DE): University of Regensburg; 2014
2. Schmidberger A, Piendl S, Mark JJP, Matysik F-M. Characterization of a laboratory-constructed miniaturized device for fast CE measurements with contactless conductivity, amperometric, and mass spectrometry detection. Monatsh Chem. 2017;148:1661–5.

8 Eidesstattliche Erklärung

Ich habe die vorliegende Arbeit selbstständig verfasst, keine anderen als die angegebenen Quellen und Hilfsmittel benutzt und bisher keiner anderen Prüfungsbehörde vorgelegt. Von den in §27 Abs. 5 vorgesehenen Rechtsfolgen habe ich Kenntnis genommen.

Regensburg, den 26.01.2023

…….

Daniel Böhm